Development of an advanced noise propagation model for noise optimization in wind farm

Barlas, Emre

Publication date:
2017

Document Version
Publisher's PDF, also known as Version of record

Development of an advanced noise propagation model for noise optimization in wind farm

Department of Wind Energy PhD Report 2017

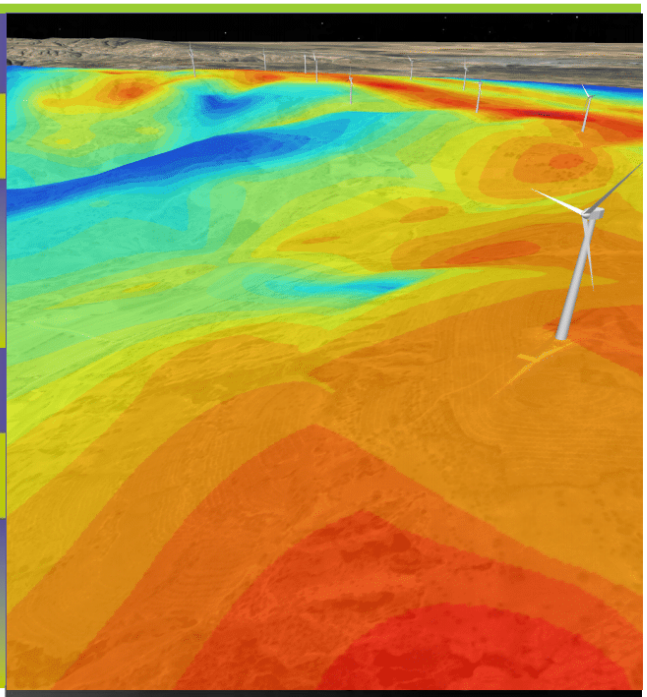

Emre Barlas

DTU Wind Energy PhD-0080(EN)

Oktober 2017

DTU Wind Energy
Department of Wind Energy

Authors: Emre Barlas

Title: Development of an advanced noise propagation model for noise optimization in wind farm

Department: Fluid Mechanics Section

DTU Wind Energy PhD-0080(EN)
Oktober 2017

Education:
PhD

Supervisors:
Wen Zhong Shen
Jens Nørkær Sørensen
Wei Jun Zhu

Technical University of Denmark
Department of Wind Energy
Nils Koppels Allé
Building 403
2800 Kgs. Lyngby
Denmark
Telephone

www.vindenergi.dtu.dk

Preface

This thesis is submitted in partial fulfilment of the requirements for the *Doctor of Philosophy* degree from the Technical University of Denmark. The research was conducted during the period from November 2014 to October 2017 at the Department of Wind Energy, Fluid Mechanics Section.

I would like to thank my supervisors Wei Jun Zhu, Wen Zhong Shen and Jens Nørkær Sørensen for the time that they have allocated for my questions. In addition, I would like to thank Mark Kelly from DTU Wind Energy Risø campus for adding valuable input to the project from different technical perspectives. I also want to acknowledge my gratitude to Patrick Moriarty from NREL as he has been a very nice host during my external stay. During my stay I also had the opportunity to have fruitful discussions with Vladimir Ostashev from NOAA on fundamental applications of the methods used in the thesis. Furthermore, collaborating with Wu Ka Ling and Fernando Porté-Agel from EPFL helped me to investigate various topics and increased the value of my work.

I am also thankful to many other colleagues from DTU Wind Energy, particularly FLU section. Lastly, I would like to thank Kaya Onur Dag for the discussions on the physical interpretations and numerical implementation issues that I have encountered during the three years.

Abstract

Increasing demand in renewable energy has resulted in large wind energy deployment. Even though wind turbines are among the most environmentally friendly way of generating electricity, the noise emitted by them is one of the the main obstacles for further installation. Wind farm developers rely on noise mapping tools for environmental impact assessment studies. Inaccurate noise mapping during wind farm development phase may result in under or overprediction of the sound pressure levels. The former causes downregulation of wind turbines under certain atmospheric conditions (e.g. for some incoming wind directions or time of the day). The latter causes turbines to be located at less resourceful sites in advance. Both of these scenarios increase the cost of energy. Hence there is a need for more accurate noise mapping tools. The thesis addresses this issue via development of a new tool based on combined source, propagation and flow models.

The parabolic wave equation method is used for modelling the frequency dependent wave propagation. Different numerical techniques such as FFT's or finite difference methods are implemented to solve the equations. The wind speed and temperature distributions are obtained either from Large Eddy Simulation or Reynolds-Averaged Navier-Stokes computations. The source levels and locations are obtained from aeroelastically coupled semi empirical airfoil noise models. Via the developed tool the effects of various atmospheric phenomena and turbine operation conditions on far field noise are investigated. Classical propagation effects (i.e. shadow zones at the upwind of the turbine, absorbing character of grass versus hard ground) and source level changes due to the operational conditions are well captured. Additionally, throughout the thesis the effects of wake on far field sound pressure levels are addressed both in steady and unsteady manner. Enhanced far field amplitude modulation is observed and associated with the wake dynamics and the rotating blades. Lastly, the developed tool is used for an onshore wind farm noise prediction taking the terrain and the flow field around it into account.

Dansk resumé

Øget efterspørgsel i vedvarende energi har resulteret i stor udnyttelse af vindenergi. Selvom vindmøller er blandt de mest miljøvenlige måder at generere elektricitet på, er den støj, der udsendes af dem, en af de største hindringer for yderligere installation. Vindmøllepark udviklere er afhængige af støjkortlægningsværktøjer til undersøgelser af miljøkonsekvens. Ukorrekt støjkortlægning under vindparkens udviklingsfase kan resultere i under eller overprediktion af lydtrykniveauerne. Den førstnævnte forårsager nedregulering af vindmøller under visse atmosfæriske forhold (fx for nogle indkommende vindretninger eller tidspunkter på dagen). Sidstnævnte forårsager at vindmøller bliver opstillet på steder med færre vindresourcer. Begge disse scenarier øger omkostningerne ved energi. Derfor er der behov for mere præcise støjkortlægningsværktøjer. Afhandlingen omhandler dette problem via udvikling af et nyt værktøj baseret på at kombinere kilde, udbredelses- og flowmodeller.

Den parabolske bølge lignings metode anvendes til modellering af frekvensafhængig bølgeudbredelse. Forskellige numeriske teknikker såsom FFT'er eller Finite Difference implementeres for at løse ligningerne. Vindhastigheden og temperaturfordelingen opnås enten fra Large Eddy Simulation eller Reynolds-Averaged Navier-Stokes beregninger. Kildeniveauerne og lokaliteterne er opnået fra aeroelastisk koblede semi empiriske vingeprofil støjmodeller. Via det udviklede værktøj undersøges virkningerne af forskellige atmosfæriske fænomener og turbine operationsforhold på støj. Klassiske udbredelseseffekter (dvs. skyggezoner opstrøms for vindmøllen, græs absorberende karakter i forhold til hård jord) og ændringer i kildeniveauet på grund af driftsforholdene er godt modelleret. Derudover behandles effekten af kølvandet på lydtryksniveauer langt nedstrøms både på en stabil og ustabil måde. Forstærket amplitude modulering observeres og er forbundet med kølvandets dynamik og de roterende blade. Endelig er det udviklede værktøj brugt til en prognose for vindmølleparker på landområder, hvor der tager hensyn til terrænet og strømningsfeltet omkring det.

List of Publications

Journal Articles

Barlas E, Zhu W J, Shen W Z, Kelly M and Andersen S J (**2017**) Effects of wind turbine wake on atmospheric sound propagation. Appl. Acous. **122**, 51-61.

Barlas E, Zhu W J, Shen W Z, Dag K O and Moriarty P J (**2017**) Consistent modelling of wind turbine noise propagation from source to receiver. J. Acoust. Soc. Am. **142** (5), 3297-3310.

Barlas E, Ling W K, Zhu W J, Porte-Agel F and Shen W Z (**2017**) Variability of wind turbine noise over a diurnal cycle. J. Ren. En. (submitted - July 2017)

Kelly M, Barlas E and Sogachev A (**2018**) Statistical prediction of far-field wind-turbine noise, with probabilistic characterization of atmospheric stability. J. Ren. Sust. En. **10** (1), 013302.

Zhu W J, Shen W Z, Barlas E, Bertagnalio F and Sørensen J N (**2018**) Wind turbine noise generation and propagation modeling at DTU Wind Energy: A review. J Ren. En. Rev. (accepted)

Conference Articles

Barlas E, Zhu W J, Shen W Z, Dag K O and Moriarty P J (**2017**) Investigation of amplitude modulation noise with a fully coupled noise source and propagation model. 7th Int. Conf. on Wind Turbine Noise.

Barlas E, Zhu W J, Shen W Z and Andersen S J (**2016**) Wind Turbine Noise Propagation Modelling: An Unsteady Approach. J. Phys. Conf. Ser., Vol. 753

Ostashev V E, Wilson D K, Finn A, Rogers K and Barlas E (**2016**) Spectral broadening of acoustic tones generated by unmanned aerial vehicles in a turbulent atmosphere. J. Acoust. Soc. Am. **140**(4).

Shen W Z, Zhu W J, Barlas E, Sørensen J N (**2017**) Modelling activities in wind turbine noise aeroacoustics at DTU Wind Energy. 7th Int. Conf. on Wind Turbine Noise

Poster Presentations

Barlas E, Zhu W J, Shen W Z (**2016**) Sensitivities of wind farm noise propagation to the input parameters, Wind Europe Workshop: Wind Turbine Sound 2016

Barlas E, Zhu W J, Shen W Z (**2015**) Development of Wind Turbine Noise Propagation Models, DCAMM 16th Internal Symposium, Horsens.

Zhu W J, Shen W Z, Barlas E (**2014**) Development and comparisons of wind turbine noise propagation models EWEA Workshop: Wind Turbine Sound 2014

List of Symbols

Acronyms

ABL	Atmospheric Boundary Layer
ASL	Atmospheric Surface Layer
DTU	Technical University of Denmark
ECN	Energy research Centre of the Netherlands
EPFL	École Polytechnique Fédérale de Lausanne
FFP	Fast Field Program
GFPE	Green's Function Parabolic Equation
GTPE	Generalized Terrain Parabolic Equation
LEE	Linearised Euler Equations
LES	Large Eddy Simulation
MPI	Message Passing Interface
NAPE	Narrow Angle Parabolic Equation
NOAA	National Oceanic and Atmospheric Administration
NREL	National Renewable Energy Laboratory
PE	Parabolic Equation
RANS	Reynolds Averaged Navier-Stokes
RT	Ray Tracing
SPL	Sound Pressure Level
WAPE	Wide Angle Parabolic Equation

Symbols

δ	boundary layer thickness	m
λ	wavelength	m
ρ	density	kg/m^3
c	speed of sound	m/s
f	frequency	Hz
α	absorption coefficient	dB/m
ω	angular frequency	rad/s
k	wave number	rad/m

Sub- and Superscripts

amb	value relative to the ambient
eff	effective

Executive Summary

This thesis investigates the long-range sound propagation of wind turbine noise from source to receiver under various atmospheric conditions. The basis of the propagation model is built on the parabolic wave equation (PE) method. This technique has been extensively used in outdoor and underwater acoustics. It can take into account the complex ground impedance over the whole source-receiver range, vertical and horizontal sound speed profiles, turbulence, and irregular terrain. Although the implementation of the PE method is relatively trivial, obtaining the aforementioned inputs is the main challenge. The innovative contributions of this thesis are as follows:

1. The consideration of the background flow/wake unsteadiness: with increasing computational resources, the representation of atmosphere within the PE model has inevitably become more realistic. There are studies (though limited) that incorporated unsteady atmospheric input obtained from Large Eddy Simulations to the PE method. Nevertheless, the interaction of wind turbines with the atmosphere is another story. The complexity of wake evolution undeniably complicates the downwind sound propagation. The first significant advancement that this work puts forward is the unsteady representation of wake fields within PE via successive simulations. This allowed us to gain insight of the wake effects on outdoor sound propagation and forced us to raise more questions.

2. The consideration of the unsteady nature of wind turbine noise: the unsteadiness is a result of constant variation of noise source generation and propagation. To address this, a numerical technique is developed that combines the aforementioned two phenomena. The initial coupling was carried out using aero-elastic codes with semi-empirical airfoil noise calculations. This is not necessarily the state of the art; however, the source representation in an unsteady and quasi 3D manner within the PE is the major advancement of this step. Additionally, the usage of high fidelity flow solvers output for both generation and propagation allows us to model the phenomena consistently. One

of the most important applications of the developed technique is the numerical investigation of the far-field amplitude modulation (AM). This was not previously possible (earlier works mostly focus either on near field AM with simple numerical models or field experiments for AM detection after the wind farm installation phase). Via the consistent wind turbine noise generation-propagation model it can be possible to narrow down the conditions (both wind turbine operation and atmospheric) and find solutions to mitigate it accordingly.

3. The investigation of wind turbine noise variation during a diurnal cycle: as researchers, we usually have opportunities to look into various issues more in depth thanks to the large computational resources as well as projects with long term goals. Nevertheless, we should always remember the relevant outcomes for possible future implementations or tunings of the existing engineering models via our outputs. In this regard, the developed tool was used to investigate the wind turbine far field noise variation over a diurnal cycle. The interest in these topics was emphasized on several occasions during our interaction with various companies. The technical advancement of this step is the incorporation of the realistic temperature and wind fields including source generation variation (day and night), wake evolution, and wind shear and turbulence variation.

4. In addition to the physical conclusions, we can derive from this thesis an important contribution that should not be ignored is the development of a Fortran/MPI code that is readily available to use for future work. The code's capabilities such as the incorporation of various flow and source models for single wind turbines or wind farms are the significant improvements that DTU Wind Energy will be taking advantage of.

Although the developed source-propagation coupling technique can be used to study wind turbine noise at large distances, it is worthwhile noting the shortcomings/limitations:

1. Even though the parabolic equation is a physics-based method and derived from the governing wave propagation equations, the assumptions that are used during the mathematical derivation arise some limitations. First, it is a one-way propagation method. In other words, the terms that represent the backscattering are neglected, and thus the results under multiple scattering are not reliable (e.g. a source located between two screens). However, for wind turbines, this is rarely the case. Second, the angular limitation of the method can be an important aspect. Depending on the expansion of the so-called square-root operator during the mathematical derivation, the region where the results are

valid can be extended further. Nevertheless, throughout the thesis a wide-angle implementation of parabolic wave equation is used. This is valid within ± 35 degrees in the paraxial direction. This can be an issue particularly for an elevated source like a wind turbine if the near field levels are of interest. Lastly, the effective speed of sound approach is a crucial point. It is an approach where the moving atmosphere is replaced by a hypothetical motionless medium with the effective sound speed. It is expected to perform well when the source and receiver are close to the ground, as the sound propagation direction is nearly horizontal and the scattering angle (angle between the sound wave and the wave scattered by turbulence) do not exceed a certain limit. However, it was shown in the first article of the thesis that the error decreases as a result of turbulence introduced random phase shifts.

2. Apart from the classical limitations of the PE method, a two-dimensional (2D) approach which was employed in this thesis is another drawback. The axisymmetric approximation allows us to reduce a 3D problem to a 2D problem, which neglects the azimuthal variations. This approximation is shown to perform sufficiently accurate in many cases; however, the effect of complexity of wind turbine flow field is yet to be quantified.

3. Even though the increasing computational power allows us to simulate more things than before, the PE method can still be a limited tool for long distance propagation of high frequencies. Depending on the distance and source spectra, this issue should be considered carefully.

4. It is also important to note that throughout the thesis, atmospheric attenuation is kept constant, as the focus of the study is mostly on calculation of transmission loss. However, the variation of temperature and humidity will result in change of attenuation factor and this should be taken into account for a more rigorous study.

Contents

Chapter 1

Introduction

1.1 Wind turbine noise

Wind turbine noise is a highly multi disciplinary topic. Starting from the aerodynamic sound emitted at the airfoil scale, propagating through the turbulent atmosphere over complex terrain and transforming to annoyance for the resident living nearby, the issue requires the involvement of a broad range of disciplines. While aero-acousticians are deeply interested and very much capable of modelling the airfoil noise generation with different fidelity models [1, 2, 3, 4], an atmospheric scientist might focus more on the sound wave propagation through inhomogeneous moving medium and how the medium causes both short and long term far field noise variability [5, 6]. Another scientific community would like to emphasize the human response to wind turbine noise [7, 8] as well as the reasons that lie behind the higher annoyance of wind turbine noise than other noise sources [9]. Addressing the whole chain of wind turbine noise issue is indeed a difficult task.

Nevertheless, because the noise is one of the main obstacles achieving a broader public acceptance of wind energy, the accurate assessment of noise generated from wind turbines/farms is even more of a necessity than ever. This starts with a good estimation of the source characteristics. The aerodynamic sound generation from airfoils has been reviewed by many authors [10, 11]. The underlying physics relevant for wind turbine noise can be narrowed down to airfoil self noise and the turbulent inflow noise. Single steady airfoil noise is an issue on one hand, the rotating blades that are exposed to complicated flow field on the other hand, the wind turbine noise generation is a complicated phenomenon. Variation of the dominant source location, directivity, strength and spectral characteristics are some of the issues to be addressed for an accurate source level estimation [12, 13].

Furthermore, for accurate modelling of wind turbine noise at far field requires not only a good knowledge of source characteristics but also a realistic representation of the medium between the rotating blades and the receivers. Variation of ground characteristics (e.g. snow or grass covered), terrain undulations (e.g. flat or complex terrain), atmospheric conditions combined with unsteady nature of wind turbine wakes result in an intricate and fundamentally random propagation phenomenon. There is an increasing interest in investigation of peculiar far field characteristics of wind turbine noise that are not clearly well understood [14], hence so far poorly modelled.

The estimation of overall wind turbine far field noise is a complex task that depends on a wide range of parameters and both short and long term variations. The following subsection gives an overview of the existing prediction tools and the motivation of the present work.

1.2 Motivation and Objectives

The wind turbine noise generation and propagation are inherently unsteady phenomena as a result of the constant variation of turbine operation and atmospheric conditions. However, the existing tools for wind turbine noise estimations at far field receivers are not capable of handling this complexity. The basic approach for far field noise prediction is assuming an overall source power level for a wind turbine depending on the rotor diameter and using a propagation relationship based on hemispherical spreading. Even though this neglects most of the physics, it has been the standard for some years [15]. A more advanced method is the Nord2000 that is based on a semi-analytical ray model which deals with the refraction effects using a linear approximation for the speed of sound profile [16]. There are other corrections applied for undulating terrain and ground impedance. Even though this model has shown to predict more accurately than many other models [17], there are certain shortcomings. For example, the source model is still somewhat simple since a monopole at the hub height is used to represent the wind turbine noise source irrespective of the diameter and the source strength does not depend on the inflow conditions.

More sophisticated noise source models exist [18, 19] that divide the wind turbine blades into airfoil segments and sum up the contribution of each segment's noise levels that are calculated based on semi-empirical relationships. This source model along with simple propagation calculations is used in the computational tool called SILANT (developed by ECN)[20]. A similar source model is employed and coupled with the ray tracing model in [21]. Neither of these tools consider the complicated

three dimensional flow field around a wind turbine and its effect on sound generation and propagation.

There is a clear need for developing a wind turbine far field noise prediction tool, that takes into account the interaction between the incoming turbulent flow and the wind turbine noise generation and propagation physics. The thesis addresses this gap via the objectives listed below:

- Development of a high-fidelity sound propagation model that is accurate but with reasonable computational demand.
- Development of a suitable source model that can handle the variability of wind turbine noise generation.
- Investigation of various effects such as wind and temperature gradient, ground cover, atmospheric and wake turbulence, turbine operation conditions.
- Lastly, preparation of a code to be applied for wind farm noise mapping and/or optimization.

1.3 Thesis outline

The thesis is outlined as an attempt to get a consistent message across to the reader. Ch. 2 starts with a very brief review of the physics underlying the sound propagation phenomenon with an emphasis on refraction. Subsequently an overview of modelling techniques is given, followed by the elaboration of the methodology used in the thesis. Lastly, ch. 2 shows some validation studies with experiments and benchmark cases of the developed codes.

The following 4 chapters have the same structure. An overview of the relevant phenomenon is outlined in the first section and the corresponding publication is added in the second section. Ch. 3 elaborates the effects of wind turbine wakes on sound propagation. The emphasis is on the description of the physical phenomenon and the consequences. Ch. 4 employs a statistical approach to investigate the downwind propagation of wind turbine noise considering the probability of various atmospheric conditions. Thereby not only extreme stable or unstable atmospheric conditions were investigated, but also a generalized outcome was obtained

While chapters 3 and 4 focus solely on the propagation phenomena, Ch. 5 introduces a new combined model that includes the variability of both wind turbine noise generation and propagation. The source model is more advanced and more representative than the previous chapters. The corresponding publication gives a

detailed model description and shows applications for various wind speeds and surface roughness values for a neutral atmosphere. This chapter also investigates the amplitude modulation of wind turbine noise in a more consistent manner. Ch. 6 extends the new model applications with a different flow solver to investigate the diurnal variability of wind turbine noise. Again the unsteady simulations are used to investigate the amplitude modulation variation. In Ch. 7 a preliminary study on wind farm noise is carried out using the developed tool. This is the basis for a new wind farm noise mapping tool that can readily be used within noise assessment studies. Finally, conclusions and future works are given in Ch. 8.

Chapter 2

Atmospheric Acoustics & Modelling

2.1 Atmospheric Acoustics

Sound propagation in atmosphere is a complex phenomenon that is influenced by a large number of parameters. Various review papers exist for the discussion of the topic in depth [22, 23]. Early observations date back to 1800s when a large volcano explosion was heard thousands of kilometres away [24]. Throughout the history the variability in sound propagation changed the course of wars [25, 26], modified the perception of the church bells [27] or caused some *strange sounds* in the atmosphere [28]. The physics that lie behind these interesting events are detailed in the aforementioned review papers. The structures of these papers are similar and start from the geometrical spreading of sound waves from a point source (a decrease of the sound intensity inversely proportional to the distance square). Then it continues with the atmospheric absorption phenomenon which causes a loss of energy and originates from two processes: relaxation and dissipation. These phenomena have been well studied [29] and the resulting parameter, the absorption coefficient (α), depends on acoustic frequency, humidity and temperature, and to a lesser extent on atmospheric pressure. Throughout the thesis the frequency dependent absorption coefficient in ISO 9613-1 is used for a constant humidity (80 %) and a constant temperature (20°C), thereby the variability due to air absorption is neglected.

Following the geometrical spreading and absorption phenomena; effects of ground (reflection), effects of wind and temperature gradients (refraction), effects of terrain topography and obstacles (reflection, diffraction) are discussed. The thesis focuses predominately on the refraction effects on sound waves, therefore this section fo-

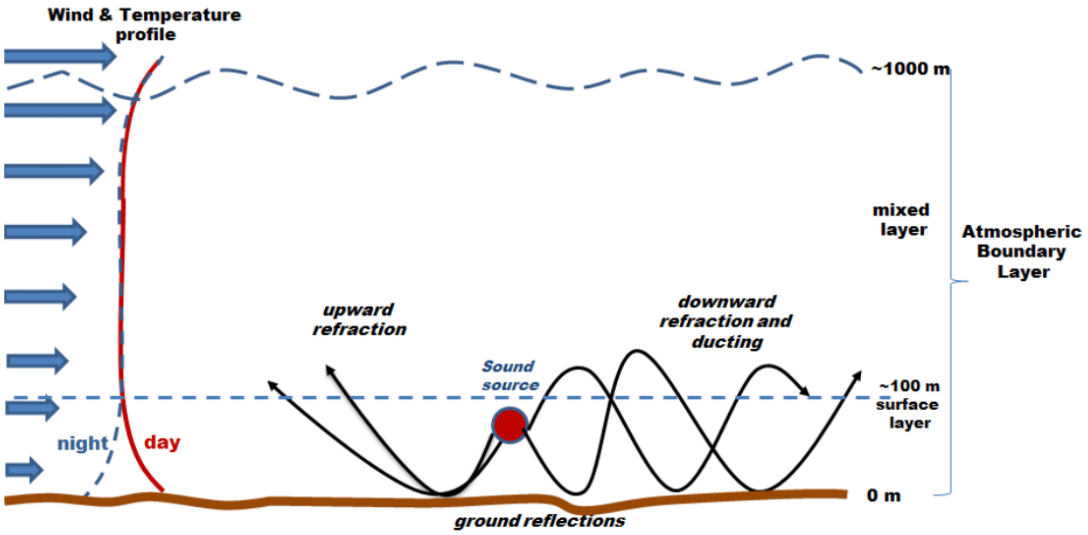

Figure 2.1: Near-ground sound propagation for a high-wind condition. Wind direction is from left to right. (adapted by [30]).

cuses on the effects of both time averaged and instantaneous wind and temperature gradient.

To give an overall picture a more recent review paper [30] is followed in which the atmospheric sound refraction is parametrized with the so-called effective speed of sound parameter. This parameter is defined as $c_{eff} = c + \mathbf{v}\, cos\, \theta$, where c is the actual sound speed, $\mathbf{v}$ is the wind speed, and θ is the angle between the direction of sound propagation and the wind velocity vector. As seen from the relationship the effective speed of sound is implicitly affected by the temperature (c(T)) and explicitly by the wind distribution ($\mathbf{v}$). With the variation of atmospheric conditions and propagation direction these parameters play a role in favour of sound pressure level amplification or attenuation for the ground level receivers. At very high wind speeds, the atmospheric stratification is generally close to the neutral due to the strong turbulent mixing induced by the wind shear. A sketch of the resulting sound propagation phenomena is shown in Fig. 2.1. If the wind speed is low, the stratification will vary with the atmospheric conditions that change the radiative transfer between the ground and air. While in a clear day an unstable stratification is observed due to the heat that is conducted to the overlying air from the ground heated by the sun, in a clear night stable stratification is observed due to the cooling of the ground. A near-neutral stratification can be observed when a thick stratus cloud

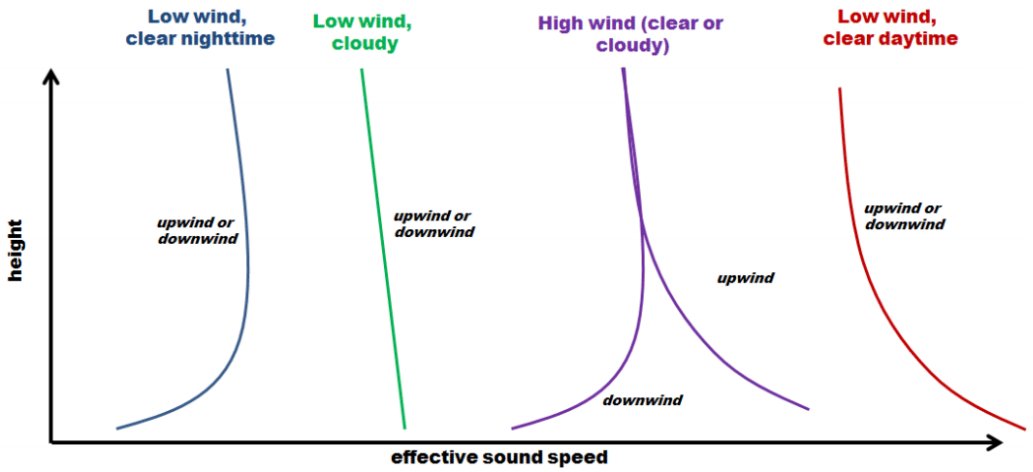

Figure 2.2: Characteristic effective sound speed profiles for 4 limiting cases of the surface layer. The profiles are arbitrarily offset along the horizontal axis (adapted by [30]).

layer covers the area.

Following [30] four fundamental sound propagation regimes can be defined:

High wind (day or night): Nearly neutral stratification. Refraction depends primarily on wind shear and hence on the propagation direction.

Low wind, clear, daytime: Unstable stratification and upward refraction. Buoyancy instabilities create a strong turbulence.

Low wind, cloudy (day or night): Weak refraction, generally upward all directions. Turbulence tends to be weak.

Low wind, clear, nighttime: Ground-based temperature inversions often form, which lead to the prevalence of a strong downward refraction. Turbulence is suppressed by the stable stratification but may occur intermittently.

Fig. 2.2 shows the effective speed of sound profiles listed above. This classical picture changes significantly when we discuss the sound propagation behind a wind turbine due to the wake deficit effects. This issue will be further investigated in ch. 3.

Apart from the average wind and temperature gradients, the fluctuations of these parameters also affect the sound propagation. A way to interpret the atmospheric

turbulence is depicting it to be composed of a broad range of eddies with various characteristic lengths (vary in size from millimetres to hundreds of meters). The wavelengths (λ) within a broadband signal propagating through this cascade of eddies also vary significantly (e.g. $0.017 \text{ m} < \lambda < 17 \text{ m}$). Depending on the specific wavelength, propagation distance and turbulent scales, the effects on sound propagation may change (see [31] for a review). For example, there can be localized effects which cause single scattering (scattering of the wave outside the initial direction of propagation) or when propagation through an extended region of turbulence is considered (large distance compared to characteristic turbulent length scales) it can cause multiple scattering which results in wave front distortion, loss of coherence and strong intensity fluctuations. Some numerical simulations are carried out in [32, 33] for single or multiple scattering. One can briefly state that the temperature fluctuations cause random changes in the local speed of sound and the velocity fluctuations cause the wave convection at different speeds. If one refers to the effective speed of sound approach these two separate looking effects boil down to one. And the turbulence causes the so-called refractive index fluctuations. These fields to be used within the propagation models can be either synthetically generated with respect to a prescribed spectrum or obtained via solving the governing equations of fluid dynamics. The latter is computationally much more demanding than the former. A study that investigates the representation of the atmosphere with various techniques can be found in [34]. Moreover, there are comprehensive papers discussing the interaction of the relevant turbulent scales and sound waves [35, 36]. Additionally, a poster that addresses this issue to a certain extent is attached to the end of the thesis.

Overall, the sound propagation in a stratified turbulent atmosphere is a complicated field with an increasing interest from the research community. The interested reader is referred to [6] for rigorous mathematical derivations and an overview of applications.

2.2 Overview of Modelling Techniques

There is a variety of numerical techniques for modelling the atmospheric sound propagation phenomenon. Each technique's equations can be derived from a complete set of fluid dynamics equations and the methods differ from each other with different assumptions. Each comes along with its advantages and disadvantages. The scope of this section is limited with a brief overview rather than a scrutinized derivation of equations which can be found in ch. 2 of Ref. [6]. Here, the modelling techniques are divided into two groups namely, geometrical acoustics and wave-based methods,

and an overview is given.

Geometical Acoustics Based Methods

1. Ray Tracing (RT) Techniques

   Ray tracing is based on the high frequency approximation to the full wave equation. The high frequency approximation/limit implies that the waves behave like particles and travel along rays [37]. Conceptually, these rays may be regarded as the particle trajectories as they move through the fluid at a certain speed of sound and fluid velocity [6]. There is a variety of formulations of RT techniques. The fundamental idea is the same for all. First, the determination of the ray paths is carried out and then the contribution of each ray to overall sound pressure is calculated. Some of the formulations can only handle a linear speed of sound [38] with an effective speed of sound approach, while more advanced ones (e.g. Hamiltonian ray tracing [21]) are not restrained with these limitations. Nevertheless, as it is pointed out in [6] geometrical acoustics may not be the best method to handle low frequencies and other phenomena such as small scale turbulence scattering, diffraction effects can not be accounted for. Additionally, the ray models produce inaccurate results at focusing areas called caustics. Even though there are ways to overcome this as presented in [39] the problems do not seem to be fully overcome.

   Considering that a long range propagation is dominated by the low frequencies (due to atmospheric absorption), RT technique's inherent high frequency assumption appears as the most important drawback.

   The starting point of the mathematical derivation of the ray models is the Helmholtz equation. In Cartesian coordinates this yields:

$$\nabla^2 p + \frac{\omega^2}{c^2(\mathbf{x})} p = -\delta(\mathbf{x} - \mathbf{x}_0) \tag{2.1}$$

   To obtain the ray equations, we seek a solution of the Helmholtz equation in the form:

$$p(\mathbf{x}) = e^{i\omega\tau(\mathbf{x})} \sum_{j=0}^{\infty} \frac{A_j(\mathbf{x})}{(i\omega)^j} \tag{2.2}$$

   This is called the ray series. It is generally divergent, but in certain cases it can be shown to be an asymptotic approximation to the exact solution. Taking derivatives of eq. 2.2 yield:

$$p_x = e^{i\omega\tau}\left[i\omega\tau_x \sum_{j=0}^{\infty} \frac{A_j}{(i\omega)^j} + \sum_{j=0}^{\infty} \frac{A_j, x}{(i\omega)^j}\right] \tag{2.3}$$

$$p_{xx} = e^{i\omega\tau}\left\{[-\omega^2\tau_x^2 + i\omega\tau_{xx}] \sum_{j=0}^{\infty} \frac{A_j}{(i\omega)^j} + 2i\omega\tau_x \sum_{j=0}^{\infty} \frac{A_j, x}{(iw)} + \sum_{j=0}^{\infty} \frac{A_j, xx}{(i\omega)^j}\right\} \tag{2.4}$$

where subscripts stand for derivatives.

Substituting this result into the Helmholtz equation and equating terms of same order in ω, we obtain the following infinite sequence of equations for the functions $\tau(\mathbf{x})$ and $A_j(\mathbf{x})$,

$$\begin{aligned} O(\omega^2) &: |\nabla\tau|^2 = c^{-2}(\mathbf{x}), \\ O(\omega) &: 2\nabla\tau \cdot \nabla A_0 + (\nabla^2\tau)A_0 = 0, \\ O(\omega^{1-j}) &: 2\nabla\tau \cdot A_j + (\nabla^2\tau)A_j = -\nabla^2 A_{j-1}, \quad j = 1, 2, ... \end{aligned} \tag{2.5}$$

The $O(\omega^2)$ equation for $\tau(\mathbf{x})$ is known as the *eikonal equation*. The remaining equations for $A_j(\mathbf{x})$ are known as the *transport equations*.The standard simplification made is to ignore all but the first term in the ray series, which is evidently a high-frequency approximation. The solution for these equations are further detailed in [40].

Wave-Based Methods

In this section starting from the linearised Euler equations (LEE), which constitute the basis of Time Domain Techniques, wave equation, Helmholtz equation and then the parabolic wave equation is shown. LEE is the linearized equations of fluid dynamics with certain assumptions such that the atmosphere is assumed to be an ideal gas, the magnitude of the flow speed ($\mathbf{v}$) is smaller than the adiabatic speed of sound (c), spatial variations in ambient air pressure are neglected, and the internal gravity waves are of no concern.

$$\frac{\partial p}{\partial t} = -(\mathbf{v} \cdot \nabla)p - \rho c^2 \nabla \cdot \mathbf{w} + \rho c^2 Q \tag{2.6}$$

$$\frac{\partial \mathbf{w}}{\partial t} = -(\mathbf{w} \cdot \nabla)\mathbf{v} - (\mathbf{v} \cdot \nabla)\mathbf{w} - \frac{\nabla p}{\rho} + \frac{\mathbf{F}}{\rho} \tag{2.7}$$

where $\mathbf{w}$ is the acoustic particle velocity vector, p is the acoustic pressure, the quantities F and Q represent sources: the former is a force acting on the medium, whereas the latter is a mass source. These may be interpreted as dipole and monopole sources, respectively. The terms $(\mathbf{v} \cdot \nabla)p$ and $(\mathbf{v} \cdot \nabla)\mathbf{w}$ represent the transport of the sound wave by the atmospheric wind, also called advective terms. The term $(\mathbf{w} \cdot \nabla)\mathbf{v}$ in eq. 2.7 represents enhancement/diminishment of the acoustic particle velocity by spatial variations in the wind field. As the methodologies are explained in each subsection the equations and the corresponding simplifications will be referred.

1. Time Domain (TD) Techniques

   Time domain techniques are based on solving linearised Eulerian equations (LEE) [41]. In comparison to the other wave based methods it has the fewest simplifying assumptions, thus is capable of representing most of the physics. For example, the convection, refraction and scattering of sound waves by an inhomogeneous and moving atmosphere is included explicitly in the equations. Synthetically generated kinematic turbulence [42], Large Eddy Simulation over flat terrain [43] or more complex meteorological models [44] are some of the previously used methods to obtain the background flow input. Furthermore, multiple reflections, diffractions and scattering from objects such as noise barriers [45] [46] or trees [47] can also be considered and ground reflections can be modelled with various techniques [48] [49]. A broad frequency response is obtained by performing a single simulation with TD techniques, as opposed to frequency domain methods that solve one at a time.

   Despite all its advantages time domain methods are still fundamentally limited by the cost of discretizing a large domain for long distance sound propagation. The most commonly used discretization technique is finite difference method mostly due to its implementation simplicity [50]. Even though new trends exist to exploit spectral methods such as Fourier [51] or Chebyshev polinomial [52] discretization techniques, time domain models still remain a computationally expensive tool for the distances considered for this study. Additionally, the source representation for broadband sources such as wind turbines is still a difficult task for TD techniques.

2. Frequency Domain (FD) Techniques

   Transition from TD techniques to FD ones starts with the manipulation of the previously given first order LEE to derive the second order wave equation. This can be done by taking the time derivative of eq. 2.6 and the divergence of eq 2.7. For a non moving medium this yields the classical wave equation;

$$\frac{1}{c^2}\frac{\partial^2 p}{\partial t^2} - \nabla^2 p = \mathbf{S} \tag{2.8}$$

where $\mathbf{S}$ represents all the source terms caused by non uniform force field and fluctuations of viscous stress, mass and entropy. A more rigorous formulation including moving medium is;

$$\frac{1}{c^2}\frac{\partial^2 p}{\partial t^2} - \nabla^2 p + (\mathbf{v}\cdot\nabla)^2 p = \mathbf{S} \tag{2.9}$$

Eq. 2.9 constitutes the basis of the parabolic equations explained below. PE method is a frequency domain method thus a conversion from time domain to frequency domain is carried out using the relationship;

$$p(\mathbf{r}, t) = Re(\exp^{-iwt}\psi(\mathbf{r})) \tag{2.10}$$

where $\psi(\mathbf{r})$ is some complex valued scalar function and the real part is taken, since $p(\mathbf{r}, t)$ is real. Thus the Helmholtz equation (shown later eq. 2.13) stands for monochromatic waves, or waves of some given frequency. In addition to the substitution of the expression 2.10 to eq. 2.9 one can further assume that the characteristic scale of velocity variations, L, is large in comparison to the acoustic wavelength, λ, then the operator $(\mathbf{v}\cdot\nabla)^2$ can be replaced by $v_i v_j \nabla_i \nabla_j$ which yields;

$$\left[\nabla^2 + k^2(1+\epsilon) + 2ik\sqrt{1+\epsilon}\frac{v_i}{c}\nabla_i + \frac{v_i v_j}{c^2}\nabla_i\nabla_j\right]\psi(r) = 0 \tag{2.11}$$

where $k = \omega/c_0$ (ω is the radian frequency of the sound, c_0 is the reference speed of sound), $\epsilon = (c_0/c)^2 - 1$. One can see that velocity gradient does not appear 2.11, therefore a more correct representation including both velocity and its gradients is:

$$\left[\nabla^2 + k^2(1+\epsilon) - \frac{2i}{\omega}\frac{\partial v_i}{\partial x_j}\frac{\partial^2}{\partial x_i \partial x_j} + \frac{2ik}{c_0}\mathbf{v}\cdot\nabla\right]\psi(r) = 0 \tag{2.12}$$

Note that, both eq. 2.11 and eq. 2.12 reduces to a classical Helmholtz equation if $\mathbf{v} = 0$:

$$[\nabla^2 + k^2(1+\epsilon)]\psi(r) = 0 \tag{2.13}$$

The additional terms in eq. 2.11 and eq. 2.12 in comparison to eq. 2.13 represent the effects of the moving medium. Third term on the left hand side of eq. 2.11 is proportional to the Mach number and the spatial derivative of the pressure. This term represents the convection of the sound by the velocity field. The fourth term on the left hand side is second order in Mach number and is proportional to the second spatial derivative.

In eq. 2.12 the new terms represent the wave scattering by dipoles through the wind terms (third term) and by quadrupoles through the gradient terms (fourth term). Therefore, for sound propagation through turbulence, this equation will describe more accurately scattering effects. These equations will be used in sec. 2b

(a) Fast Field Program (FFP)

In addition to the time domain transformation, spatial domain transformation is carried out with the FFP method. FFP is a numerical method for computing the sound field of a monopole source in a layered atmosphere above a ground surface. The ground surface is described by the ground impedance and the atmosphere is represented by the vertical profiles of the wind velocity and the temperature gradients. The FFP approximates the atmosphere by dividing it into horizontal homogeneous layers with constant temperature and wind velocity. The sound field in each layer is computed from the field in the horizontal wave number domain by an inverse Fourier transformation. Therefore the FFP method is sometimes called a wave number integration method [53]. This is a 2D method for an axisymmetric atmosphere with the effective sound speed accounting for wind. Since the Fourier transformation to the horizontal wave number domain occurs in the FFP it is limited to predictions incorporating a layered atmosphere and a homogeneous ground surface. Systems with a range-dependent sound speed profile or a range-dependent ground impedance cannot be modeled with the FFP [54].

(b) Parabolic Equation (PE)

The parabolic equation method is based on an approximate form of the wave equation with a preferred direction of propagation. Following the notation in [55] the PE methods can be divided into two groups: scalar and vector PE. The scalar PE is the conventional approach wherein the

moving atmosphere is replaced by a hypothetical motionless medium with an effective sound speed. For the vector PE, the vector properties of the velocity field are maintained, thus the propagation equation contains new terms. The scalar PE method is expected to perform well when the source and receiver are close to the ground because the sound propagation direction is nearly horizontal and the scattering angle (angle between the sound wave and a wave scattered by turbulence) do not exceed a certain limit.

Depending on the basis equation that the derivation starts from the PE method changes character. (e.g. derivation that starts from eq. 2.11 is referred to as the Mean Wind Wide Angle PE (MW-WAPE), eq. 2.12 is referred to as the Turbulent Wind Wide Angle PE (TW-WAPE) and eq. 2.13 are referred to as the Wide Angle PE (WAPE) or as the Narrow Angle PE (NAPE)). The mathematical manipulation is carried out both in [56] and in [57].

For all methods (vector and scalar PE) the procedure starts with the separation of forward and backward propagating waves. Subsequently, the latter one is neglected therefore, the PE method is generally referred to as one way propagation technique. In other words, only the waves propagating from source to receiver are accounted for (e.g. backward scattered waves from an obstacle are neglected). As a result of splitting process, a square root operator appears in the equations. Based on the order of the approximation scheme to the square root operator, the PE method is categorized as a narrow angle PE (NAPE), a wide angle PE (WAPE), or a higher-order PE. These equations can be solved with various numerical methods (e.g. finite difference and finite element methods [53]).

A completely different numerical technique solving the eq. 2.13 is based on Kirchoff-Helmholtz integral equation [58]. This methodology yields so called Green's Function PE (GFPE) for a refracting atmosphere. GFPE accounts for direct, reflected and surface wave separately. GFPE is superior to the other numerical techniques because the range steps (horizontal grid) can be of the order of multiple wavelengths. However it can be numerically unstable for long distances. A numerically stable formulation was recently proposed in [59]

Propagation over undulating terrain can be incorporated to the PE method with various techniques. A general solution is provided in [60] based on a non-orthogonal terrain following coordinate transformation. This method is referred to as Generalized Terrain PE (GTPE). Another method

which can be incorporated with all the previously mentioned PE methods (GFPE, WAPE etc.) is the so called rotated reference frame method. In this method the undulating terrain is approximated by a succession of constant slope segments. At the start of each segment the initialization is carried out with the interpolation of the predecessor segments sound field. This method was used with MW-WAPE in [61] and with GFPE in [62]. Some other methods to include terrain undulation into PE methods are Beilis-Tappert transformation [63], stair-steps method [64] [65] and conformal mapping [53].

2.3 Model Selection and Implementation

As seen from the previous sections there is a wide range of modelling techniques for outdoor sound propagation. For this thesis, a model that is capable of handling range dependent flow, complex terrain and varying ground characteristics was needed. Considering a reasonable computational demand was one of the bottlenecks of the selection process, PE method is used throughout the thesis.

First implementation phase is carried out in MATLAB for NAPE, WAPE, MW-WAPE, TW-WAPE, GFPE including rotated reference frame method and GTPE. The experience gained from the flat terrain simulations showed that (see sec 3.2) the random phase shifts caused by the turbulence help to decrease the error committed by the effective speed of sound assumption. Thus a computationally less demanding scalar PE method (tri-diagonal solution matrices) were chosen instead of vector PE (penta-diagonal solution matrices). Additionally, due to the sensitivity of the results with respect to the selected GFPE input parameters, Crank Nicolson numerical scheme was used.

For the terrain representation, two of the aforementioned models were evaluated (terrain following coordinates and domain decomposition). Experience gained from the simulations was that an automatized terrain decomposition procedure (e.g. selection of domain transformation locations) for any given complex terrain for wind farm noise mapping simulations was a very difficult task. Additionally, the results were very susceptible to change depending on the locations of the reference frame transformations. Hence the conclusion was to use GTPE for complex terrain. Over flat terrain on the other hand mostly WAPE and NAPE is used for near and far field receivers, respectively.

After model selection procedure and various test simulations the code was transformed to FORTRAN. The parallelization of the code was carried out using MPI in three different ways depending on the usage. Note that, there can be other ways

to exploit parallelization developing tailored cut routines for the corresponding flow solver input (velocity and temperature).

- Method 1: Most of the large simulation sets during the thesis period were carried out using pre-stored time dependent flow fields with equidistant grid in each direction. When the flow fields are already available, an efficient and easy way of parallelization is allocating each core to each time step. For example, 20 nodes in DTU's jess cluster corresponds to 400 cores. For a simulation set with 400 time steps all cores would calculate one time step. These are all independent simulations and the load in each core is equal to each other, so the scalability is ideally linear.

  At each time step (each core) two-dimensional computation domains are constructed from all sources to all receivers and the flow fields are interpolated to a common grid (e.g. 2 m resolution vertically and horizontally). This resolution is usually lower than the one that is required for the frequency dependent PE calculations, thus it is referred to as *low resolution interpolation step*. Subsequently, the interpolated flow fields are stored in a variable and then used for each PE simulation that are carried out for each frequency. Just to give an idea for the computational time required for one time step, let us consider a simulation of 17 frequencies (from 20 Hz to 1000 Hz), for a single receiver 2000 m away from the turbine which is represented with three sources around the blade tip regions. For each source a PE domain is constructed as they propagate through different flow fields, and thus the solution matrices are updated at approximately every wavelength. This simulation takes 1.5 minutes on one core.

- Method 2: If the code is coupled with a flow solver that outputs the time dependent results at each time step (e.g. the flow is not pre-stored as in Method 1) then the cores should be distributed in a different way. For a grid with uniform spacing and flat terrain the *low resolution interpolation step* does not take much time. Therefore it is simply carried out by Core 0. Core 0 reads in the three-dimensional flow field, interpolates and then broadcasts to all cores. Here we describe a new term called **pejob**. It refers to a single frequency simulation (a two-dimensional PE domain) for each source and receiver. For example if one-third octave band centre frequencies are simulated from 31.5 Hz up to 1000 Hz, for a single turbine represented with three point sources and ten different receiver locations, this would sum up to 480 independent **pejobs**. (16 frequencies, 3 sources, 10 receivers). These are all treated as independent simulations that are distributed to each available core. For a 1

node job in jess cluster this would mean 24 pejobs for each core. Each pejob's workload is not identical due to varying frequencies and distances (source-receiver). Therefore the core assignment can be made more efficiently. There is room for improvement depending on the future usage of the code.

- Method 3: Similar to the Method 2 if the flow fields are not pre-stored this option is preferred. Different to the Method 2 if a non-uniform complex terrain grid is used for the solver then the *low resolution interpolation step* takes time. Therefore this method first uses all the cores to execute the interpolation. Once the low resolution two-dimensional fields are obtained the rest of the calculations is identical to Method 2.

2.4 Validation Cases

This section is devoted for various comparison cases between the developed codes and experiments as well as other benchmark simulations in the literature.

Flat Terrain

Benchmark Case

A commonly used benchmark case is detailed in [66]. Four different profiles are used in that article however, only one selected case with non-constant vertical gradient (linearly increasing speed of sound profile) is shown here. The source is located at 5 m height in the beginning of the domain and the receiver is at 1 m height along the propagation path. Fig. 2.3 shows a comparison between the benchmark case and GFPE and WAPE codes developed for the thesis. It is observed that, WAPE and benchmark is in good agreement for the whole range, however GFPE has a phase error clearly visible after 3000 m. The input parameters were tried to be tuned however the error did not change. The error is attributed to be an inherent problem for GFPE refraction term which has a remedy in [59]. However, as aforementioned the long range propagation will inevitably be affected by the atmospheric turbulence which in turn causes random phase fluctuations. Thus turbulent simulations over flat terrain were carried out with GFPE as well and the results are more satisfactory (see next section).

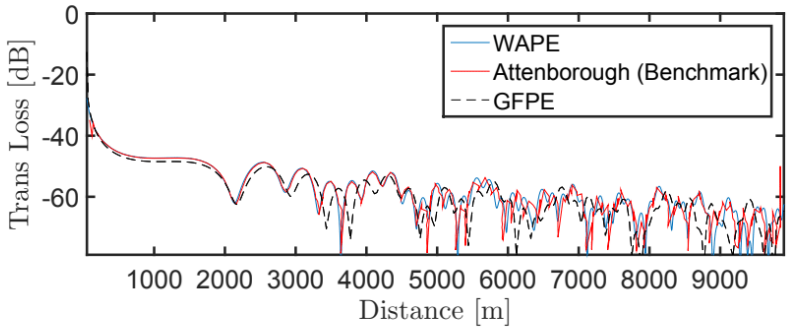

Figure 2.3: Comparison of transmission loss for 10 Hz at 1 m height between the benchmark case number 2 in [66] and the developed codes.

Experiment

First case is the experimental study in the literature [67]. Simulations are carried out for a weak upwards refractive atmosphere;

$$c_{eff} = \begin{cases} c_0 - 0.5\, ln(z/d) & z \geq z_0 \\ c_0 - 0.5\, ln(z_0/d) & z < z_0 \end{cases} \tag{2.14}$$

where z_0=0.01 m and d=0.0006. The source is located at 3.7 m height and 424 Hz is simulated. The turbulence is synthetically generated using the method explained in [53]. Von Karman spectral density function is used with the parameters: normalized structure functions for temperature and wind speed $C_T^2/T_0^2 = 6\times10^{-7}m^{-2/3}$, $C_v^2/c_0^2 = 3.5\times10^{-6}m^{-2/3}$, $K_0 = 1$, number of modes $N = 200$.

Fig. 2.4 shows the results for a receiver height of 1.5 m with increasing number of realizations. It is observed that the simulation without turbulence severely underestimate the experiments. The results including turbulence converge after 50 realizations. Only the GFPE results are shown in the plot, however similar results are obtained with WAPE.

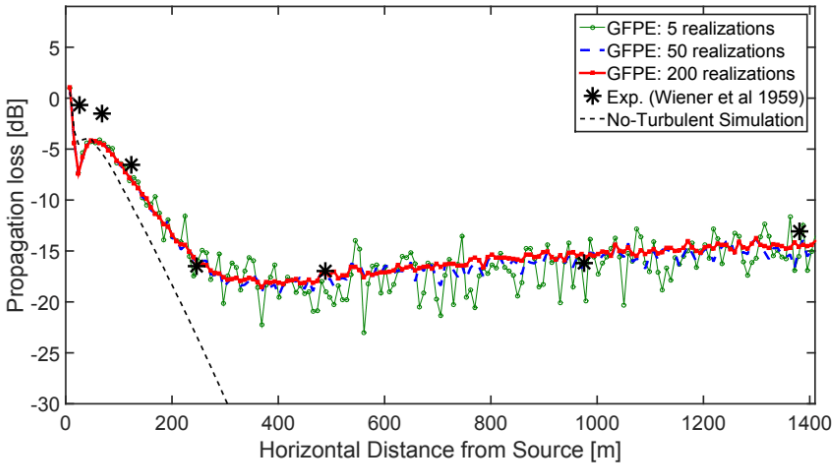

Figure 2.4: Experimental comparison (f=424 Hz) over flat terrain for weak upwards refraction case in [67].

The second comparison study with experiments was carried out using the data obtained in [17]. The experiments were carried out with an elevated speaker over flat terrain. The transmission losses for two source heights (30 m and 50 m) and

two receiver heights (2 m and 5 m) were investigated for downwind propagation. For each case 50 WAPE realizations were carried out using the synthetically generated turbulence explained in [53]. The von Karman spectral density function was used with the parameters: $C_T^2/T_0^2 = 6 \times 10^{-7} m^{-2/3}$, $C_v^2/c_0^2 = 2 \times 10^{-6} m^{-2/3}$, $K_0 = 0.06$, number of modes $N = 200$. Subsequently, the average frequency-dependent SPL is compared with experiments. Figures 2.5 and 2.6 show the comparison. It was observed that computations with hard ground impedance match the experiments much better than grass covered land computations. Hence, they are presented here. The agreement is satisfactory for most of the cases. The near and far field predictions match well for a 30 m source height, while the far field predictions are relatively better for the 50 m source height. The PE method has been validated with other experiments in the literature, on the other hand it is important to note that the inputs to the PE method such as atmospheric and ground conditions may significantly vary the results.

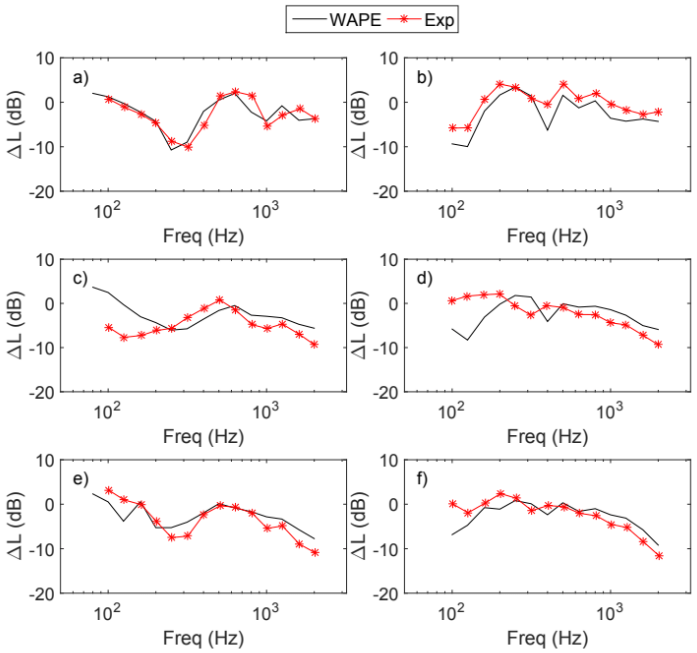

Figure 2.5: Flat terrain experimental comparison source height 30 m. From top to bottom a) 500 m b) 1000 m and c) 1500 m distance from source. From left to right receiver height 2 m and 5 m.

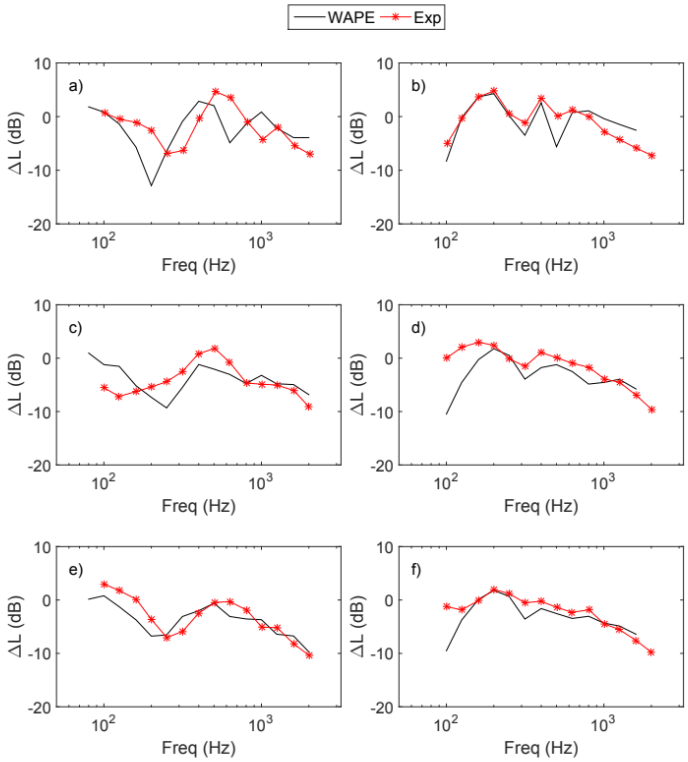

Figure 2.6: Flat terrain experimental comparison source height 50 m. From top to bottom a) 500 m b) 1000 m and c) 1500 m distance from source. From left to right receiver height 2 m and 5 m.

Complex Terrain

Over complex terrain there are not that many field experiments were found in the literature. Additionally, simulation accuracy of the flow field that is affected by the topography arises as another problem for such comparison cases. Here the comparative studies were restricted with other codes using two different cases in the literature.

Gaussian Hill

First the propagation over two dimensional Gaussian hill is evaluated. The comparison is carried out using the developed codes GTPE and GFrPE with the ones found in literature [53]. While GTPE results are identical with the literature GFrPE results slightly deviate at the top of the hill. This is mostly due to the domain decomposition accuracy. As explained in the previous section the results are prone to change depending on the domain decomposition parameters. However, overall agreement is satisfactory for both codes.

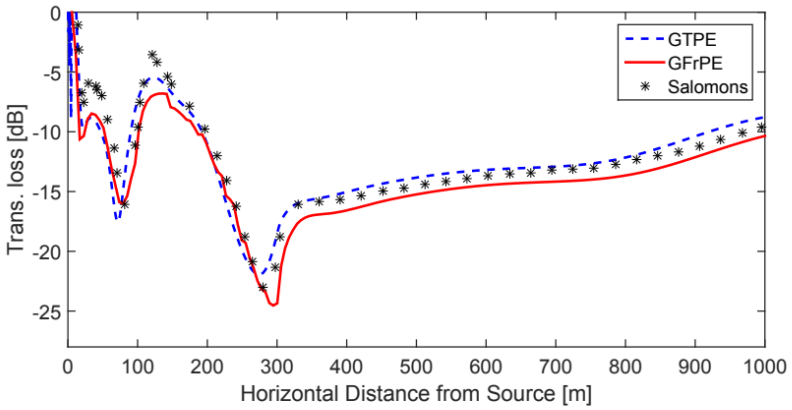

Figure 2.7: Transmission loss for receiver at 2 m height over a Gaussian hill.

Undulating Terrain

Another comparison case is the undulating terrain shown in Fig. 2.8. The details are given in [68] and the simulation results obtained from different models as well as the terrain distribution are downloadable in [69]. A constant and linearly increasing speed of sound profile is used for the two comparison cases. Single impedance representative for grassland is used for the whole domain and the source height is 10 m. Fig. 2.8 shows the propagation loss for a ground level receiver for constant speed profile and a good agreement is observed for the developed codes (GFrPE, GTPE) and the others. Fig. 2.8 shows the same terrain for linearly increasing speed of sound profile which causes downward refraction and more interference with the reflected waves. GTPE and the other methods are in good agreement. However GFrPE seems to have deeper dips and multiple reflections towards the end of the domain. This was further investigated to tune the parameters such as the domain

decomposition and interpolation in between segments, however the results were very prone to change depending on the parameters. Therefore it was concluded not to use GFrPE for a generalized noise mapping situations where the domain between turbines and receivers have to be arbitrarily decomposed.

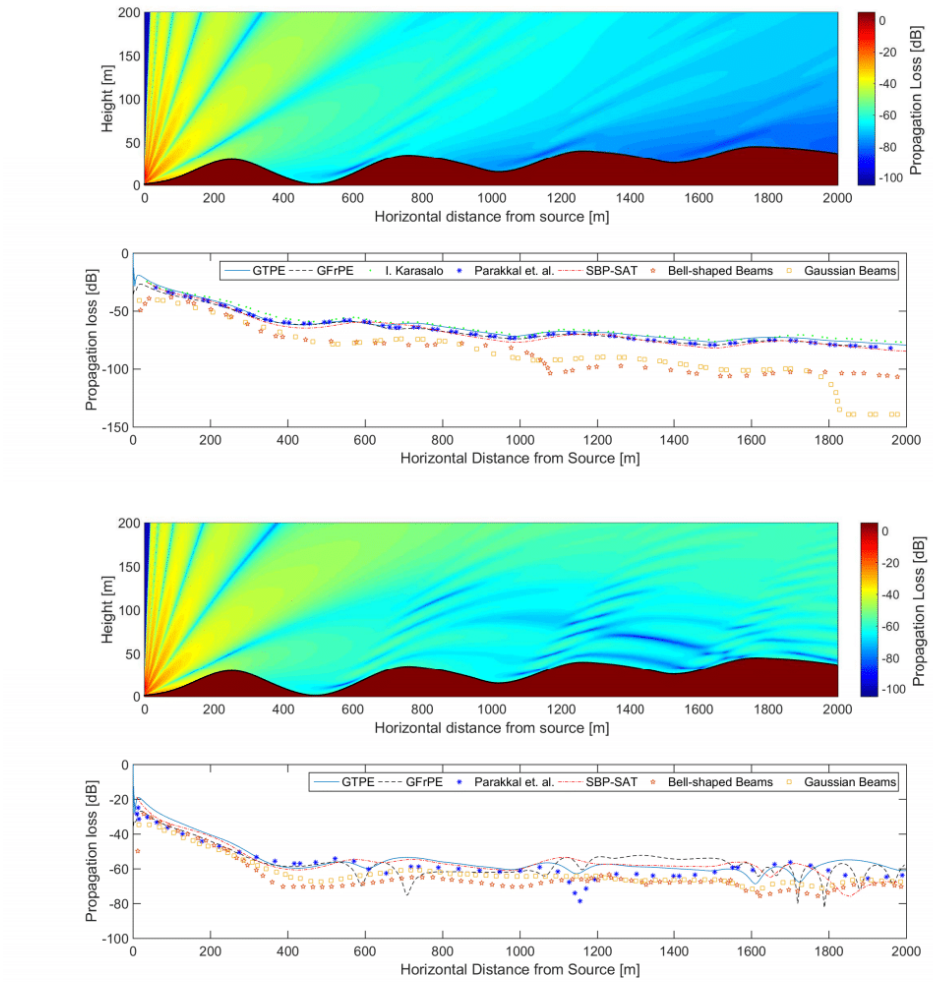

Figure 2.8: Contour plots of the propagation loss and the distributions at 1 m above ground obtained from various numerical techniques in [68] and the codes developed in the thesis. The top two subplots show constant speed of sound results. The bottom two subplots show linearly increasing speed of sound results.

Chapter 3

Sound Propagation & Wind Turbine Wake

3.1 Chapter Overview

Wind turbine wakes have attracted increasing interest as we move towards more clustered wind farms. The main focus of the research has been on the two effects of the wake, namely the reduced power production and increased fatigue of the downstream turbines. In addition to these two phenomena the wake influences also the sound propagation. The turbine induced wind speed deficit causes sound waves to go through local upwind and downwind refracting regions. The corresponding publication in this chapter (Sec. 3.2) addresses this issue using the parabolic equation method and various flow inputs.

The outcome of the paper shows a non-negligible effect of wind turbine wakes on the sound waves emitted from both steady and moving point sources. The wake deficit redistributes the acoustic energy and results in a severe downwards refracting region at the far field (corresponds to the region where the wake breaks down). The incoming turbulence intensity is the main parameter that determines the wake evolution, and thus the SPL amplification/attenuation regions. The largest difference obtained from the unsteady simulations with and without wakes is observed for the laminar inflow case (7 dB). This value decreases with increasing turbulence but, the SPL amplification regions become wider. For the 10 % incoming turbulence intensity, the differential SPL values reach 5 dB and the region width extends from 600 m to 2000 m.

3.2 Publication

Applied Acoustics 122 (2017) 51–61

Contents lists available at ScienceDirect

Applied Acoustics

journal homepage: www.elsevier.com/locate/apacoust

Effects of wind turbine wake on atmospheric sound propagation

Emre Barlas *, Wei Jun Zhu, Wen Zhong Shen, Mark Kelly, Søren Juhl Andersen

Department of Wind Energy, Technical University of Denmark, 2800 Kongens Lyngby, Denmark

ARTICLE INFO

Article history:
Received 23 February 2016
Received in revised form 11 February 2017
Accepted 19 February 2017

Keywords:
Atmospheric acoustics
Vector parabolic equation
Wind turbine sound
Wind turbine wake

ABSTRACT

In this paper, we investigate the sound propagation from a wind turbine considering the effects of wake-induced velocity deficit and turbulence. In order to address this issue, an advanced approach was developed in which both scalar and vector parabolic equations in two dimensions are solved. Flow field input was obtained using the actuator line (AL) technique with Large Eddy Simulation (LES) to model the wind turbine and its wake and from an analytical wake model. The effect of incoming wind speed and atmospheric stability was investigated with the analytical wake input using a single point source. Unsteady acoustic simulations were carried out with the AL/LES input for three cases with different incoming turbulence intensity, and a moving source approach to mimic the rotating turbine blades. The results show a non-negligible effect of the wake on far-field noise prediction. Particularly under stable atmospheric conditions, SPL amplification reaches up to 7.5 dB at the wake centre. Furthermore, it was observed that when the turbulence intensity level of the incoming flow is higher, the SPL difference between the moving and the steady source is lower.

1. Introduction

Noise is one of the main obstacles achieving a broader public acceptance of wind energy. In order to reduce the transmission cost, wind farms are often placed close to populated areas. This demands accurate noise prediction tools and noise reduction techniques which are difficult tasks due to the complexity of wind turbine noise generation and propagation mechanisms. Turbines emit time dependent sound that varies with the incoming flow (i.e. wind speed and turbulence levels), and the turbine design and operation conditions (i.e. rotational speed and rotor design). Moreover, downwind propagation of the emitted sound is influenced by the turbine induced velocity deficit and turbulence. This issue is addressed by Heimann et al. [9] with a ray-based sound particle method where the flow field input is obtained either from full scale experiments or meteorological micro scale models. The study considers a single night case with a temperature inversion and a low-level jet whose wind speed maximum is below the rotor plane crest. Depending on the meteorological model used for the flow field input method the results show variations (overall sound pressure levels are either higher or lower than the case without the wake deficit) in the near field (up to 700 m). The far field noise (700–1000 m) is found to be consistently higher for all simulations when the wake is taken into account. Lee et al. [11] uses parabolic equation method for the acoustic simulations and a Reynolds Averaged Navier Stokes based solver for the flow field input. Different to Heimann et al. [9] the simulations were carried out for four incoming flow wind shear values and the computational domain extends up to 3000 m in the streamwise direction. The results show considerable variations depending on the incoming wind profile. They found that for a small wind shear case, the wake flow tends to increase the far-field noise levels while the opposite is observed for much higher wind shear values.

The present work employs an approach by coupling the high resolution Actuator Line (AL)/Large Eddy Simulation (LES) solutions with the Parabolic Equation (PE) method in order to investigate the unsteady downwind sound propagation in the wake of a wind turbine. Using the time dependent flow input, frequency dependent acoustic simulations are carried out successively. Three different incoming turbulence intensity cases are simulated with AL/LES, each yielding a different velocity distribution thus changing the refraction patterns of sound waves. Additionally the superposition of various incoming wind profiles with analytical wake models is also used for flow field input. Thereby, comparative studies are carried out to assess the need for unsteady turbulent flow input. Another comparison is carried out with two types of source modelling. The conventional approach is to represent the wind turbine with a single point source located at hub height. In this study an unsteady approach was used to mimic the rotation of the wind turbine blades. Thereby, the amplitude modulation due to blade passage is captured. The main objectives of the study are grasping

* Corresponding author.
E-mail address: ebarlas@dtu.dk (E. Barlas).

http://dx.doi.org/10.1016/j.apacoust.2017.02.010
0003-682X/

a better understanding of the relationship between wake dynamics and far field noise levels as well as assessing the influence of turbulent flow input and source modelling for wind turbine sound propagation.

The structure of the paper is as following; first the computational models used in this study are described for both acoustic and flow simulations, respectively. Then the results are discussed in four different subsections. First part is the validation and grid independence study for the PE method. In the second part single PE simulations are carried out with the flow input obtained from the analytical wake model superposed with various wind profiles. This part is called the steady case. The third part uses the flow input obtained from LES and referred to as the unsteady case. The fourth part deals with comparison of the aforementioned two methods and finally a discussion and a conclusion sections are included.

2. Computational models

2.1. Models for sound propagation

Wind turbines significantly modify the flow behind them, hence a sound propagation method that can handle the range dependent flow field (varying along the propagation path) is required. On the other hand, distances on the order of 2–3 km restricts the usage of computationally demanding time domain methods. Therefore, a two-dimensional Parabolic Equation (PE) method was chosen as a compromise between accuracy and computational resources.

Following the notation in Blanc-Benon et al. [5] the PE method can be divided into two groups, namely scalar and vector. The former is the conventional approach where the moving atmosphere is replaced by a hypothetical motionless medium with the effective sound speed $c_{eff} = c + v_x$, where v_x is the wind velocity component along the direction of propagation between source and receiver. In the latter approach, the vector properties of the velocity field are maintained. Thus the equation contains new terms. The scalar PE method is expected to perform well when the source and receiver are close to the ground, as the sound propagation direction is nearly horizontal and the scattering angle (angle between the sound wave and the wave scattered by turbulence) do not exceed a certain limit. For both cases the derivation can be carried out starting from the equation for the sound field P' in inhomogeneous moving medium Ostashev et al. [15] (here given with uniform density assumption);

$$\left[\nabla^2 + k^2(1+\epsilon) - \frac{2i}{\omega}\frac{\partial v_i}{\partial x_j}\frac{\partial^2}{\partial x_i \partial x_j} + \frac{2ik}{c_0}\mathbf{v}\cdot\nabla\right]P'(r) = 0 \qquad (1)$$

where $k = \omega/c_0$ (ω is the radian frequency of the sound, c_0 is the reference speed of sound), $P'(r)$ is the monochromatic sound field, $\epsilon = (c_0/c)^2 - 1$. Note that, Eq. (1) reduces to a classical Helmholtz equation if $\mathbf{v} = 0$; $[\nabla^2 + k^2(1+\epsilon)]P'(r) = 0$. Further mathematical manipulation in order to reduce these equations to a one way parabolic equation is carried out in Ostashev et al. [15]. If the derivation starts from Eq. (1) and maintains the terms with wind velocity then it reduces to Turbulent-Wind Wide Angle Parabolic Equation (TW-WAPE) and it is also referred to as the vector PE. If further manipulation is carried out by setting all velocities to zero, then it reduces to Wide Angle Parabolic Equation (WAPE) and it is referred to as the scalar PE. In this study both scalar and vector PE methods are used. The aim is to test and present the limitations of WAPE in comparison to TW-WAPE for an elevated source such as wind turbine, with range dependent velocity profiles. For both methods a semi-implicit marching scheme is used, with central differences in the vertical direction (z) and the Crank-Nicolson method in the horizontal direction (x). These two PE methods yield either tri-diagonal (WAPE) or penta-diagonal matrices (TW-WAPE) to be solved at each space step. The spatial resolution for both directions is set to one-eighth of the wavelength ($\Delta x = \Delta z = \lambda/8$); where λ is the wavelength of the solving frequency. Only flat terrain is considered and the ground impedance was characterized using the Delany-Bazley model Delany and Bazley [8]. An effective flow resistivity value of 200 kPa s/m^2 was chosen, as this is a typical value for grassland where onshore turbines are commonly located.

The PE methods require a starter function which essentially represents the sound source. In this study the starter function derived in West et al. [20] is used. One approach to mimic the dynamics of the wind turbine sound is treating the wind turbine to be composed of lumped sources located near the tips, i.e., at 85% of the blade span. This approach is a result of the source location studies carried out by Oerlemans et al. [14] which states that the sound is produced in the outer part of the blades. Considering a wind turbine rotating in and out of 2D PE plane, three separate simulations are carried out for each atmospheric condition. For each simulation the single point source is located either at top tip height (114 m) or hub height (80 m) or bottom tip height (46 m). This set of simulations is referred to as the steady case. The unsteady case employs a moving source approach. The main difference between steady and unsteady cases is that the flow field input for each PE simulation is updated every 0.11 s for the unsteady case and at each time step a point source is translated either up or down taking the turbine rotational speed, the diameter and the hub height into account (see Section 2.2.2). Since the focus of this study is the flow field effects on propagation, the source power levels are kept constant for all simulations.

2.2. Models for the flow field input

The PE methods described in the preceding section need flow field input, either as scalar or vector. These profiles were obtained with two different methods that are elaborated in the following subsections.

2.2.1. Case with analytical wake method

In the steady case the streamwise velocity profile is obtained using the analytical wake model proposed by Bastankhah and Porte-Agel [4]. The model uses the mass and momentum conservation by neglecting the viscous and pressure terms and then applies it on the control volume around the turbine. Subsequently, a Gaussian profile in vertical is proposed for the velocity deficit in the wake and an expression for the normalized wind speed deficit is given. The required inputs to the model are hub height (z_h), turbine diameter (D) and thrust coefficient (C_t) which are selected to be z_h = 80 m, D = 80 m and C_t = 0.8. Additionally, a tunable parameter (k^*) for the wake growth rate is necessary. This parameter is adjusted with respect to atmospheric stability via an LES study by Abkar and Porte-Agel [2] as reference.

The ambient mean flow and temperature profiles are obtained using the Monin-Obukhov similarity theory (MOST) for three different stability conditions. The expressions used for the profiles in this study can be found in Salomons [16]. The relevant parameters are given in Table 1, with the inverse Obukhov length (L_{MO}^{-1})[1] and all simulations are carried out with a aerodynamic roughness length z_0 = 0.1 m.

The flow fields obtained via superposing the wake deficits and the upstream wind profiles under three different atmospheric stability conditions are depicted in Fig. 1. Note that, for the case with

[1] In contrast to L_{MO}, its inverse L_{MO}^{-1} is amenable to statistical characterization Kelly and Gryning [10].

Table 1
Surface-layer parameters used in the wind profile, for atmospheric stability classes considered here.

ABL classes	L_{MO}^{-1} [m]	u_* [m/s]	$\theta*$ [K]
Stable (SBL)	0.067	0.31	0.016
Neutral (NBL)	0	0.4	0
Convective (CBL)	−0.067	0.46	−0.044

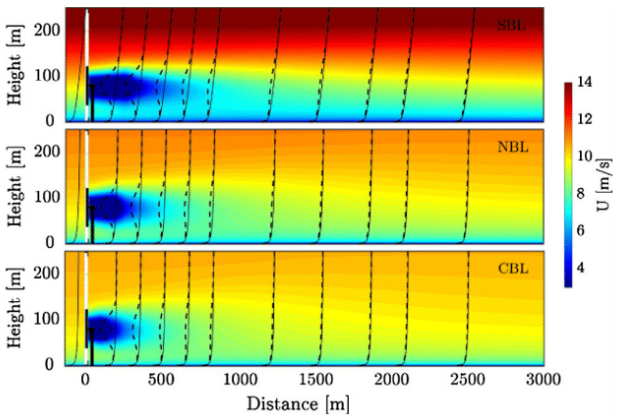

Fig. 1. Contours of streamwise velocity in the middle vertical plane for different stability conditions. The flow fields are obtained from the analytical model in Bastankhah and Porte-Agel [4]. Top: Stable conditions $k^* = 0.02$ Middle: Neutral conditions $k^* = 0.03$ Bottom: Unstable conditions $k^* = 0.04$. Other relevant parameters are given in the text. Solid Line: Incoming wind profile. Dashed Line: Wake deficit wind profile.

the analytical wake input only streamwise velocity is used while the vertical velocity is set to zero for the vector PE method. Two things are worthwhile to point out regarding these flow fields: (1) increased stability yields a longer wake; (2) incoming wind profiles are different. In Section 3.2.2 these effects on refraction will be discussed in detail.

2.2.2. Case with large eddy simulation

Flow fields are obtained from high resolution LES data for the unsteady case. The simulations are performed using the 3D flow solver EllipSys3D, which was developed as a collaboration between Technical University of Denmark [13] and Risø National Laboratory [19]. EllipSys3D solves the discretised incompressible Navier-Stokes equations in general curvilinear coordinates using a block structured finite volume approach in primitive variables. The influence of the wind turbine is simulated using the Actuator Line technique (for further details see Sørensen and Shen [18]), which imposes body forces along the rotating lines. The body forces are calculated through a full aero-elastic coupling with Flex5, which computes the aerodynamic loads, see Øye [22] for details on Flex5 and Sørensen et al. [17] for details on the coupling. The fully coupled simulations also includes a controller, which means the turbine behaves as a real turbine and adjusts according to the incoming turbulent flow field. The modelled turbine is an upscaled version of the NM80 turbine based on the original NM80 (see Aagaard Madsen et al. [1]) and the turbine is proprietary to Vestas Wind Systems A/S. The blade radius is $R = 40$ m and rated power is 2.75 MW at rated wind speed of 14 m/s. The computational domain used for this study is [40 D × 10 D × 10 D] in the streamwise, vertical and lateral directions, respectively (D represents the turbine diameter, 80 m) and the turbine is located 400 m from the inlet. The spatial resolution is 2.5 m in all directions and the computations were carried out for approximately 90 min of real time. The velocity perturbations upstream of the turbine are

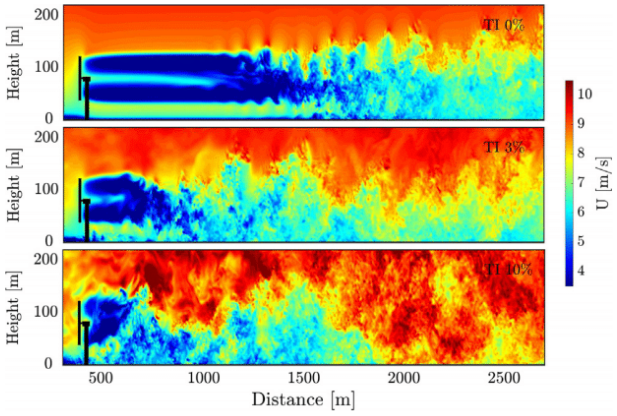

Fig. 2. Contours of instantaneous streamwise velocity (u) in the middle vertical plane for different incoming turbulence intensity $\left(\frac{u'}{U}\right)$. The flow fields are obtained from LES-AL technique. From top to bottom: TI = 0%, TI = 3%, TI = 10%.

obtained from a pre-generated turbulent wind field (see Mann [12]). The magnitude of the fluctuations were scaled in order to mimic three different incoming turbulence intensity (0%, 3%, 10%). Out of 90 min long flow simulations, two independent 10 min long data are used for each turbulence intensity case to feed into the acoustic simulations. Both vertical and streamwise velocity components are extracted at 10 Hz and subsequently fed into the acoustic simulations. Instantaneous snapshots of the flow fields are depicted in Fig. 2. It can be seen that the turbine wake becomes less stable and persistent when incoming turbulence intensity increases as the inflow turbulence assists in breaking down the wake [17]. This will influence the sound propagation as will be shown later.

3. Results

All simulations are carried out for 1/3-octave band with lower, centre and upper limit frequencies up to 630 Hz and summed logarithmically;

$$L_{p(sum)} = 10log_{10}\left(\sum_{i=1}^{N} 10^{Lp(f_i)/10}\right) \quad (2)$$

where N is the number of frequencies used and $L_p(f_i)$ is the sound pressure level defined as;

$$L_p(f_i) = L_{W-A}(f_i) - 10log_{10}4\pi R^2 - \alpha R + \Delta L \quad (3)$$

where the A-weighted source power level for a wind turbine (L_{W-A}) is obtained from the semi empirical source model Zhu et al. [23], the second term on the right hand side stands for geometrical spreading, the third term represents the atmospheric absorption where the absorption coefficient is calculated according to ISO 9613-1 for air at 20 °C with 80% relative humidity. The last term is the relative sound pressure level $\Delta L = 20log_{10}(|P'|/|P_f|)$ that represents the deviation from the free field of a source due to ground effect, atmospheric refraction, turbulence, etc.

3.1. Validation and grid independence study

The output from WAPE and TW-WAPE are compared to the work of Dallois et al. [7]. Fig. 3 shows the result for 680 Hz, where the source is located at 2 m height and a receiver at 10 m height. It is seen that with the implementation used in this paper the phase shifts as well as the dips and peaks of SPL are captured. This validates the implementation of these two methods.

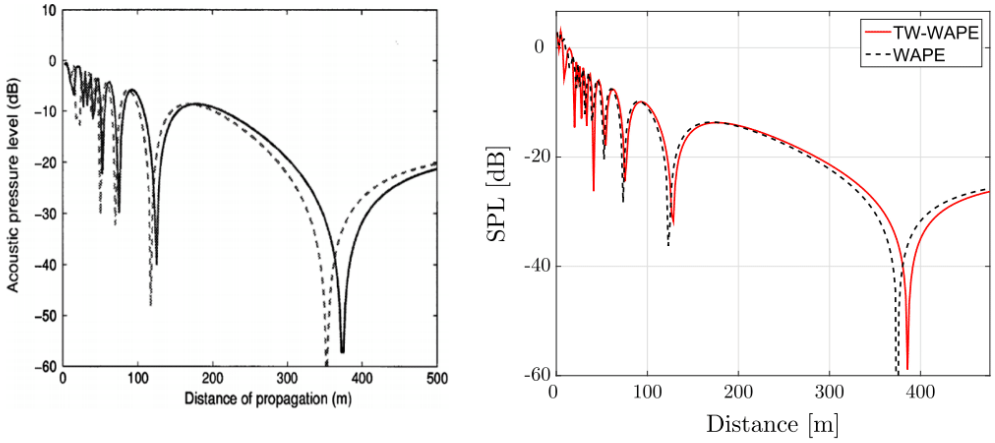

Fig. 3. Validation case. Sound pressure levels for a receiver at 10 m height Left: Taken from Dallois et al. [7] Right: Current work.

Furthermore, an error analysis is carried out in order to test how often the solution matrices should be updated in the space marching scheme for a range dependent flow field. This is done by running one benchmark case with both methods where the update is at each space step, Δx (where $\Delta x = \lambda/8$). Afterwards the error is quantified for cases with space steps of 5, 10, 50 and 100 Δx by subtracting the relative sound pressure levels from the case with Δx. The highest error is detected under stable atmospheric conditions and Fig. 4 shows the evolution with distance for a receiver at 2 m. It is clear that if the step is chosen much larger than the wavelength, i.e. 50 or 100 Δx, the committed error is considerably high for TW-WAPE. A similar trend is observed for WAPE, however the error margin is much smaller. For both methods the error is less than 0.5 dB if the simulations with 5 Δx is used. Thus from this point on the update step is set to 5 Δx.

3.2. Steady case with analytical wake model

3.2.1. Effect of wake under neutral stability conditions

The next step is to assess the difference between range dependent and independent profiles on sound propagation (also denoted with and without wake, respectively).

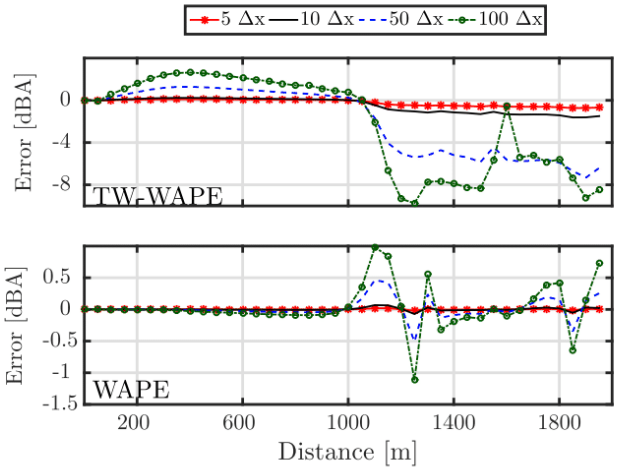

Fig. 4. Sound pressure levels for a receiver at 2 m height under stable atmospheric conditions. The error is quantified by subtracting results from the benchmark case which is the case where the flow field update is at each space step Top: TW-WAPE Bottom: WAPE.

First, the case with source height at 80 m (hub height) is studied and an interesting refraction phenomenon is captured. Fig. 5 helps to give a visual understanding of this phenomenon. Considerably higher sound pressure levels are observed after certain distance from the source. This was also reported in Heimann et al. [9] and Lee et al. [11]. The wake deficit and its downstream evolution are the key parameters which cause different refraction patterns of sound waves. Subsequently *downwards bursting zones* are generated (similar to ducting of sound waves near the ground observed in e.g. Wil-son et al. [21]). These are the regions with high sound pressure level due to turbine induced velocity gradients. Note that in the wake, the mean wind speed vertical gradient ($\partial U/\partial z$) at the

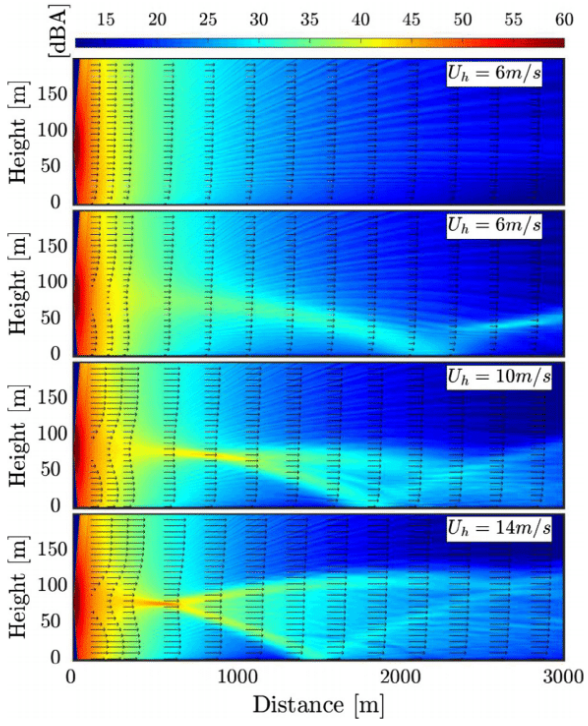

Fig. 5. Contours of sound pressure levels calculated with TW-WAPE under neutral atmospheric stability conditions for various incoming hub height wind speeds. The velocity vectors are embedded in the figure. From top to bottom: Case without wake $U_h = 6$ m/s, case with wake $U_h = 6$ m/s, case with wake $U_h = 10$ m/s and case with wake $U_h = 14$ m/s.

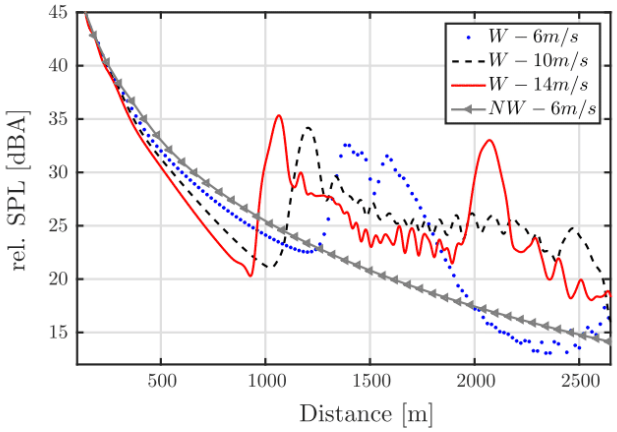

Fig. 6. Sound pressure levels for a receiver at 2 m height, neutral boundary layer case at various incoming hub height wind speeds. Case with wake (W) and case without wake (NW).

top tip height is significantly greater than at the bottom tip, thus creating a more severe downward refraction than the upward refraction. Moreover, increased incoming hub height wind speed (U_h) also yields stronger gradients. Thus the regions with higher sound pressure levels are widened. Two distinctly separated peak regions are detected for the case $U_h = 14$ m/s. The first peak is caused by initial downward refraction. The second peak is due to firstly upward and afterwards downward refracted sound waves.

Overall, the SPL differences due to the wake can reach up to 12 dB at certain ranges for a receiver at 2 m height as shown in Fig. 6. Note that the simulations with range independent profiles (without wake) yield higher sound pressure levels for the ranges before the bursting zones, namely before 1 km. Even though, only one case without wake is shown ($U_h = 6$ m/s) in this figure, this observation is valid for higher incoming wind speeds. The reason for this is that before the wake breakdown the acoustic waves are retained within the wake deficit region thus they do not reach to the ground. This results in attenuation of SPL in the near field (less than 1000 m). The refraction patterns vary depending on the source height. This is studied in Section 3.2.3.

3.2.2. Effect of atmospheric stability conditions

The incoming flow as well as the wake evolution is different for various atmospheric stability conditions. Wake recovery takes places differently due to varying mixing characteristics. For sound propagation this means that the refraction regions will vary with respect to the wake field. In Fig. 7 the effect of this is depicted with contour plots of SPL under three different stability classes. The comparison is carried out for the same incoming hub height velocity, $U_h = 12$ m/s. The results show that under stable conditions the persistence of the turbine induced velocity gradient in the wake yields a more continuous downwards refraction. Thus the region with increased sound pressure levels is widened and the start of it reaches down to a range of 1000 m. This is also important because under stable conditions the shear of the velocity profile is higher which means that the wind speed at the ground level is considerably lower than the hub height wind speed. Therefore, the background noise at the ground level is lower which causes wind turbine sound to be more noticeable.

Fig. 8 compares the cases with and without wake as well as TW-WAPE and WAPE outputs for a receiver at 2 m height. The results clearly indicate that the effect of wake, especially under stable atmospheric conditions is considerable. The difference in SPL reaches up to 10 dB for the first peak while the same value is

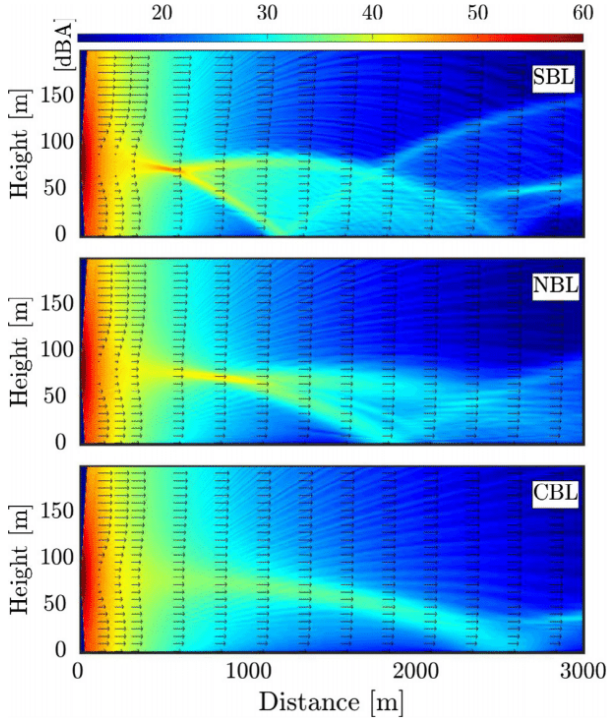

Fig. 7. Contours of sound pressure levels calculated with TW-WAPE under various atmospheric stability conditions for $U_h = 12$ m/s. From top to bottom: Stable, Neutral, Convective boundary layer.

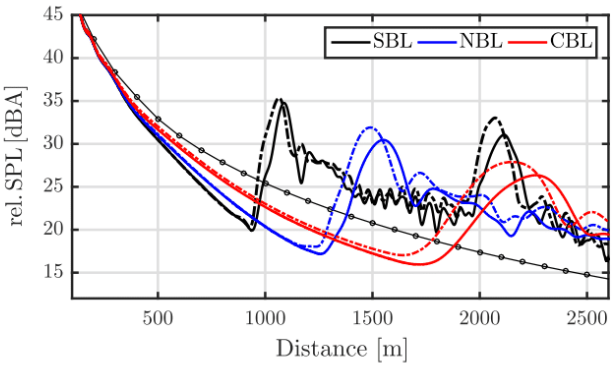

Fig. 8. Sound pressure levels for a receiver at 2 m for $U_h = 12$ m/s. Colors represent different atmospheric stability classes. Full Line: TW-WAPE with wake. Dashed Line: WAPE with wake. Line with Markers: TW-WAPE without wake.

almost 15 dB for the second peak under stable atmospheric condition. Another important observation is the phase difference between WAPE and TW-WAPE. As was pointed out in Blanc-Benon et al. [5] this cumulative phase error is introduced due to the limitation of effective speed of sound approach that is inherent to WAPE. The equations derived for TW-WAPE take into account vertical and horizontal velocity components separately and speed of sound is only function of temperature. This is not the case for WAPE (scalar PE - the effective speed of sound approach). Wind speed is simply projected and added directly to the speed of sound at each space marching step. With this approach, for example a downwards refracted wave would be accelerated towards downwards. But in reality the vertical and horizontal velocity components are affecting the sound wave refraction differently than just adding it to the speed of sound. This causes a phase error that

increases with distance as well as with wind speed. Here the results are not presented as a function of frequency however it was observed that at certain distances from the source the destructive and constructive interference regions change location. This results in more than 20 dB difference between the two methods.

3.2.3. Effect of source height

As mentioned in Section 2.1 the representation of a wind turbine as a single source at hub height may be misleading. Therefore simulations with different source heights are carried out. The results show different trends as a result of refraction pattern variations, see Fig. 9. A common feature of all the simulations with wake is both amplification and attenuation of SPL at various distances. This means that regardless of the source height, wake flow field redistributes the acoustic energy. If the source is located at 114 m, the sound waves refract such that the wake induced SPL amplification is in the near field (300–800 m). On the other hand, if the source is located at 46 m, this amplification is observed in the far field (above 1600 m). This is an interesting outcome because of two reasons; (1) as a result of continuous rotation of turbine blades the SPL increase is observed at different distances. This behaviour may help to understand the annoyance caused by amplitude modulation at the far field. (2) considering that a rotating wind turbine rotor passes through all these positions there is a cumulative effect of all source heights. This yields an overall increased SPL at all distances from the source. It is also important to mention that the study of Heimann et al. [9] concludes that wake flow favours the sound propagation only from the upper sources towards the ground. Considering that this study is limited to 1 km distance this is indeed the case. However when further distances are taken into account the amplification of SPL are more considerable and mostly caused by lower sources. The effect of source location and type will be investigated further in the following section with the unsteady approach.

3.3. Unsteady case

3.3.1. Comparison of WAPE and TW-WAPE

TW-WAPE and WAPE are compared for a five minutes long simulation. Fig. 10 shows both the mean SPL and the associated standard deviation values for a receiver at 2 m height. Unlike the steady flow approach there is no distinguishable phase error, neither with the moving source nor with the steady source. This can be explained via the turbulence effect on propagation. One of the major effects of turbulence on downwind sound propagation is the phase fluctuations of sound waves. This means regardless of the PE method (vector or scalar) each PE run will have a 'random' phase shift. If we consider a single time step (also called a single realization) the discrepancy between the two methods is large,

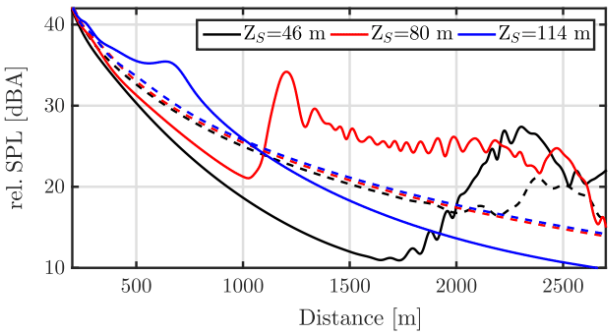

Fig. 9. Sound pressure levels for a receiver at 2 m height for $U_h = 10$ m/s and SBL. Comparison of range dependent (Full lines: with wake – W) and range independent (Dashed lines: without wake - NW) velocity profiles.

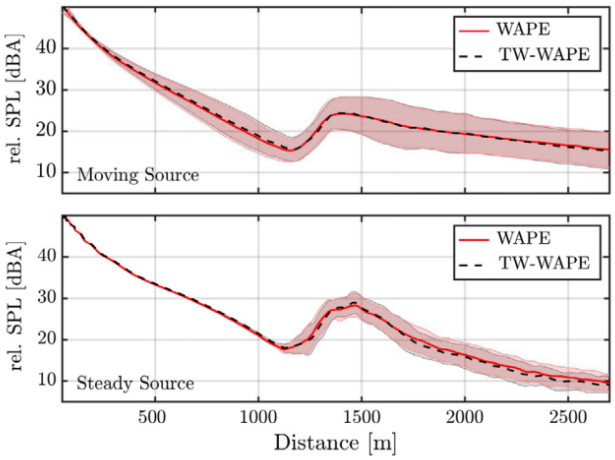

Fig. 10. Sound pressure levels for a receiver at 2 m height obtained with two different PE methods (scalar and vector) for no turbulence incoming flow case.

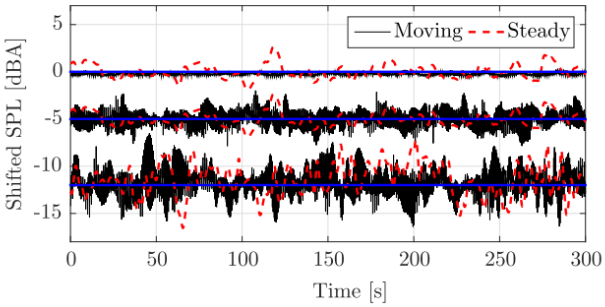

Fig. 11. Difference in SPL ($SPL_{WAPE} - SPL_{TW-WAPE}$) for a receiver at 2 m height and at three different distances. The results are shifted in y axis with the offset that blue lines represent. From top to bottom: at distances of 300 m, 1500 m and 2500 m.

but once it is averaged over many realizations, the obtained results are similar.

Further assessment is carried out with the time signals obtained from both methods. Fig. 11 shows the subtracted SPL for each instant which represents the error ($SPL_{WAPE} - SPL_{TWWAPE}$). As expected, the error is increasing with distance. Around 2500 m and at certain instances the error reaches up to 4 dB.

From these results it is concluded that the mean and standard deviation of sound pressure levels are independent of the method even though instantaneous values vary. Since the parameters of interest are restricted with those two in this study the rest of the simulations are carried out with WAPE.

3.3.2. Effect of wake deficit

In order to solely assess the effect of wake deficit dynamically three sets of simulations are carried out with moving source approach. These set of simulations are distinguished by changing the flow field input;

- LES+PE: Fully unsteady case, where every instant the flow field is updated and the source is translated up or down. This yields a twenty minutes long SPL time signal which is then averaged in time.
- Perturb+PE: Similar to the LES+PE method however, the mean wake deficit is subtracted from the flow field at each instant in time. In other words, turbine induced perturbations are superimposed to the incoming flow.

- Inflow+PE: Single logarithmic wind profile obtained from time averaged LES inflow is used along the whole propagation path (range independent, steady flow) and five PE simulations are carried out with different source heights. This yields a periodic time signal which is then averaged in time.

This comparison is conceptually similar to the steady case studies with and without wake, however for the first two methods (LES+PE and Perturb+PE) both the flow as well as the source is dynamic which is a more realistic modelling for wind turbine noise and the atmosphere. Fig. 12 shows the differential SPL of LES+PE and Perturb+PE for three different incoming turbulence intensity, namely 0%, 3% and 10%. Highest discrepancy is observed for the case with 0% (≈7 dB). The constant wake deficit ducts the acoustic energy and results in a severe downwards refracting region at the far field (corresponds to the region where the wake breaks down see Fig. 2). In addition to the ground level receivers, local upward refraction results in discrepancy for all receiver heights, but the wake induced SPL amplification mostly decreases with height. All these effects are visible in a more smeared manner with increasing incoming turbulence. In other words, the start of the downwards bursting zones gets closer to the source but the overall wake induced SPL amplification decreases (≈5 dB). From this study it can be deduced that for even higher turbulence levels wake induced SPL amplification in the far field will be lower. This is also in agreement with the wake physics, since the increased incoming turbulence results in higher mixing and subsequently shorter wake. Another common feature for all cases is that the SPL discrepancy increases with distance for receivers at ground level.

Fig. 13 shows a comparison between LES+PE and Inflow+PE. The sound pressure levels for a receiver at 2 m height illuminates the abrupt downwards bursting zone (SPL amplification) for 0% incoming turbulence intensity case, while these regions are distributed more evenly for the other two cases. It is observed that up to a range of 500 m all lines collapse. This shows that atmospheric refraction effects are only visible after this distance.

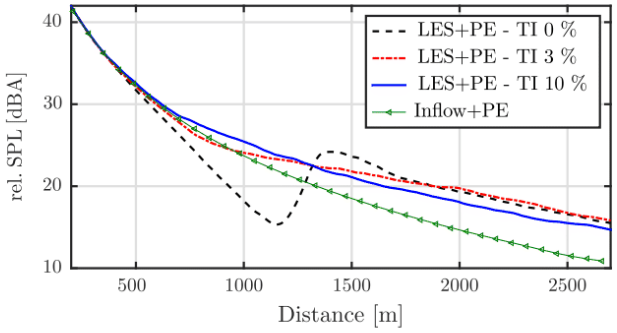

Fig. 13. Sound pressure levels for a receiver at 2 m height, for different incoming turbulence intensity levels.

3.3.3. Effect of source type

Representation of a wind turbine as a single steady point source at hub height is the conventional approach and may be an acceptable assumption for far field noise prediction. However, with the wake induced flow field the modified conditions increase the importance of source modelling type. Here this effect is investigated using moving and steady source approaches (for further explanation see Section 2.1). The comparison is depicted in Fig. 14. Note that, the study in Section 3.2.3 showed that the lower sources contribute to the SPL amplification in the far field while higher sources contribute to the near field SPL amplification. The moving source approach contains all these contributions, therefore general trend is that the SPL amplification is distributed to all distances in the domain and overall levels are mostly higher. From the

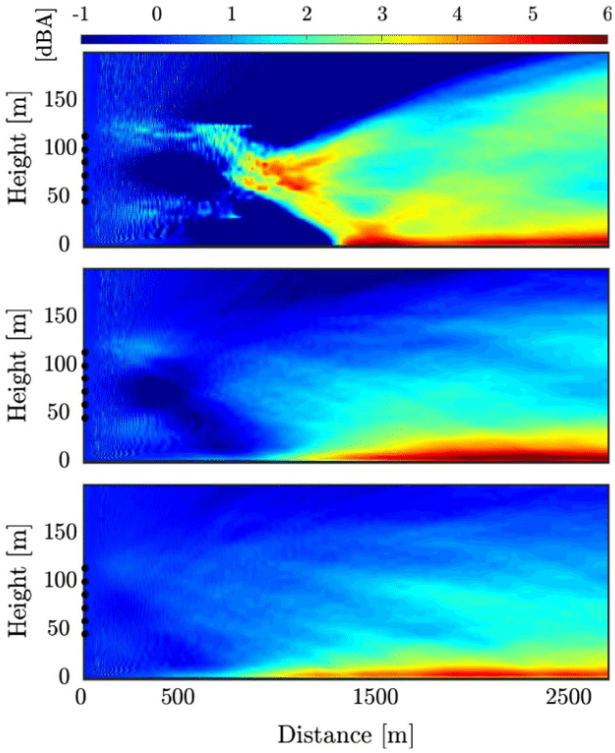

Fig. 12. Contours of differential sound pressure levels ($\Delta_{SPL} = SPL_{LES+PE} - SPL_{Perturb+PE}$) for different incoming turbulence intensity. From top to bottom: T.I. 0%, 3% 10%. Block dots represent the source heights.

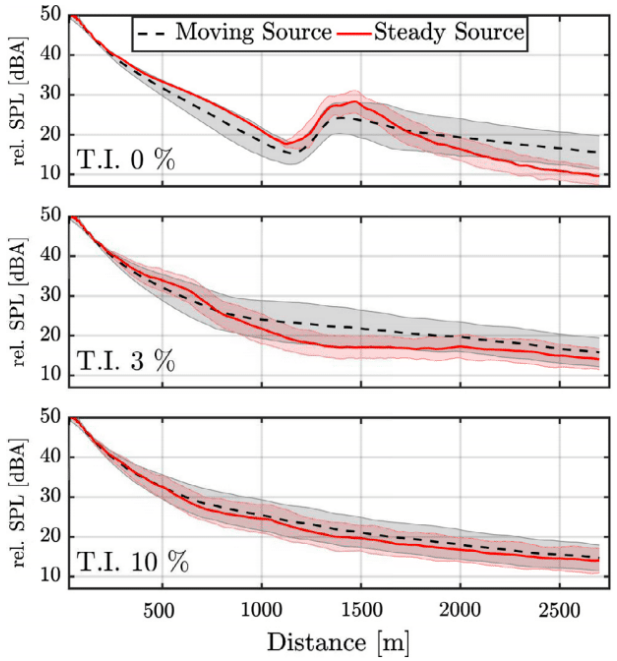

Fig. 14. Sound pressure levels for a receiver at 2 m height, for different incoming turbulence intensity levels and source types. Shaded regions represent the standard deviation.

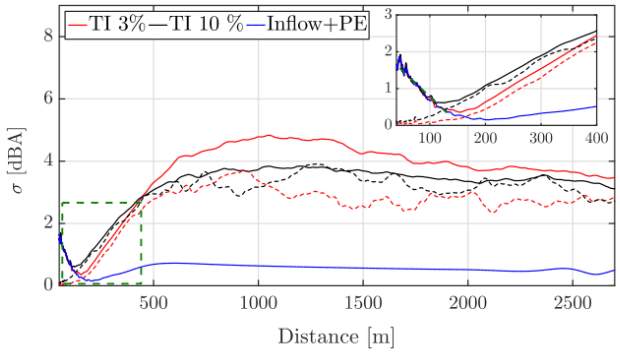

Fig. 15. Standard deviation (σ) of SPL for a receiver at 2 m height under various flow conditions and source modelling techniques. Dashed lines: Steady source. Full lines: Moving source.

two figures (Figs. 13 and 14), it can be concluded that the wake influenced sound pressure levels would be mis-predicted especially in the low turbulence cases if turbine is modelled as a single steady source at hub height.

Furthermore, the comparative study between three incoming turbulence intensity levels shows that the higher the turbulence, the less important the source type is. For example for 10% case the SPL difference between the two source modelling types is negligibly small (≈1 dB), while these values reach up to 5 dB for both cases with 0% and 3%. For the case with 0% incoming turbulence intensity the abrupt increase of SPL due to severe downward refraction is seen with both source types. However, the amplification is lower for moving source at certain distances. These observations are in agreement with the wake physics as well. Higher incoming turbulence results in more mixing and shorter wake. Hence, refraction of sound waves due to wake induced flow field is not so influential. Subsequently the source position or modelling type becomes less important.

The shaded regions in Fig. 14 represent the standard deviation of SPL. For an easier comparison these values are shown in Fig. 15. In the near field a clear effect of source type is seen. For all flow cases with moving source a linear relationship between distance and standard deviation is detected up to a certain point, after which the values for both source types collapse. This distance varies depending on the incoming turbulence intensity. These values are 180 m and 140 m for 3% and 10%, respectively. The higher the turbulence intensity, the earlier the source type loses its effect. Afterwards the fluctuations due to flow dynamics rather than the source become more important.

At the far field (above 700 m) there is almost no difference between two source types for the 10% case. However, there is a certain discrepancy for 3% case which can be explained with the longer wake. Due to more severe and persistent local downwards refracting regions the source location becomes a more important issue for the 3% case. Sound emitted from the lower sources with wake deficit results in higher contribution to downwards bursting zones. And with the movement of the source the receiver at certain distances goes in and out of these increased SPL regions. This shows that the source type is important for large distances under low turbulence intensity.

3.4. Comparison between steady and unsteady case

This part of the paper is devoted to the comparison among different flow field input methods. The simulations are carried out with the moving source approach and three different ways are used to feed the flow to the acoustic simulations;

- LES+PE: Fully unsteady case, where the flow field is updated every instant and the source is translated up and down. This yields a twenty minutes long SPL time signal which is then averaged in time.
- MeanLES+PE: In total only five simulations are carried out for five different source heights along the rotor. The flow field is obtained via time averaging the LES results and remains unchanged for all simulations. This yields a periodic time signal which is then averaged in time.
- Analytical Wake+PE (AW+PE): Similar to the method MeanLES +PE, this time the flow field is obtained from superposition of the inflow wind profile with an analytical wake model where the wake growth parameter (k^*) is tuned with respect to the LES results. This yields a periodic time signal which is then averaged in time.

Fig. 16 shows the comparison of time averaged SPL for all three methods and incoming turbulence intensities. There is a clear discrepancy between AW+PE and the other two methods. The difference decreases with increasing turbulence intensity however it is observed that the AW+PE method underestimates the SPL along the whole propagation path for all cases. For the laminar inflow case (incoming turbulence intensity 0%) SPL amplification around the range of 1250 m is captured to a certain extend. Nevertheless this increase is not as abrupt as in LES+PE or MeanLES+PE. This is because analytical wake model is a far field model. This means the method does not capture the flow characteristics in the near field and the PE method is sensitive to the flow input. In order to overcome this issue a refined wake model that is capable of capturing the near wake flow field more accurately can be used.

Another important observation is that the discrepancy between averaged SPL obtained from LES+PE and MeanLES+PE is not very significant. They both follow a similar trend and the differences in averaged SPL do not exceed 3 dB. This means the wind turbine induced turbulence does not influence the downwind sound propagation much.

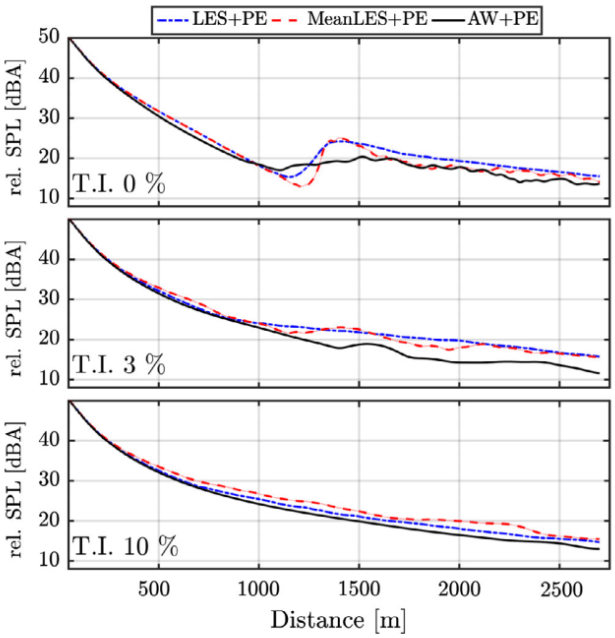

Fig. 16. Sound pressure levels for a receiver at 2 m height for three different incoming turbulence intensity and flow field input methods.

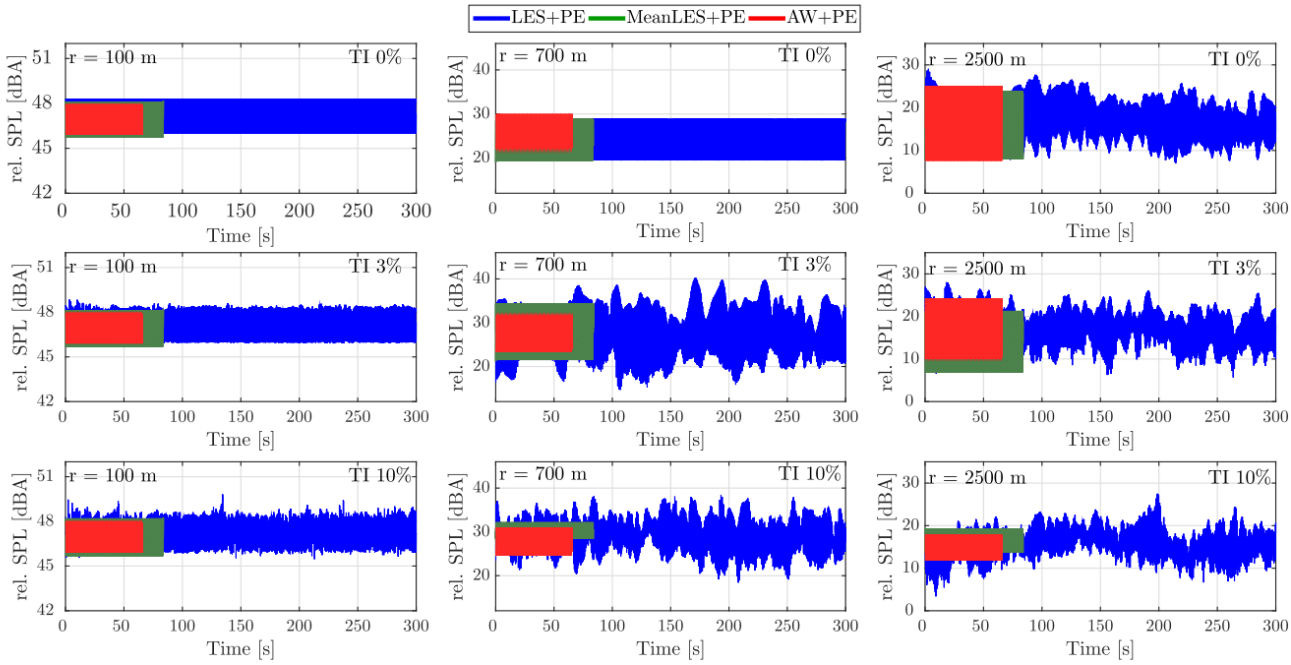

Fig. 17. Time signal of SPL for a receiver at 2 m height and different distances for cases with different incoming turbulence intensities. Three different flow field input methods are used.

Moreover, time signals of sound pressure levels are investigated. Fig. 17 shows the signals for a receiver height of 2 m at three different location, namely 100 m, 700 m and 2500 m also referred to as near field, mid-field and far field in this section. It is observed that in the near field (100 m) for all incoming TI the sound pressure levels are modulated periodically as a result of the moving source. Even though certain peaks are visible for the SPL time signal obtained with LES+PE the peak to trough ratio and the mean SPL values are same for all three methods. This implies that in the near field the source is the dominant parameter, which governs the sound pressure levels rather than the flow input.

In the mid-field (700 m) time signal of all methods collapse again for the laminar inflow case (incoming T.I. 0%). At this distance for this case the wake breakdown has not taken place therefore the moving source is again the only cause for periodic modulation that is observed for all methods. However for the other cases with higher incoming TI (3% and 10%) even though the mean SPL values are very close to each other for all three methods the behaviour of the signals are different. AW+PE and MeanLES+PE shows periodic modulation since there is no changes in the flow. LES+PE has both the modulation due to changing source height as well as the turbulent flow field. This yields higher peak to trough values at various instances in time. For example maximum values reach up to 23 dB for the case with incoming TI 3% while this is maximum 18 dB for the TI 10% case. Note that the standard deviation of LES+PE for 3% case is higher than 10% case. This observation was also underlined in Section 3.3.3 (see Fig. 15). This is because the ducted acoustic energy due to persistent wake is refracted downwards and reaches different distances at each instant in time as the source moves up and down. As a result of this the time signal at a certain receiver point has higher standard deviation.

In the far field (2500 m) time signals of AW+PE and MeanLES+PE still show a periodic modulation. However the peak to trough values decrease with increasing turbulence (i.e. 16 dB, 12 dB and 5 dB for 0%, 3% and 10% respectively). From this observation it can be concluded that if the wake is short enough (e.g. very high turbulence) the fluctuations that are seen in the far field due to the moving source will disappear. The results of LES+PE also supports this argument. They show a similar trend in terms of standard deviation. Remembering again the study in Section 3.3.3 the standard deviation of moving and steady source collapse on the same line at this distance (above 2300 m).

So far the comparison is restricted with the summed SPL values that are calculated using Eq. (2). For further investigation frequency dependent spectra for a receiver height of 2 m are depicted in Fig. 18. From summed and averaged SPL comparison it was clear that the AW+PE performs poorly and the results do not match the other two methods. The comparisons of spectra also shows that AW+PE does not capture the general trend as LES+PE or MeanLES+PE. Higher differences are observed for the frequencies over 300 Hz. The frequency dependent comparisons between LES+PE and MeanLES+PE has interesting output. MeanLES+PE captures the general trend however LES+PE has a more smeared distribution of SPL over the whole propagation path which can be explained by the phase shifts caused by turbulence. This cannot be captured by running only five simulations without changing the flow field.

4. Discussion

From this study it is clear that the acoustic energy is redistributed downwind from wind turbine, due to the wake-induced flow field. The main parameter is the persistence of the wake, particularly in stable atmospheric conditions: there the wake is long, considerably high SPL amplification is observed in the far field. There are certain shortcomings of this study that may prevent generalization to some wake cases. First of all, even though the steady case investigates three different incoming wind profiles, under more extreme conditions (i.e. friction velocity $u_* = 8$ m/s) it is possible that the wake flow may result in SPL attenuation also in far field as it was pointed out in Lee et al. [11]. Nevertheless, the cases considered in this study covers the atmospheric conditions that are commonly encountered and a more detailed study was also carried out by the authors that investigates the effect of shear and turbu-

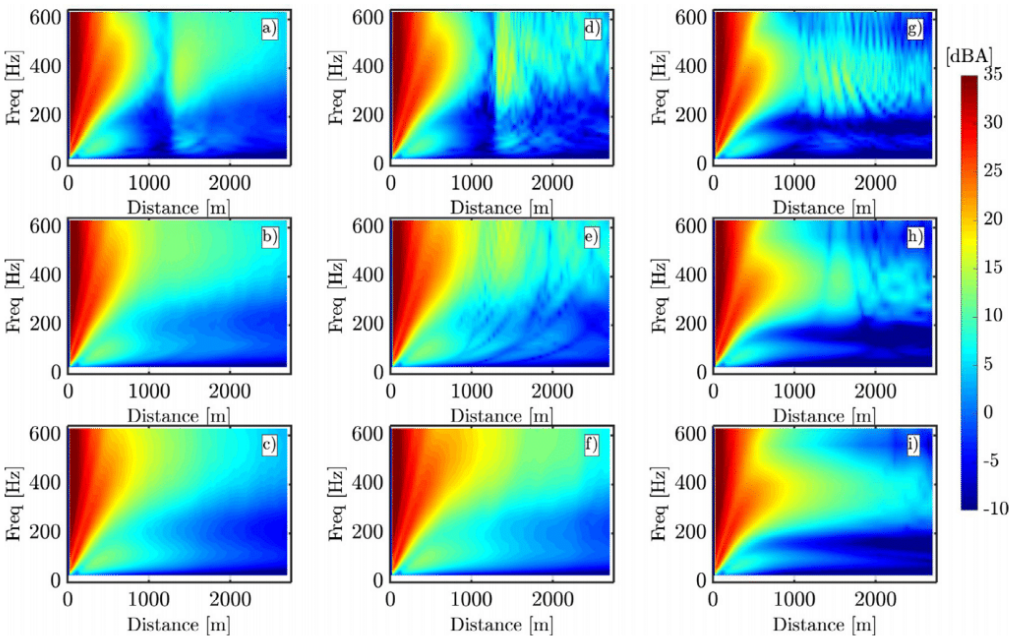

Fig. 18. Frequency dependent (1/3-octave band lower, centre and upper limit) SPL for a receiver at 2 m height for three different incoming turbulence intensity and flow field input methods. (a) LES+PE - TI 0%, (b) LES+PE - TI 3%, (c) LES+PE - TI 10%, (d) MeanLES+PE - TI 0%, (e) MeanLES+PE - TI 3%, (f) MeanLES+PE - TI 10%, (g) AW+PE - TI 0%, (h) AW +PE - TI 3%, (i) AW+PE - TI 10%.

lence on both downwind and upwind propagation from a wind turbine Bar-las et al. [3]. Additionally, it may be argued that the moving source approach is a limitation of the present study. Wind turbine blades rotate in and out of the 2D PE domain instead of only along one axis. However, the further the receiver, the more realistic it becomes to model the rotor as a single source that moves up and down. This is a source modelling technique that captures most of the dynamics, such as amplitude modulation due to blade passage.

The unsteady approach which couples PE with LES for wind turbines is state of the art. However, as comprehensively investigated in Cotté and Blanc-Benon [6], the smallest turbulent scales should be on the order of the acoustic wavelength for accurate modelling of the turbulence effect on scattering. This condition is not met considering the highest frequency resolved using PE is 630 Hz ($\lambda \approx 0.5$ m) and the LES spatial resolution is 2.5 m for all directions. On the other hand the required resolution is computationally so demanding that a fully resolved coupling is not considered in this study. Last, it is important to point out that the current study is limited to flat terrain and homogeneous ground impedance. These are important parameters that cause sound waves to reflect differently. Further investigations should be carried out to see if the dynamic wake effects are larger for sound propagation over complex terrain and inhomogeneous ground impedance.

5. Conclusion

It is known that different atmospheric conditions result in various acoustic refraction patterns. When the source is a wind turbine, the correct representation of the flow and source itself becomes even more important because of the constant variations in the source strength and flow modifications around wind turbines. In this study, both steady and unsteady approaches were employed using a 2D PE method coupled to flow fields generated by an analytical wake model and AL/LES. The main findings are:

- Sound waves go through local upward and downward refracting regions, as a result of wake deficit behind a wind turbine. This means acoustic simulations without the wake cannot properly estimate the far field noise. This is valid for all atmospheric stability conditions, incoming wind speeds and source heights that have been investigated in this study.
- It is observed that during stable atmospheric conditions, which result in long and persistent wakes, far field noise can be severely under-predicted if the correct flow field is not used.
- By comparing two different source modelling techniques (moving and steady) coupled with LES it is concluded that the effect of the moving source in far field (beyond 700 m $\approx$ 9 D) diminishes with increasing incoming turbulence intensity. On the other hand, at the near field the effect of the moving source is always felt. The standard deviation values of SPL with steady and moving source collapse first after 140 m ($\approx$1.8 D) for 10%, while this value is approximately 180 m($\approx$2.3 D) for 3%.
- For a single realization of the 2D PE there is a cumulative phase error caused by intrinsic assumption of effective sound speed approach (scalar PE - WAPE). However, the discrepancy between vector and scalar PE using the time dependent LES results, is negligibly small. This is possibly due to the random phase shifts at each instant in time caused by turbulent flow which diminish the error when averaged in time.
- The mean SPL behind a wind turbine can be predicted with time averaged input (MeanLES+PE) almost as accurately as time dependent input (max. 3 dB). However, the comparison with PE using an analytical wake model did not yield satisfactory results. This is because analytical wake models do not capture the near wake characteristics of the flow. Subsequently the sound waves are not refracted in the same way as LES results.

Acknowledgements

The work has been funded by the GreenTech Wind project, a collaboration of the EuroTech Universities. Furthermore, the proprietary data for Vestas' NM80 turbine has been used.

Appendix A. Supplementary material

Supplementary data associated with this article can be found, in the online version, at http://dx.doi.org/10.1016/j.apacoust.2017.02.010.

References

[1] Aagaard Madsen H, Bak C, Schmidt Paulsen U, Gaunaa M, Fuglsang P, Romblad J, et al. The DAN-AERO MW experiments. Denmark: Forskningscenter Risø. Risø-R. Danmarks Tekniske Universitet, Risø Nationallaboratoriet for Bæredygtig Energi; 2010.

[2] Abkar M, Porte-Agel F. The effect of atmospheric stability on wind-turbine wakes: a large-eddy simulation study. J Phys: Conf Ser 2014;524(1):012138. , <http://stacks.iop.org/1742-6596/524/i=1/a=012138>.

[3] Barlas E, Zhu WJ, Shen WZ, Andersen SJ. Wind turbine noise propagation modeling: an unsteady approach. In: Journal of physics: conference series. The Science of Making Torque from Wind 2016, vol. 753; 2016.

[4] Bastankhah M, Porte-Agel F. A new analytical model for wind-turbine wakes. Renew Energy 2014;70:116–23. , <http://www.sciencedirect.com/science/article/pii/S0960148114000317>.

[5] Blanc-Benon P, Dallois L, Juve D. Long range sound propagation in a turbulent atmosphere within the parabolic approximation. Acta Acust United Acust 2001;87(6):659–69.

[6] Cotté B, Blanc-Benon P. Estimates of the relevant turbulent scales for acoustic propagation in an upward refracting atmosphere. Acta Acust United Acust 2007;93(6):944–58.

[7] Dallois L, Blanc-Benon P, Juve D. A wide-angle parabolic equation for acoustic waves in inhomogeneous moving media: applications to atmospheric sound propagation. J Comput Acoust 2001;9(02):477–94.

[8] Delany ME, Bazley EM. Acoustical properties of fibrous absorbent materials. Appl Acoust 1970(3):105–16.

[9] Heimann D, Kaasler Y, Gross G. The wake of a wind turbine and its influence on sound propagation. Meteorol Z 2011;20(4):449–60.

[10] Kelly M, Gryning S-E. Long-term mean wind profiles based on similarity theory. Boundary-Layer Meteorol 2010;136(3):377–90.

[11] Lee S, Lee D, Honhoff S. Prediction of far-field wind turbine noise propagation with parabolic equation. In: 21st AIAA/CEAS aeroacoustics conference, Dallas, Texas; 2015.

[12] Mann J. Wind field simulation. Probab Eng Mech 1998;13(4):269–82.

[13] Michelsen J. 1992. Basis 3d-a platform for development of multiblock pde solvers, afm 92-05. Tech rep. Technical University of Denmark.

[14] Oerlemans S, Sijtsmaa P, Mendez Lopez B. Location and quantification of noise sources on a wind turbine. J Sound Vib 2007;299:869–83. , <http://www.sciencedirect.com/science/article/pii/S0022460X06006316>.

[15] Ostashev V, Juve D, Blanc-Benon P. Derivation of a wide-angle parabolic equation for sound waves in inhomogeneous moving media. Acta Acust (Stuttgart) 1997;83(3):455–60.

[16] Salomons EM. Computational atmospheric acoustics. Springer Science + Business Media B.V; 2001.

[17] Sørensen J, Mikkelsen R, Henningson D, Ivanell S, Sarmast S, Andersen S. Simulation of wind turbine wakes using the actuator line technique. Philos Trans R Soc A 2015;373(2035).

[18] Sørensen JN, Shen WZ. Numerical modeling of wind turbine wakes. J Fluids Eng 2002;124(2):393–9. http://dx.doi.org/10.1115/1.1471361.

[19] Sørensen NN. General purpose flow solver applied to flow over hills [PhD thesis]. Technical University of Denmark; 1995.

[20] West M, Gilbert K, Sack R. A tutorial on the parabolic equation (PE) model used for long range sound propagation in the atmosphere. Appl Acoust 1992;37(1):31–49.

[21] Wilson DK, Noble JM, Coleman MA. Sound propagation in the nocturnal boundary layer. J Atmos Sci 2003;60(20):2473–86.

[22] Øye S. Flex4 simulation of wind turbine dynamics; 1996.

[23] Zhu WJ, Heilskov N, Shen WZ, Sorensen JN. Modeling of aerodynamically generated noise from wind turbines. J Sol Energy Eng 2005;127(4):517–28. http://dx.doi.org/10.1115/1.2035700.

Chapter 4

Statistical Approach for Wind Turbine Far Field Noise

4.1 Chapter Overview

The previous chapter showed the significant effects of the wind turbine wake on atmospheric sound propagation. This chapter focuses on the SPL statistics downwind of a turbine under a variety of atmospheric conditions that are obtained from the long term meteorological measurements.

The corresponding publication (Sec. 4.2) makes use of the PE calculations that are driven by the inputs from a RANS solver. First, a set of simulations for the strategically selected atmospheric conditions are carried out. Subsequently, a statistical approach is used to determine the stability-integrated SPL mean and variance distributions. It was observed that when the stability-affected propagation results are aggregated the mean SPL distribution deviate maximum -2 dB (unstable-dominated site) and 1.5 dB (moderately stable site) from the neutral conditions. While these values are relatively low the variation of SPL reaches much higher values when investigated for each atmospheric condition (e.g. maximum 7 dB deviation along the propagation path for different atmospheric classes). Lastly, the publication also shows the importance of the temperature inclusion for the sound propagation calculations (especially for the stable climates) via the simulations with and without temperature distribution.

4.2 Publication

Statistical prediction of far-field wind-turbine noise, with probabilistic characterization of atmospheric stability

Mark Kelly,[1, a)] Emre Barlas,[2] and Andrey Sogachev[1]

[1)] *Wind Energy Dept., Risø Lab/Campus, Danish Technical University; Frederiksborgvej 399, Roskilde 4000 DK*

[2)] *Wind Energy Dept., Lyngby Campus, Danish Technical University; Lyngby 2800 DK*

(Dated: 26 February 2018)

Here we provide statistical low-order characterization of noise propagation from a single wind turbine, as affected by the mutually-interacting turbine wake and environmental conditions. This is accomplished via a probabilistic model, applied to an ensemble of atmospheric conditions based upon atmospheric stability; the latter follows from the basic form for stability distributions established by Kelly & Gryning (2010). For each condition, a parabolic-equation ("PE") acoustic propagation model is driven by an atmospheric boundary-layer ("ABL") flow model; the latter solves Reynolds-Averaged Navier-Stokes ("RANS") equations of momentum and temperature, including the effect of stability and ABL depth, along with the drag due to the wind turbine.

Sound levels are found to be highest downwind for modestly stable conditions not atypical of mid-latitude climates, and noise levels are also elevated for very stable conditions. The probabilistic modelling gives both the long-term (ensemble-mean) noise level and variability as a function of distance, per site-specific atmospheric stability statistics. The variability increases with distance; for distances beyond 3km downwind, this variability is highest for stability distributions that are modestly dominated by stable conditions. However, mean noise levels depend on the widths of the stable and unstable parts of the stability distribution, with more stably-dominated climates leading to higher mean levels.

[a)] Electronic mail: mkel@dtu.dk

I. INTRODUCTION

Noise emitted by wind turbines can be a major concern for residents living nearby—and is subsequently an important consideration for the viability of potential wind farms. Turbine-associated sound levels may vary considerably due to the differing atmospheric conditions that occur, from e.g. day to night and season to season. Both the mean sound pressure level (SPL), as well as its variability (i.e. the standard deviation σ_{SPL}) are thus of interest for wind-farm planning and associated tasks. As part of the internal cross-cutting activity on wind turbine noise propagation at the Danish Technical University (DTU) in 2016, to address the aforementioned, we developed a statistical model; the model—along with models for turbine noise-source, propagation, and atmospheric flow—accounts for sound propagation from turbine blades through an ensemble of simulated atmospheres incorporating both stability (buoyancy) and the wind turbine wake. Here we first introduce the various components of the problem.

a. Medium-range outdoor sound propagation. Sound propagation through the atmospheric boundary layer [ABL], for distances over which turbine noise is relevant (on the order of hundreds of meters to several kilometers, which we refer to here as 'medium-range') is a complex phenomenon that is influenced by a number of potentially competing effects. These include geometric spreading, atmospheric (molecular) absorption, attenuation and reflection by the ground, as well as spatio-temporal deviations in the speed of sound. Theoretical[1–5], numerical[6–8], and experimental[2,9–11] works have shown that due to the last aspect, some atmospheric conditions can result in far-field SPL that may exceed the noise levels predicted when considering only geometric spreading, atmospheric absorption, and ground effects. From field measurements it is clear that wind farm noise can be exceedingly higher than such predictions[12]. This relative increase in SPL—particularly its aggregate effect on long-term low-order statistics—is not well-quantified with extant noise models or tools.

b. Stability and the atmospheric boundary layer. The primary contributors to fluctuations in the speed of sound are local fluctuations in the wind velocity and temperature fields (e.g. Embleton[13], Salomons[14]). The velocity and temperature fields can each be decomposed in terms of a 'background' profile which varies in the vertical, plus three-dimensional turbulent (local) fluctuations[15]. The background profiles are considered constant for 10 minutes or longer (up to perhaps ∼1 hour according to stationarity in the ABL[15,16]), while the

turbulent fluctuations vary over time scales ranging from seconds to minutes. The latter are generally responsible for acoustic scattering and SPL fluctuations over time scales of minutes or shorter, while a given stability condition is associated with background profiles of temperature and wind speed—and thus the short-term mean (background) sound speed profile, which we denote $c(z)$. Here we are interested in long-term representative statistics, and so we focus on modelling the sound speed profile, via atmospheric stability, as elucidated below. The sound speed profile is affected by vertical gradients in both the wind speed (shear) and temperature (lapse rate); the ABL 'top,' which is characterized by a strong positive temperature gradient, can occur at heights ranging from ∼100-200 m (winter/nighttime) up to 1 km or more (sunny day), with shallow ABL's having a dramatic impact upon both turbine wake structure and sound propagation.

c. Use of RANS for ABL flows with wind turbines. We wish to model the flow field encountered by a wind turbine and also including the turbine wake, as affected by atmospheric stability (buoyancy); we desire to characterize the resultant multi-dimensional velocity and temperature fields for use as input to our acoustic propagation calculations. A computational method which allows such modelling is the solution of the Reynolds-Averaged Navier-Stokes (RANS) equations; this permits output of the mean flow for a given stability condition, including the variation of temperature and wind gradients in space.[17] The buoyancy-affected gradients, in turn, are affected by (and affect) the turbine wake; such interacting effects of a turbine on the flow are also readily modeled within RANS (e.g. Sharpe[18], Troldborg *et al.*[19], Crasto *et al.*[20]). The solver that we use, SCADIS, also gives realistic ABL depths for a given surface-layer stability; both are important for establishing the vertical gradients which cause acoustic refraction and ultimately affect the transmission loss.

d. Statistical aspect. In the lower ABL where wind turbines exist, given the importance of wind shear and vertical temperature gradients on the sound speed profile, the state of the atmosphere can be characterized by the surface-layer stability[21,22] and also ABL depth (height of temperature inversion[15,23]). But climatologically, the effect of stability on the mean vertical profiles—and thus long-term means and variability—depends on the *distribution* of stability, and also ABL depth[24,25]. Here we adopt the probabilistic framework of Kelly and Gryning[25] which gives a form for universal stability distributions, allows them to be expressed in through long-term statistics. Thus e.g. multi-year low-order noise-level statistics (mean and variance) are comprised of an ensemble of noise fields, where each mem-

ber of the ensemble corresponds to a representative atmospheric condition; the probability of each condition dictates the relative contribution of the noise field in that condition to the long-term noise statistics.

e. Propagation Modeling. The ISO-9613-2 standard[26] includes a parameterization for meteorological (stability) effects; however it is crude (does not depend on actual stability), and only has a valid range of wind speeds up to 5 m/s—below the wind speeds relevant for wind turbines[27]. Improvements on the ISO-9613-2, such as the Nord2000[28] and HARMONOISE[29] models, have been made by building upon ray-tracing approaches. But these cannot capture e.g. range-dependent sound-speed profiles, or multiple ground reflections, respectively[30]; the former is relevant due to wind-turbine wakes, and the latter is an issue in winter and nighttime (stable) conditions. Further, these models do not readily facilitate prediction of variability per observable stability statistics (again we are interested here in finding climatologically representative noise statistics). On the other hand, propagation calculations based on the parabolic wave equation can handle varying atmospheric conditions and multiple reflections[31,32]; we employ such a method[33] in this work.

Structure of this article

The structure of this paper is as follows: first we present our statistical model to represent turbine noise propagation via a probabilistic stability framework, including the necessary theory. Secondly we introduce the computational flow model used to simulate an ensemble of atmospheric flow and temperature fields, including the dynamical effect of a turbine. Then we introduce the parabolic-equation sound propagation model, with the turbine noise-source modeling; the latter includes both physical representation and inflow effect, as well as the simulated noise source. Finally we show results of the aggregate modelling, discussing and summarizing.

II. THEORY AND MODELLING

The basis for the acoustic propagation modelling is the parabolic equation (PE) method, with a 2-dimensional implementation and solver as outlined in Barlas *et al.*[34]. This solver, which can also account for temperature-induced sound-speed profile deviations[35],

is driven by 2-D wind fields generated for different atmospheric stability regimes by an atmospheric boundary-layer (ABL) flow model; the latter is the Reynolds-averaged Navier-Stokes (RANS) flow solver ScaDis[36].

The mean flow is calculated including the wake effect, via an actuator disc implementation in ScaDis; this is done because the combined effect of atmospheric stability and the turbine wake on the flow is crucial in calculating the environmental propagation of turbine noise. Such sensitivity is primarily due to the fact that the curvature of sound rays can be dominated by the mean wind profile $U(z)$ as affected by stability (caused by the surface heat flux), with the temperature profile $T(z)$ often playing a less direct role; this is elucidated later.

A. Probabilistic model of atmospheric representation and propagation

In order to arrive at meaningful turbine-noise propagation statistics, e.g. mean sound loss as a function of distance downwind, we start by attempting to account for the statistical behavior of the primary variable characterizing the (aggregate) atmospheric effect on turbine-to-ground propagation: the Obukhov length. In particular, the inverse Obukhov length, $L^{-1} = \kappa(g/T_0)H/u_*^{-3}$, defined by fluxes of heat (H) and momentum (u_*^3) in the surface layer ($\sim$10-30m above ground), is a direct measure of the atmospheric stability. Further, its distribution $P(L^{-1})$ tends to follow a universal form that is effectively scalable from site to site, as found by Kelly and Gryning[25]; this form has been shown to predict the mean profile $U(z)$ at various sites[37]. The wind profile dominates the sound speed profile, so effect of stability on the sound speed profile is through the wind shear, particularly approaching receivers near ground; since we know the range of L^{-1} to be expected across (typical) turbine sites in practice, then knowing the form $P(L^{-1})$ allows us to sample a number of L^{-1} and calculate the propagation for each situation. Specifically, we simulate the flow field—including turbine-induced wake—for a representative range of stability cases, calculate the propagation loss for each case, and then we are able to compute a weighted sum of the case results based on the widths of the unstable ($L < 0$) and stable ($L > 0$) sides of the stability distribution.

The stability distribution for the Lille Valby (DK) site is shown in Figure 1, calculated from two years of sonic-anemometer measurements taken at 10 m above ground. This is

typical for mid-latitude sites[25], and will be later used to represent climatological conditions for the Risø-DTU turbine noise measurement campaign.

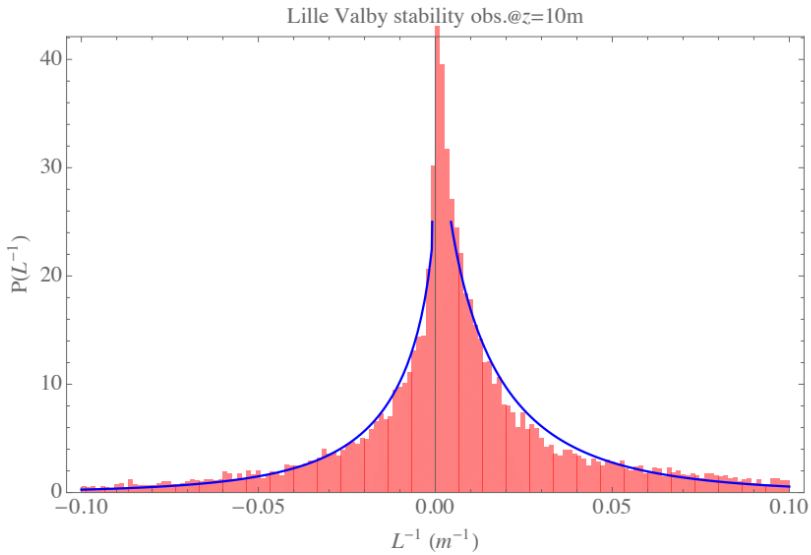

FIG. 1. Distribution of stability (inverse Obukhov length) for Lille Valby site. Shaded/red: observations; blue line is 'universal' stability distribution[25].

For our study, we selected 15 stabilities spanning the distribution shown in Figure 1, including the neutral case of $L^{-1} = 0\,\mathrm{m}^{-1}$. While Barlas *et al.*[35] calculated propagation results for only a significantly stable and unstable case, here we address the need to model the various propagation conditions over the range of stabilities. This is necessary because sound attenuation can be most significantly reduced for slightly- to modestly-stable cases, particularly at distances greater than 1 km from a turbine; i.e., the most stable cases do not cause the loudest signals at long distances. Less stable high-wind conditions, which happen more frequently[25], can enhance propagation, as can ABL depths that tend to occur in such conditions.

A basic probabilistic model is devised here, which allows estimation of low-order statistics of turbine noise propagation (and loss) due to varying flow conditions in the ABL. Most simply, the model calculates a weighted average of sound pressure loss (*transmission loss*, TL) by sampling over the relevant range of atmospheric stabilities, with the weights taken as the respective stability probabilities; this is analogous to—and follows from—the stability-

affected weighted-mean wind profile model of Kelly *et al.*[25,37]. Ideally we have

$$\mathrm{TL}(r,f) = \int \mathrm{TL}(r,f|L^{-1})P(L^{-1})dL^{-1} \tag{1}$$

as a function of frequency f and distance from source r, as well as height above ground (z) and propagation angle from mean wind direction ($\Delta\varphi$); however, we do not yet consider the last two aspects, and thus suppress them here in the notation. The integral is in practice approximated by a sum, sampling the stability distribution $P(L^{-1})$; thus written as a weighted average, it is

$$\mathrm{TL}(r,f) = \sum_i a_i \mathrm{TL}(r,f|L^{-1})P(L_i^{-1}). \tag{2}$$

Here a_i is the weight for each case, proportional to the sampling interval in L^{-1}-space (or bin-width for each L_i^{-1}). The 2-sided stability distribution is modelled[25,37] by

$$P_\pm(L^{-1}) = \frac{n_+}{\Gamma(5/2)}\frac{C_\pm}{\sigma_\pm}\exp\left[-\left(\left|L^{-1}\right|C_\pm/\sigma_\pm\right)^{2/3}\right] \tag{3}$$

where "+/-" subscripts indicate values for either stable ($L^{-1}>0$) or unstable ($L^{-1}<0$) conditions: $\sigma_\pm$ are the variability[38] in L^{-1}, $n_\pm$ is the fraction of occurence and $\{C_+, C_-\} = \{1, 3\}$ for stable/unstable conditions, respectively (see Kelly and Gryning [25] for more details). The widths $\{\sigma_+, \sigma_-\}$ of the stability distribution for stable and unstable conditions and the fraction of stable conditions ($n_+ = 1-n_-$) determine the distribution $P(L^{-1})$, so for a given $\{\sigma_+, \sigma_-, n_+\}$ we can calculate $P(L^{-1})$, and from it the a_i, from a limited number of RANS and PE simulations.

We choose 15 stability cases which span the range stabilities encountered 98% of the time on the stable side for Lille Valby, giving priority/weight to stable conditions (smaller sampling interval)—because L^{-1} has a greater effect on $U(z)$ and SPL in stable conditions, and because unstable conditions have an effect which does not vary much with L^{-1} and which saturates for more negative L^{-1} (i.e. the atmosphere is well-mixed for any cases more unstable than the minimum value we chose). The stabilities L_i^{-1} sampled for simulation and analysis are $-12.3, -9.5, -7.7, -5, -3.5, -2.3, -1.6, 0, 9.7, 12.7, 19.2, 23.2, 32.1, 46.5,$ and $67.8\,\mathrm{km}^{-1}$; looking at Figure 1, we can see these cover the range of stabilities encountered at the site considered here. Again, for stabilities $L^{-1} < -0.01\,\mathrm{m}^{-1}$ the lower ABL is mixed enough to not give different propagation conditions; for $L^{-1} > 0.04\,\mathrm{m}^{-1}$ (as shown later in this work) the attenuation does not increase, and there is also very little probability mass there as seen in Figure 1.

B. Atmospheric boundary-layer flow model

The SCADIS [SCAlar-DIStribution] flow model is a Reynolds-Averaged Navier-Stokes (RANS) solver employing a two-equation turbulence closure scheme[36], including a self-consistent atmospheric stability formulation that gives results satisfying Monin-Obukhov theory[39]. The code includes the effect of the Coriolis force as well as cloud cover (radiation), and reproduces both the diurnal cycle as well as associated ABL depth variations. It was run in 2-D mode with 10m resolution, using the k-ω equations[40] for turbulence closure. Diurnal cycles were run with various geostrophic winds (G=$\{$8,10,12,14$\}$ m/s) in clear conditions, and 50% and 100% cloud cover conditions were also run for G=10m/s. In aggregate, 15 simulation cases were taken, which span the range of stabilities as mentioned above in section II A.

The turbine rotor is located at $x = 0$ from heights 60 m$\leq z \leq$140 m (virtual hub-height of 100 m) above ground level, and is simulated using the common actuator disc method. The effect of wind turbine on airflow was prescribed via drag force distributed between 50 and 150 m above the ground. The force was also 'smeared' over adjacent computational nodes in the horizontal direction, with three nodes used to smooth the horizontal pressure gradient like Troldborg *et al.*[41]. A uniformly-distributed drag-coefficient C_d=0.2 was used in the central node of canopy location, and tapered symmetrically in the vertical around the hub height to account for the cross-sectional area in the cross-stream direction.

Two sample mean flow fields are shown in Figure 2, corresponding to (top) mildly stable conditions with $L^{-1} = 0.013\,\mathrm{m}^{-1}$ (i.e. higher wind speeds at turbine rotor heights) common during nights and winter; and (bottom) weakly unstable conditions with $L^{-1} = -0.012\,\mathrm{m}^{-1}$, commonly found during sunny or partly-cloudy days. One can see these are relatively common by noting that the values of L^{-1} are near the peak region of $P(L^{-1})$ shown in Figure 1 above. The flow fields were generated using ScaDis, for different geostrophic (driving) wind speeds, above a uniform rural/field roughness (z_0=10 cm) and flat terrain. One can see the effect of stability on both the wind profile upwind of the turbine, as well as upon the wake recovery, from Figure 2. In the wake, the stability affects the "competition" between recovering ambient high shear versus turbulent mixing, and the distance over which these effects (and the flow) equilibrate.

Another stability-related aspect of the ABL that affects the flow and propagation, which

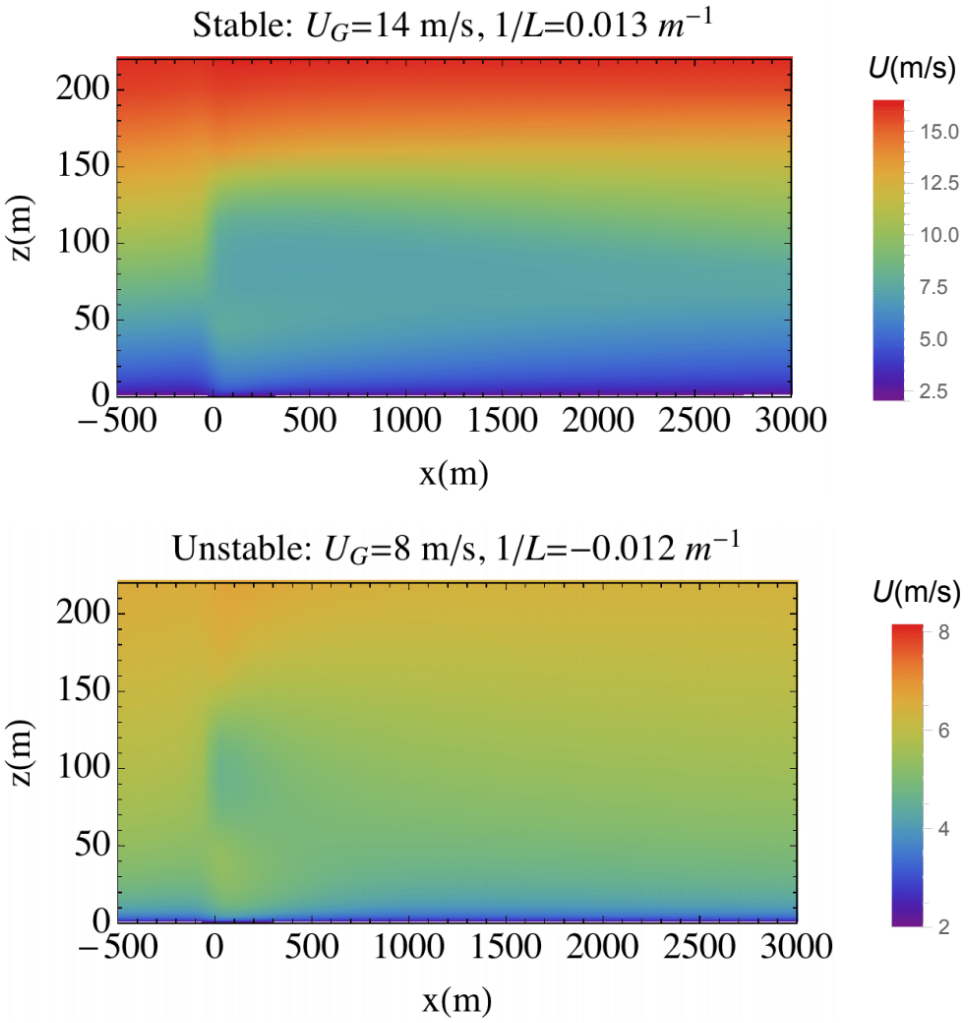

FIG. 2. Input wind fields for weakly stable and unstable regimes, produced by ScaDis. Turbine rotor (actuator disc) is located at $x = 0$, $z = 100 \pm 40\,\mathrm{m}$.

is implicitly incorporated in our probabilistic model (2) via ScaDis, is the ABL depth h_{ABL}. In the cases shown in Figure 2, h >250m, but for more stable conditions the ABL can be shallower than 200m (or even 100m in more extreme cases). ScaDis captures the stability-affected depth by simulating the evolving ABL, as well as cloud cover (which causes more neutral conditions and also affects h_{ABL}). For example, the most stable case simulated ($L^{-1} = -0.012\,\mathrm{m}^{-1}$) had a depth h_{ABL} ≈100m and associated mean 'jet' spanning part of the rotor, resulting in negative shear in the wake of the rotor; the flow field from this rarest of simulated cases is shown in Figure 2. Situations like the stable, shallow-ABL case shown in Figure 2 can lead to ducting and enhanced long-range propagation, or also increased

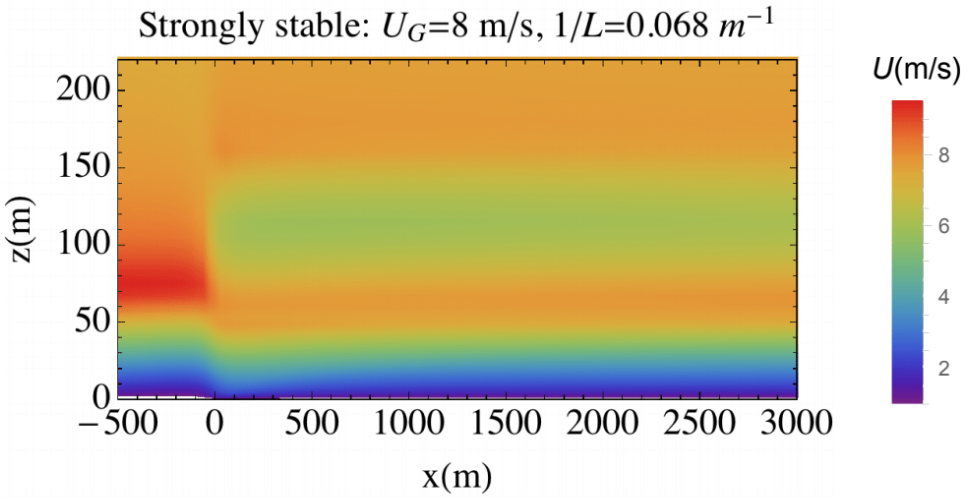

FIG. 3. Input wind fields for most stable (rarest) sample/case simulated by ScaDis.

attenuation, depending on the ABL depth and the terrain; in fact the latter is more likely for the case in the figure, as shown in the sections below.

C. Sound Propagation Model

For propagation modelling DTU's WindSTAR-PRO (Wind turbine Simulation Tool for AeRodynamic Noise PROpagation)[34,35] was used. The tool includes several parallelized (MPI) implemetations of Parabolic Equation (PE) models, solved per frequency and realization. In this study, a two-dimensional wide-angle PE method[31] is employed, where the moving atmosphere is replaced by a hypothetical motionless medium having an effective speed of sound c_{eff} that accounts for refraction due to wind speed gradients: $c_{\text{eff}}(x,z) = c(x,z) + V_p(x,z)$, where V_p is the component of mean wind velocity along the direction of propagation between source and receiver, and c is the speed of sound calculated via $c = \sqrt{\gamma RT}$, where γ is the specific heat ratio, R is the gas constant and T is the temperature (obtained from the flow solver, see also sec. II B). The spatial resolution in both directions is set to one eighth of the wavelength ($\Delta x = \Delta z = \lambda/8$; where λ is the wavelength of the considered frequency). Only flat terrain is considered and the ground impedance is characterized using the four-parameter model developed by Attenborough[42,43] with effective flow resistivity of 200 kPa m^{-2}s representative for grassland. The other parameters of the impedance model are kept constant: pore shape factor ($s_p = 0.75$), Prandtl

number ($N_{Pr} = 0.72$), grain shape factor ($n' = 0.5$), porosity ($\Omega = 0.3$), ratio of specific heats ($\gamma = 1.4$) and density ($\rho = 1.19$ kg/m^3). All simulations are carried out for $\frac{1}{3}$-octave band centre frequencies from 20 Hz to 800 Hz and the corresponding sound pressure levels are summed logarithmically to obtain the overall SPL

$$\mathrm{SPL_{tot}} = 10\log_{10}\Big(\sum_{i=1}^{N} 10^{\mathrm{SPL}(f_i)/10}\Big), \tag{4}$$

where N is the number of frequencies used. The sound pressure level $\mathrm{SPL}(f_i)$ is defined as

$$\mathrm{SPL}(f_i, r) = L_W(f_i) - 10\log_{10}\left(4\pi r^2\right) - r\alpha(f_i) + \mathrm{TL}(f_i, r), \tag{5}$$

where the first three terms on the right-hand side represent the source power level, geometrical spreading, and atmospheric absorption, respectively. The absorption coefficient is calculated according to ISO 9613-2[26] for air at 20°C with 80% relative humidity.[44] The last term represents the transmission 'loss': the deviation from the free field of a source due to ground effects, atmospheric refraction, turbulence, etc.; this last term is calculated using the PE method.

1. Source modelling: inflow and physical representation

Wind turbines are three-dimensional, complex noise sources, considering the rotation of the blades and the unsteady flow field around them. Recently a coupled wind turbine noise generation-propagation model was proposed in Barlas *et al.*[33], where the source is represented in a three-dimensional and unsteady manner within the PE solver. In this study our focus is on the mean sound pressure levels downwind of the turbine, so we use a mean two-dimensional approach, i.e. with a simplified source representation. Before all the simulations were carried out for this study, mean integrated sound pressure levels obtained from the various techniques are compared, in order to justify our simplified choice; these techniques are described below.

- 3D Weighted Unsteady Source + Unsteady LES Flow (3D-WUS-UF):
  At each time step a two-dimensional PE domain is constructed from each blade's noisiest element to each receiver location, while the source coordinates remain three-dimensional (see Fig 4). The background flow field is obtained using LES and interpolated and updated at each time step for each 2D PE domain. The source levels are

obtained from aero-elastically coupled wind turbine noise generation model[34]. The propagation simulations are carried out for a 10-minute duration, with 0.1 s time step. This method is taken as the reference, to which the following three methods' results are compared. Figure 5 shows the time-variation of source power level and height for this technique.

- 3D Weighted Unsteady Source + Mean LES Flow (3D-WUS-MF):
  Source representation and weighting of the source levels are identical with the previous technique, but only the time-averaged LES flow field is used as input.

- 2D Weighted Unsteady Source + Mean LES Flow (2D-WUS-MF):
  The lateral (y-) coordinate of each source is set to 0, i.e. the 2D PE domain lies in the x-z plane (Fig. 4). The source levels from the unsteady 3-d (3D-WUS-UF) method are used, and simulations are carried out for one full revolution.

- 2D Unweighted Unsteady Source + Mean LES Flow (2D-MUS-MF):
  The source coordinates are identical to 2D-WUS-MF technique, but time-averaged source levels are used for all sources and all times.

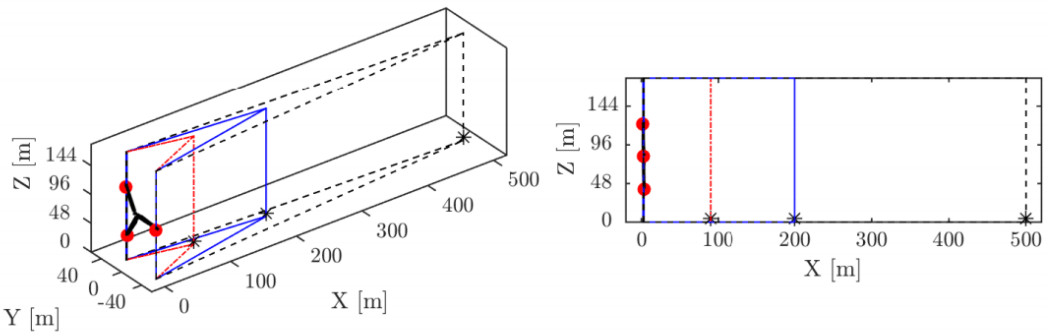

FIG. 4. Source representation within the propagation model. **Left**: Three dimensional and unsteady approach. **Right**: Two-dimensional and steady approach.

Figure 6 shows the error ensuing from use of the various source-modelling approaches, relative to the time-varying 3D-WUS-UF PE simulations. Here 'error' is described as the time-averaged overall SPL difference between the aforementioned source representation techniques at each receiver location. It is seen that the error in the mean 2D source representation

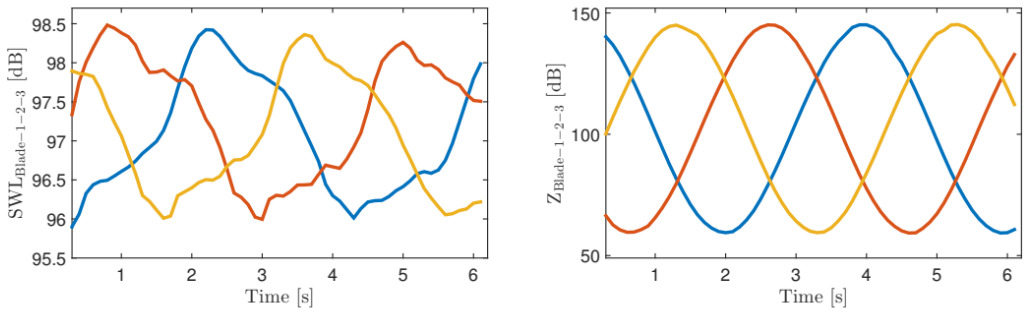

FIG. 5. Time-varying source power level (left) and vertical location (right) of each blade, for 3D-WUS-UF (each source within PE model).

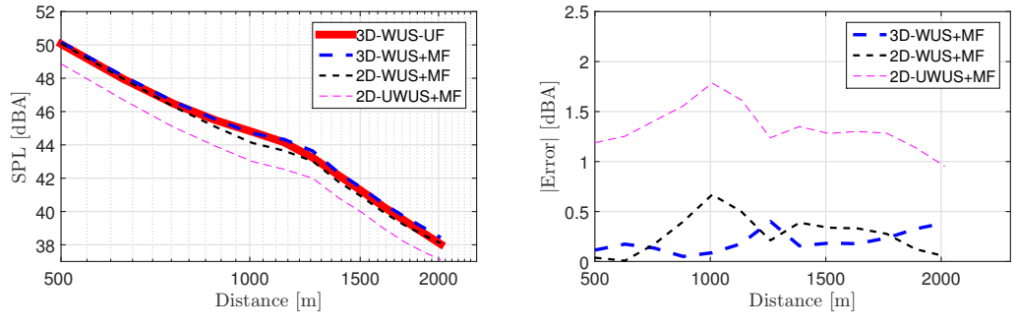

FIG. 6. **Left:** Sound pressure level versus distance for different source and flow field representations. **Right:** Error committed with the simplifications of the source and flow field representations.

basically follows the same pattern as the 2D unsteady source method; both vary a small amount ($\lesssim$0.8dBA) with distance. The relatively small error—and yet smaller variation in error—incurred when using a mean 2D source formulation allows the error to simply be modelled as a bias. The focus of this study is the mean propagation per atmospheric conditions based on stability, rather than detailed unsteady representation. Thus the mean 2D source representation is used here, with acknowledgement of the underestimation of SPL indicated in Fig. 6.

2. Turbine noise source

The PE solver calculates the frequency-dependent propagation, given a source spectrum; more details can be found in Barlas *et al.* (2016, 2017). The turbine noise source was mod-

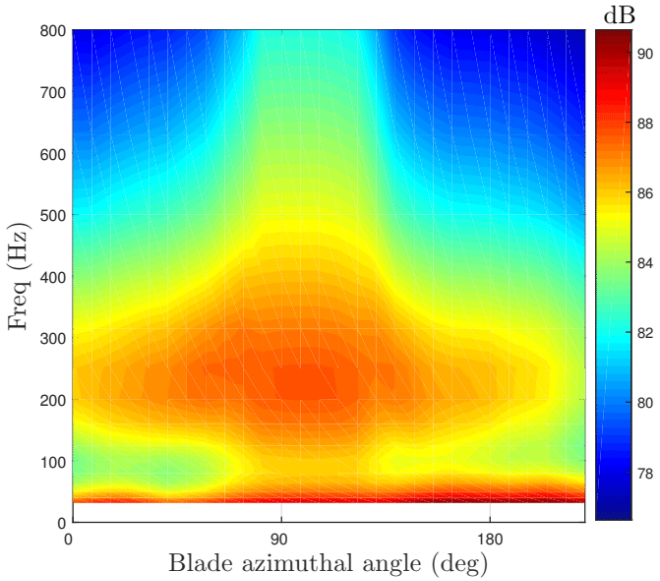

FIG. 7. Single source power level distribution with respect to blade azimuthal angle.

elled with the 2D weighted unsteady source technique described in II C 1. The simulations were carried out for one full rotation. Subsequently the sound pressure levels were averaged. The frequency-dependent source power level $L_W(f_i)$ is shown in Figure 7. This plot shows the variation of the frequency-dependent source power level of a single blade with respect to its azimuthal angle. The distribution shows a peak around 120 degrees blade location which is in agreement with the experimental source identification studies that are carried out by Oerlemans *et al.*[45]. The total propagation result per frequency f_i for distance r downwind from the source is found via eq. (5).

III. RESULTS AND DISCUSSION

The sound pressure levels found via the PE propagation code and eqns. (2)–(5), where the PE calculation has not (yet) included dT/dz, are shown in Figure 8 for all cases considered. The results are plotted as a function of distance, for a receiver height of 2 m above ground. In addition to the different stability cases (colored lines), Fig. 8 shows the total result (solid black line) calculated using all the cases with the probabilistic model (5) using the Lille Valby values for the stability distribution (corresponding to Fig. 1).

The stable cases contribute most to elevating the sound pressure level at longer distances,

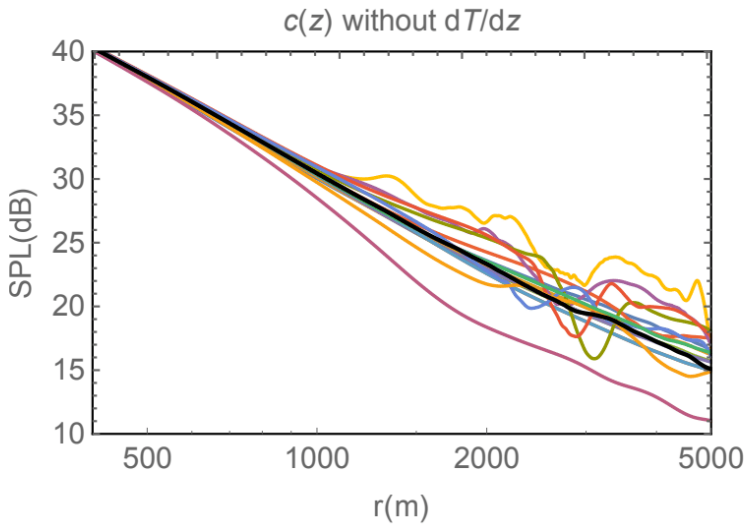

FIG. 8. Total SPL for all cases (colored lines), ignoring dT/dz within $c(z)$; solid black line is probability-weighted mean.

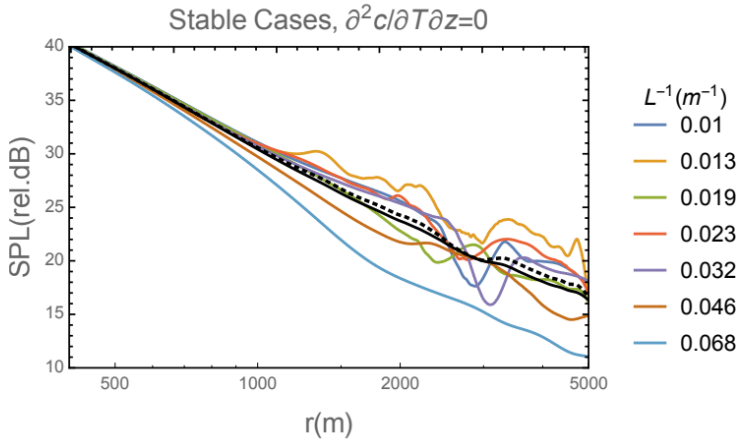

FIG. 9. Total SPL ignoring dT/dz within $c(z)$, as in Fig. 8, but for stable cases; also, probability-weighted mean for all (solid black) and for all stable(dotted black) cases.

due to (wake-affected) shear-induced refraction. Figure 9 shows the stable cases together, indicating the stability for each case; in addition to the total weighted mean (solid black as in Fig. 8), the figure also displays the weighted mean SPL for the stable cases only (dotted black).

From Figure 9 one can see that the most stable cases lead to noise *reduction*, due also to the shallow ABL depth accompanying them in the modeled flow field. From the light-blue

and brown lines (L^{-1} of 0.046 and 0.068 m^{-1}) one sees that these most stable cases, with ABL depths and associated jets occurring below rotor top (as seen in Figure 3), give the lowest sound levels. Cases with modest stability, which are accompanied by ABL depths greater than twice the rotor top height in the RANS simulations, show the loudest levels at long distances.

In the analysis and results thus far, we have not included the effects of the temperature profile. Although ScaDis provides $T(z)$, the vertical variation of T was not initially used in the effective sound speed profile $c_{\mathrm{eff}}(z)$ for the PE solver, because the wind speed profile—notably the shear, dU/dz—contribute much more to $c_{\mathrm{eff}}(z)$. But for very stable cases with a shallow ABL, the temperature may have a significant effect. Indeed, incorporating the temperature profile into $c_{\mathrm{eff}}(z)$ changes the results for such cases, as evinced in Figure 10. The figure shows results including the effect of $T(z)$. One can see in Fig. 10 that the weakly-stable case, which has the least transmission loss (i.e. loudest noise, orange lines), is not affected much by inclusion of the temperature profile; however, the most stable cases are significantly impacted by accounting for $T(z)$ in $c_{\mathrm{eff}}(z)$, with an increase of several dB in SPL for distances beyond 1 km. Thus inclusion of $\partial T/\partial z$ for very stable cases increases the long-range SPL predictions, though the weighted mean (dotted black line for stable cases, black for all cases in Fig. 10) changes modestly because increasingly stable cases occur with decreasing frequency. However, we note that the SPL for stable cases is still higher than in unstable cases.

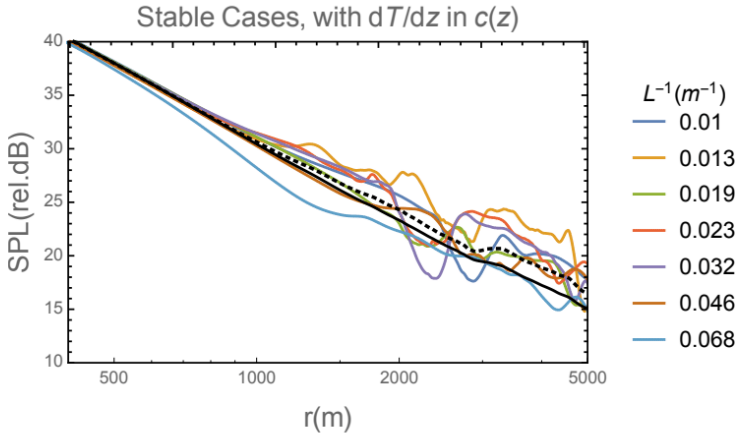

FIG. 10. SPL including $T(z)$ within $c(z)$; probability-weighted mean for all (solid black) and for all stable(dotted black).

To further demonstrate the utility of the probabilistic method, as driven by a strategically sampled set of PE and RANS simulations, Figure 11 displays the total SPL for different representative climates, calculated using (2); the bottom plot in the figure also displays the integrated SPL for each respective climate minus the neutral climate's integrated SPL, as a function of distance downwind, i.e. the overall change compared to having no surface-induced stability effects. The climates are: the typical mid-latidude/temperate case (Lille Valby) considered above; a very unstable climate (Basel, Switzerland) and stabler conditions (Cabauw, NL) found by Kelly and Gryning[25]; a neutral climate; and a very stable climate. The stability distribution $P(L^{-1})$ and consequent simulation-case weights a_i corresponding to the first three were found based on the measured $\{n_+, \sigma_+, \sigma_-\}$ from each site; then the weighted average of all cases was calculated for each site via (2). The 'very stable' climate has $\{n_+, \sigma_+, \sigma_-\}$ equal to $\{0.86, 0.06\text{m}^{-1}, 0.02\text{m}^{-1}\}$, while the neutral-dominated case has $\{n_+, \sigma_+, \sigma_-\} = \{0.5, 0.03\text{m}^{-1}, 0.01\text{m}^{-1}\}$.

From Figure 11 one can see that overall, there does not appear to be a large difference in SPL, when stability-affected propagation results are aggregated (in effect, averaged with weights) according the distribution of stability conditions at typical sites: there is less than 1 dB difference between the modestly stable (Cabauw), typical (Lille Valby), and neutral cases. This is not completely surprising, since neutral conditions dominate the stability distribution at such sites. The unstable/convectively-dominated Basel site results do show up to 2 dB lower SPL, which could likely be reduced yet further if turbulent scattering were also included[5,13]. The very stable climate shows increasing SPL relative to neutral conditions for distances from ∼1–2 km, with levels more than 1 dB louder at ∼3-4.5 km downwind. The figure further indicates that over distances up to ∼1 km the propagation (which also includes atmospheric absorption and geometrical spreading) is roughly approximated by $r^{-2.55}$ ($^{-18/7}$, dotted line). However for distances beyond $\sim 20 z_{\text{hub}}$ the modeled long-term mean SPL downwind has a distance-dependence more like r^{-2} (dot-dashed line); i.e. wake, stability, and ground effects roughly cancel the effect of atmospheric absorption, when summed over audible frequencies.

To show the expected long-term variability in SPL for each case (climate), Figure 12 displays the $P(L^{-1})$-weighted variance, i.e. the probability-weighted integral of the square of SPL difference from climate-mean, as a function of distance downwind. One can see the effect of stability on the variability, considering the weighted-variances of SPL plotted in

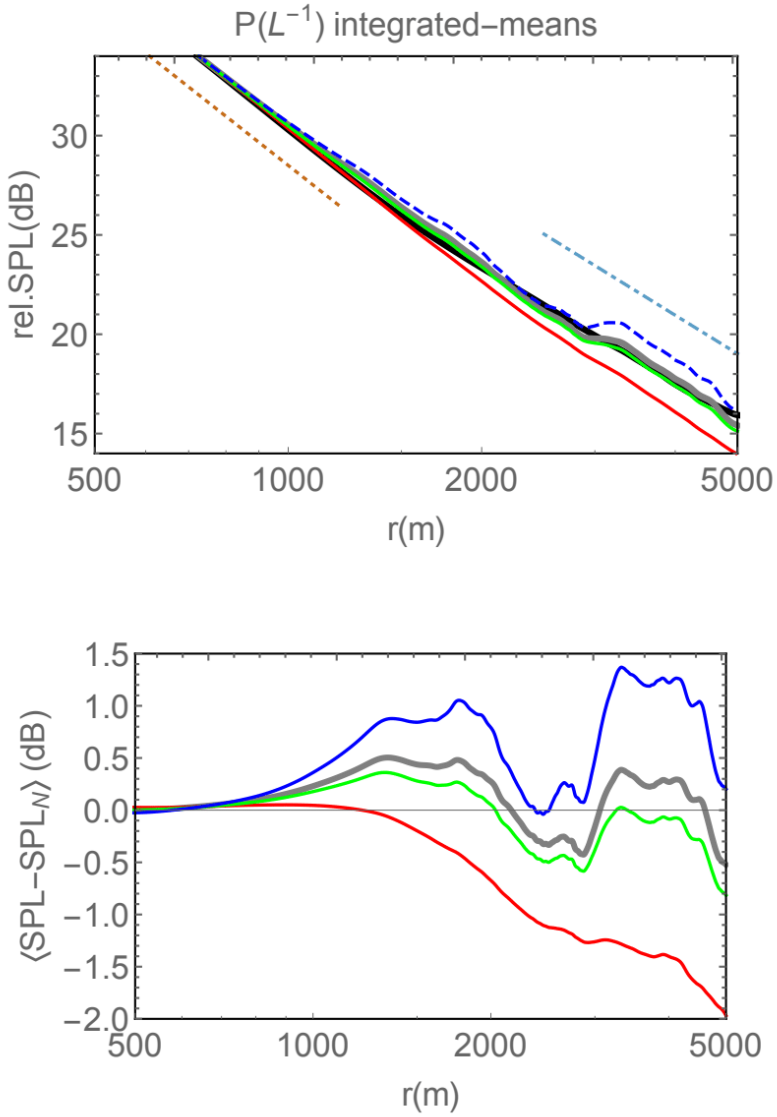

FIG. 11. Top: Overall (stability-integrated) mean SPL for different climates; bottom: difference between overall SPL and neutral result. Black (top): neutral climate; gray/thick: typical mid-latitude (Lille Valby, as in Figs. 9–10); green: modestly stable climate (Cabauw); red: unstable climate (Basel); blue: very stable climate.

Fig. 12; the 'neutral' climate is again defined above as having a very narrow distribution, and for a purely neutral climate then the relative SPL variability σ_{SPL} would be 0. Fig. 12 also shows that for very stable climates, the variability is slightly higher than for more typical

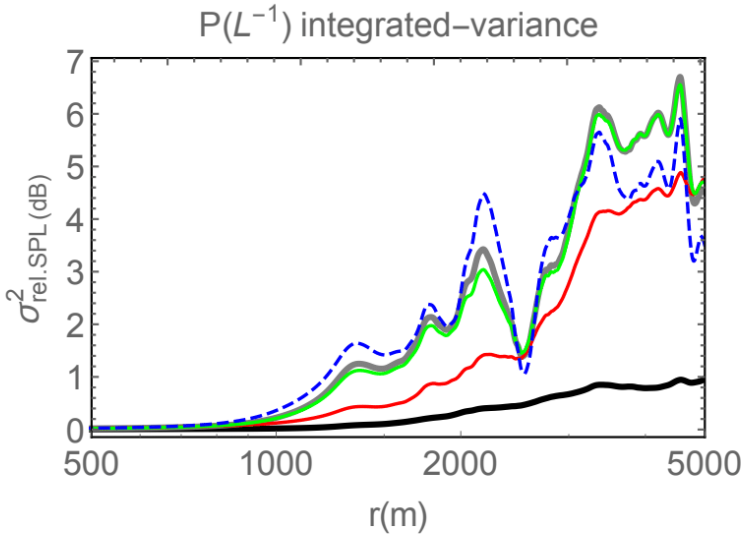

FIG. 12. Stability-integrated variance of SPL relative to the respective mean for different climates, as a function of distance downwind. Black: neutral climate; gray/thick: typical mid-latitude (Lille Valby, as in Figs. 9–10); green: modestly stable climate (Cabauw); red: unstable climate (Basel); blue: very stable climate.

climates dominated by stable conditions, at least for distances downwind up to roughly 3 km. Beyond that distance downwind, something potentially counter-intuitive happens: the more *modestly stable* distributions (more typical climates) show higher $\sigma_{\rm SPL}$ for r from ∼3km–5km. These variances are equivalent to rms SPL deviation amplitudes that grow from roughly 1dB to 2.5dB as one considers distances that increase from ∼1.3km to 4.5km downwind. The distribution dominated by unstable conditions (Basel site) shows less variability, but this is partly due to our propagation model not including turbulent scattering.

Regarding downwind propagation and stability

The results seen in Figures 9–12 are also supported by theory, which can also give a guide to inclusion or exclusion of vertical temperature gradients in the acoustic modelling. Considering downwind propagation, the effective speed of sound (including the wind speed)[46] has a vertical derivative

$$\frac{dc_{\rm eff}}{dz} = \frac{\partial c}{\partial T}\frac{\partial T}{\partial z} + \frac{\partial c_{\rm eff}}{\partial V_p}\frac{\partial V_p}{\partial z} = \frac{\partial U}{\partial z}\left[\cos(\varphi_p - \varphi_U) + \frac{c}{2T_0}\frac{\partial T/\partial z}{\partial U/\partial z}\right] \qquad (6)$$

where $c(z) = \sqrt{\gamma RT(z)}$ is the temperature-dependent speed of sound, γ is the specific heat ratio, R is the gas constant, V_p is the component of mean wind velocity along the direction of propagation, U is the mean wind speed, and $\varphi_p - \varphi_U$ is the angle between the direction of propagation and mean wind. For propagation directly downwind from a wind turbine, $\cos(\varphi_p - \varphi_U)$=1; since in the ABL one may invoke similarity to write $\partial U/\partial z = (u_*/\kappa z)\Phi_m(z/L)$ and $\partial T/\partial z = (\theta_*/\kappa z)\Phi_h(z/L)$, then

$$\left.\frac{dc_{\text{eff}}}{dz}\right|_{\varphi_p=\varphi_U} \simeq \frac{\partial U}{\partial z}\left[1 + \frac{c}{2u_*}\frac{\theta_*}{T_0}\frac{\Phi_h(z/L)}{\Phi_m(z/L)}\right] \sim \frac{\partial U}{\partial z}\left[1 + \frac{cu_*}{gL}\right] \tag{7}$$

because Φ_h and Φ_m do not differ much (see e.g. Businger *et al.*[47])—particularly for the stability range considered. Then one sees in (7) that for $L^{-1} \ll g/cu_*$, we can ignore the $\partial T/\partial z$ contribution to dc_{eff}/dz. For most stability distributions, such as those we have treated, we see that the the tails of $P(L^{-1})$ are at L^{-1} which do not allow such ignorance of $\partial T/\partial z$—as evidenced by the difference between the results in Fig. 9 (caclulated without dT/dz in c_{eff}) and Fig. 10 (calculated including dT/dz). From (6) one may also note that $\partial T/\partial z$ becomes more relevant for propagation directions differing more from the mean wind direction; i.e. for L^{-1} not negligible compared to $\sim g\cos(\varphi_p - \varphi_U)/(cu_*)$ then temperature effects can matter. Climatologically, this means that for directions deviating from downwind, then temperature gradients, e.g. the inversion at ABL top, become more important.

IV. SUMMARY AND CONCLUSION

In this work a probabilistic model for propagation conditions was developed, facilitating prediction of long-term (multi-year) wind turbine noise propagation statistics downwind. A universal analytic form of the probability density function of surface-layer stability $P(L^{-1})$ over land[25] (where L is Obukhov length), which depends on three parameters calculable from long-term meteorological (sonic anemometer) measurements, allows calculation of frequency-weighted statistics representative of yearly atmospheric conditions for a given site (ultimately over a turbine lifetime). Based on the form of the stability distribution and the range of stability conditions possible for turbine sites, an ensemble of stability conditions, i.e. atmospheric classes, were made; a corresponding set of simulations were carried out using the atmospheric RANS solver ScaDis. For each class the simulation has a different mean wind speed and surface heat flux (thus stability), as well as corresponding ABL depth

via the solution. The flow field for each simulation was used as input to drive the PE acoustic propagation model, which gave distance-dependent results for each atmospheric class. Noise propagation statistics were obtained using statistical weights according to the stability distribution, for a number of climates spanning conditions expected at wind farm sites.

Predicted noise levels were highest for modestly stable conditions, which occur during winter and nighttime in mid-latitude climates, while modelled SPL was also elevated for very stable (rarer) conditions. The latter is due to reduced depth of the ABL with increasing near-surface stability and the turbine wake. The effect of the ABL-capping temperature inversion on sound refraction via both the wind shear *and* temperature gradient is crucial, and captured via the flow model—which also accounts for the variation of ABL depth with surface stability. We again note the role of the temperature gradient (including its value within the ABL-capping 'inversion') in the sound propagation calculations, especially for stable climates; herein we have also introduced a basic scaling analysis to gauge the importance of dT/dz relative to dU/dz on the propagation.

For the unstable-dominated climate (Basel, heat-island) the $P(L^{-1})$-weighted mean SPL was lower than the neutral SPL, with the difference (SPL$-$SPL$_{\text{neutral}}$) increasing with distance downwind for $r >\sim 1$ km; the difference grew to -2 dB at a distance of 5 km for this case. For typical (non-tropical) turbine sites dominated more by stable conditions (due to buoyancy affecting wind shear more in stable conditions than in unstable conditions[21,25]), the mean SPL was a bit higher ($\sim \frac{1}{2}$ dB) than in absolute neutral conditions for distances of $\sim$1–2 km and $\sim$3–4.5 km, but similar to or less than the neutral result at $\sim$2–3 km and $\sim$4.5–5 km downwind. For an extremely stably-dominated climate, i.e. with a relatively long tail on the stable side of the $1/L$ distribution (such as what could be found in some climates with harsh winters and/or typically clear nights much colder than daytime), then a more significant relative increase in noise level is found beyond $\sim$1 km downwind—with [SPL$-$SPL$_{\text{neutral}}$] approaching 1.5 dB for the stability statistics outlined in section II A for this stability distribution.

While the mean SPL differences (relative to neutral conditions) may seem relatively small, the variability of SPL is significantly larger, especially for typical climates. The probability-weighted variability σ_{SPL} generally increases with distance. For $r >\sim 3$ km downwind, σ_{SPL} is highest for stability distributions commonly found in mid-latitudes (modestly dominated

by stable conditions, e.g. Lille Valby and Cabauw shown above) between 2–3 dB in that range. We point out that such variability can be significant, given that the overall levels predicted at distances beyond ∼3 km are ∼15-20 dB—not far from the audibility threshold of the human hearing considering the effect of e.g. sleeping indoors with open windows.

Discussion and outlook

As is the case with all modelling, the methodology using in this work involved some simplifying assumptions. The aim was to show long-term mean and rms turbine noise levels, as affected by the interacting wake and ABL including buoyancy. This begins with the assumption that surface-layer stability (reciprocal Obukhov length L^{-1}) can be used to build an ensemble of members which together represent the propagation conditions. Thus we effectively reduce the joint-distribution of near-surface friction velocity (u_*) and surface heat flux, collapsing such into $P(L^{-1})$; such an assumption becomes tenuous e.g. offshore or across lakes[37]. We have also used the ABL depths simulated by SCADIS based on each representative condition's surface heat flux (and cloudiness) and (geostrophic) wind speed, with a predefined value of 'free-atmosphere' temperature gradient above the ABL; to expand our analysis to be more complete, we wish to repeat the modelling for different free-atmosphere dT/dz. Further, we have only used a single ABL depth (z_i) per surface-stability; expanding the ensemble to include multiple z_i for each $1/L$, e.g. via the distribution[48] of z_i (such as was characterized by Liu and Liang[24]), also would refine our results.

Note also that the turbine representation (actuator disc) within the RANS flow-solver could be refined; here we began with a basic implementation which reproduces the key spatially- and stability-dependent flow features such as the wake, its decay, and associated $\{dU/dz, dT/dz\}$. A more sophisticated thrust-coefficient (and thus drag) description could be attempted, and e.g. the wake-decay and its sensitivity to parameterization could be investigated.

We note that the use of the 2D mean-flow source function involves another assumption, in effect: that stability and associated wind shear does not appreciably affect the 'bias' incurred relative to use of a 3D source with unsteady inflow. As shown in section II C 1 and Fig. 6, this bias (mean error) is less than 0.5 dB at 2 km distance downwind, diminishing to ∼0.1 dB at 5 km downwind; thus the stability-affected bias is not likely to be significant,

but could be explored.

In this work we have presented unweighted SPL, integrated over frequency, in order to show overall noise statistics. Further Frequency-dependent analysis, particularly over different surfaces and for a larger number of cases (the latter mentioned in the paragraphs above), is a subject of future work; this is relevant e.g. for domicile interaction and indoor noise (such as rattling windows) as well as supporting investigation of noise modulation.

ACKNOWLEDGMENTS

MK is thankful for internal support from DTU (2016 cross-cutting activity on turbine noise) for this work.

REFERENCES

[1]B. Gutenberg, "Propagation of sound waves in the atmosphere," Journal of the Acoustical Society of America **14**, 151–155 (1942).

[2]U. Ingård, "A review of the influence of meteorological conditions on sound propagation," Journal of the Acoustical Society of America **25**, 405–411 (1953).

[3]A. Kriebel, "Refraction and attenuation of sound by wind and temperature profiles ovr a ground plane," J. Acoust. Soc. Am. **51**, 19–23 (1972).

[4]T. Embleton, G. Thiessen, and J. Piercy, "Propagation in an inversion and reflection at the ground," J. Acoust. Soc. Am. **59**, 278–282 (1976).

[5]J. E. Piercy, T. F. W. Embleton, and L. C. Sutherland, "Review of noise propagation in the atmosphere," Journal of the Acoustical Society of America **61**, 1403–18 (1977).

[6]A. Ziemann, K. Balogh, and K. Arnold, "Modelling and measuring the atmospheric excess attenuation over flat terrain during night time conditions," Meteorologische Zeitschrift **16**, 429–441 (2007).

[7]K. Bolin, M. Boué, and I. Karasalo, "Long range sound propagation over a sea surface," The Journal of the Acoustical Society of America **126**, 2191–2197 (2009).

[8]D. Heimann, "Wide-area assessment of topographical and meteorological effects on sound propagation by time-domain modeling," The Journal of the Acoustical Society of America **133**, EL419–EL425 (2013).

[9]W. Wilken, "Experimental study of the influence of varying atmospheric conditions on sound propagation close to the ground," Acustica **62**, 55–65 (1986).

[10]O. Öhlund and C. Larsson, "Meteorological effects on wind turbine sound propagation," Applied Acoustics **89**, 34–41 (2015).

[11]A. Bigot, C. Mirabel, and P. Dutilleux, "Influence of vertical temperature gradient on backround noise and on long-range noise propagation from wind turbines," Proceedings of the ... International Congress on Sound and Vibration (2016).

[12]M. Stigwood, S. Large, and D. Stigwood, "Cotton farm wind farm–long term community noise monitoring project–2 years on," in *6th International Meeting on Wind Turbine Noise* (2015).

[13]T. F. W. Embleton, "Tutorial on sound propagation outdoors," The Journal of the Acoustical Society of America **100**, 31–48 (1996).

[14]E. Salomons, *Computational atmospheric acoustics* (Kluwer Academic Publishers,, 2001) p. 335 p.

[15]J. C. Wyngaard, *Turbulence in the Atmosphere* (Cambridge University Press, 2010) p. 393.

[16]D. H. Lenschow, J. Mann, and L. Kristensen, "How long is long enough when measuring fluxes and other turbulence statistics?" J. Atmos. Ocean Technol. **11**, 661–673 (1994).

[17]A. Sogachev and M. Kelly, "A note on two-equation closure modeling of canopy flow," Boundary-Layer Meteorology **130**, 423–435 (2009).

[18]D. Sharpe, "A general momentum theory applied to an energy-extracting actuator disc," Wind Energy **7**, 177–188 (2004).

[19]N. Troldborg, F. Zahle, P.-E. Rthor, and N. N. Srensen, "Comparison of the wake of different types of wind turbine cfd models," American Institute of Aeronautics and Astronautics. Meeting Papers on Disc **4**, 3407–3417 (2012).

[20]G. Crasto, A. R. Gravdahl, F. Castellani, and E. Piccioni, "Wake modeling with the actuator disc concept," Energy Procedia **24**, 385–392 (2012).

[21]A. S. Monin and A. M. Yaglom, *Statistical Fluid Mechanics*, Vol. 1 (The MIT Press, 1971) p. 453.

[22]T. Foken, "50 years of the Monin-Obukhov similarity theory," in *16th Symposium on Boundary Layers and Turbulence*, Fundamental studies of turbulence: observations, theory, and models session (Amer. Met. Soc., Portland, ME, 2004) p. article 7.1.

[23]J. Kaimal and J. J. Finnigan, *Atmospheric Boundary Layer Flows* (Oxford University Press, 1994) p. 304.

[24]S. Liu and X.-Z. Liang, "Observed diurnal cycle climatology of planetary boundary layer height," J. Climate **23**, 5790–5809 (2010).

[25]M. Kelly and S.-E. Gryning, "Long-term mean wind profiles based on similarity theory," Boundary-Layer Meteor. **136**, 377–390 (2010).

[26]ISO 9613-2:1996(E), "Attenuation of sound during propagation outdoors. Part 2: General method of calculation." Standard (International Organization for Standardization, 1996).

[27]K. Kaliski and E. Duncan, "Propagation modeling parameters for wind power projects," Sound and Vibration **42**, 12–14 (2008).

[28]J. Kragh and B. Plovsing, "Nord2000. comprehensive outdoor sound propagation model. part I–II." DELTA Acoustics and Vibration Report 1849–1851/00, 2000 (Danish Electronics, Light and Acoustics, 2001).

[29]E. Salomons, D. van Maercke, J. Defrance, and F. de Roo, "The HARMONOISE sound propagation model," Acta Acustica United With Acustica **97**, 62–74 (2011).

[30]C. R. Hart, N. J. Reznicek, D. K. Wilson, C. L. Pettit, and E. T. Nykaza, "Comparisons between physics-based, engineering, and statistical learning models for outdoor sound propagation," Journal of the Acoustical Society of America **139**, 2640–2655 (2016).

[31]M. West, K. Gilbert, and R. A. Sack, "A tutorial on the parabolic equation (PE) model used for long-range sound propagation in the atmosphere," Applied Acoustics **37**, 31–49 (1992).

[32]D. K. Wilson, J. M. Noble, and M. A. Coleman, "Sound propagation in the nocturnal boundary layer," J. Atmos. Sci. **60**, 2473–2486 (2003).

[33]E. Barlas, W. J. Zhu, W. Z. Shen, K. O. Dag, and P. J. Moriarty, "Consistent modelling of wind turbine noise propagation from source to receiver," J. Acoust. Soc. Am. **TBA**, TBA (2017).

[34]E. Barlas, W. J. Zhu, W. Shen, and S. J. Andersen, "Wind turbine noise propagation modelling: An unsteady approach," Journal of Physics: Conference Series–The Science of Making Torque from the Wind **753**, 022003 (2016).

[35]E. Barlas, W. J. Zhu, W. Z. Shen, M. Kelly, and S. J. Andersen, "Effect of wind turbine wake on atmospheric sound propagation," Applied Acoustics **122**, 51–61 (2017).

[36]A. Sogachev, G. Menzhulin, M. Heimann, and J. Lloyd, "A simple three-dimensional

canopy-planetary boundary layer simulation model for scalar concentrations and fluxes," Tellus **54**, 784–819 (2002).

[37]M. Kelly and I. Troen, "Probabilistic stability and "tall" wind profiles: theory and method for use in wind resource assessment," Wind Energy **19**, 227–241 (2016).

[38]The variability in stability is $\sigma_{\pm}$ =...

[39]A. Sogachev and M. Kelly, "Consistent two-equation closure modelling for atmospheric research: Buoyancy and vegetation implementations," Boundary-Layer Meteorology **145**, 307–327 (2012).

[40]D. C. Wilcox, *Turbulence Modeling for CFD* (DCW Industries, La Cañada, Calif./USA, 1994) p. 460.

[41]N. Troldborg, N. Srensen, P.-E. Rthor, and P. van der Laan, "A consistent method for finite volume discretization of body forces on collocated grids applied to flow through an actuator disk," Computers & Fluids **119**, 197–203 (2015).

[42]K. Attenborough, "Acoustical impedance models for outdoor ground surfaces," J. Sound Vib. **99**, 521–544 (1985).

[43]K. Attenborough, "Sound propagation close to the ground," Annual Reviews of Fluid Mechanics **34**, 51–82 (2002).

[44]The temperature in the different runs varies from 16° to 30° along the propagation path of a receiver at 2 m height, but this results in only a 0.2 dB difference on the overall SPL, due to the source power levels dominated by the low frequencies.

[45]S. Oerlemans, P. Sijtsma, and B. M. López, "Location and quantification of noise sources on a wind turbine," Journal of sound and vibration **299**, 869–883 (2007).

[46]A. D. Pierce, *Acoustics: an introduction to its physical principles and applications* (Acoustical Society of America through the American Institute of Physics, 1994) pp. xxv+678.

[47]J. A. Businger, J. C. Wyngaard, Y. Izumi, and E. F. Bradley, "Flux-profile relationships in the atmospheric surface layer," J. Atmos. Sci. **28**, 181–189 (1971).

[48]M. Kelly, I. Troen, and H. E. Jørgensen, "Weibull-k revisited: 'tall" profiles and height variation of wind statistics," Boundary-Layer Meteor. **152**, 107–124 (2014).

Chapter 5

Consistent Modelling of Wind Turbine Noise Propagation

5.1 Chapter Overview

So far the focus of the thesis has been on the atmospheric effects on sound propagation. However, the issue that we are addressing is the wind turbine noise and its variation. This variation is a result of both the constant change in source levels (due to the interaction of the rotating blades and the turbulent inflow and changes in operating conditions) and the unsteady and inherently random propagation through turbulent atmosphere.

The corresponding publication in this chapter (Sec. 5.2) addresses this issue with a new model that combines the modelling of wind turbine noise generation and propagation. The main objective is to propose a model that takes into account both phenomena consistently in an unsteady and quasi three dimensional manner. First, the models are introduced and the coupling procedure is explained in detail. Second, the simulations are carried out for two different hub height wind speeds and surface roughness values. The results are presented mostly in a differential way (difference in source only and coupled source-propagation simulations) to underline the effects of propagation on both time averaged and time dependent results. The possible explanations for the increased far field modulation levels are discussed and attributed to the wind turbine blade rotation and unsteady wake dynamics.

5.2 Publication

Consistent Modelling of Wind Turbine Noise Propagation from Source to Receiver

Emre Barlas[b], Wei Jun Zhu[a],* Wen Zhong Shen[b], and Kaya O Dag[b]
[a] *School of Hydraulic, Energy and Power Engineering, Yangzhou University, CN*
[b] *Dept. of Wind Energy, Technical University of Denmark, Kgs. Lyngby, 2800 Denmark*

Patrick Moriarty[c]
[c] *National Wind Technology Center, National Renewable Energy Laboratory, CO, USA*
(Dated: October 13, 2017)

The unsteady nature of wind turbine noise is a major reason for annoyance. The variation of far-field sound pressure levels is not only caused by the continuous change in wind turbine noise source levels but also by the unsteady flow field and the ground characteristics between the turbine and receiver. To take these phenomena into account, a consistent numerical technique that models the sound propagation from the source to receiver is developed. Large eddy simulation with an actuator line technique is employed for the flow modelling and the corresponding flow fields are used to simulate sound generation and propagation. The local blade relative velocity, angle of attack, and turbulence characteristics are input to the sound generation model. Time-dependent blade locations and the velocity between the noise source and receiver are considered within a quasi 3D propagation model. Long-range noise propagation of a 5 mega-watt wind turbine is investigated. Sound pressure level time series evaluated at the source time are studied for varying wind speeds, surface roughness, and ground impedances within a 2000 m radius from the turbine.

PACS numbers: PACS: 43.30.Vh, 43.60.Ac, 43.60.Bf, 43.60.Hj

I. INTRODUCTION

As a result of increasing demand for renewable energy, fewer suitable land-based sites are available for wind farms. Given that noise is a primary obstacle for gaining broad public acceptance, the accurate noise assessment of wind turbines is a necessity. Accurate predictions of far-field wind turbine noise require the knowledge of the source levels and a realistic representation of the medium between the turbines and the receivers in which the sound propagation takes place. This is a complex task as both phenomena depend on a wide range of parameters.

The classical approach for far-field noise predictions assumes an overall source power level for a wind turbine dependent on its rotor diameter (RD) and uses a propagation relationship based on hemispherical spreading. Even though this approach neglects many physical processes, it has been the standard for some years [1]. A more advanced method is the Nord2000 that uses a semianalytical ray tracing model that models refraction effects using a linear approximation for the sound speed profile [2]. There are other corrections applied for undulating terrain and ground impedance. Even though this model was demonstrably more accurate than many other models [3], there are certain shortcomings. For example, the source model is a monopole at hub-height used to represent the wind turbine irrespective of RD and the source strength is independent of the inflow conditions. The ray tracing method has been used for predicting noise from single wind turbines as well as wind farms in Refs. [4, 5]. Effects of various parameters, such as wind direction, ground impedance, and turbulence, were studied. Moreover, full-scale meteorological experiments and micro-scale models were used as input for the ray-tracing model and the effects of wakes were investigated [6]. Apart from the ray-tracing models, the parabolic equation (PE) method has also been used to address far-field wind turbine noise. Results obtained from the PE method were compared with various engineering models in Ref. [7] and suggestions for further research, such as realistic source representation and inclusion of terrain, were proposed. Flow fields obtained from Reynolds-averaged Navier-Stokes simulations were incorporated with the PE method in Ref. [8] and the variation of the wake effects on far-field noise for different incoming shears were studied. A similar methodology was employed in Refs. [9, 10] using large eddy simulation (LES) flow fields with unsteady source representation. While high-fidelity models used in these studies modelled the propagation physics more accurately, they did not consider the source characteristics in detail.

A commonly used method to model the wind turbine noise source was described in Refs. [11, 12]. The method divides the wind turbine blades into airfoil segments and sums the contribution of each segment's noise levels calculated using semiempirical relationships. This source model along with simple propagation calculations were used in Ref. [13] and the results were compared to near-field experiments. A similar source model was employed and coupled with the ray-tracing method in Ref. [14]. Even though these models represented the source more accurately, the propagation effects were not well studied.

The aforementioned models tend to focus on one side of the phenomenon (i.e., either a detailed source rep-

* wjzhu@yzu.edu.cn

resentation is used but propagation physics are disregarded or the opposite.) Another major shortcoming of most modelling techniques is their steady nature. Listening room experiments [15–17] and dose-response relationship studies [18, 19] showed a correlation between the source unsteadiness and the annoyance, particularly for wind turbines. Additionally, field experiments emphasized the considerable modification of far-field noise levels and characteristics under various atmospheric conditions [20, 21]. A recent study showed qualitative results relating the wind direction and the number of complaints received from various wind farms [22]. They highlighted that the downwind receivers, who characterized the noise as thumping, were the most annoyed for distances greater than 2.5 km.

Although previous field experiments have underlined the effect of atmospheric conditions, the existing prediction tools do not consider the complicated flow around wind turbines and its effect on sound generation and propagation. There is a need for a model that includes the interaction between the incoming turbulent flow and the wind turbine, and the propagation physics consistently. The modular methodology proposed in this article attempts to fill the aforementioned gap. Here, the name "modular" refers to the fact that the models are loosely coupled such that the flow, source, and propagation models can be replaced with alternatives in the future. The technique uses a sound-generation model based on semiempirical modelling of airfoil noise within an aeroelastic tool and a propagation model based on the PE method. LES with an actuator line (AL) technique is employed for flow modelling. Using the LES flow fields as inputs to the aeroelastically coupled aeroacoustic simulations provides the ability to model wind turbine noise generation including its structural dynamics and interaction with the incoming turbulent flow. Although the aeroacoustic source models were obtained with the assumption of rigid bodies, the angle of attack change due to the flexibility of the blade is considered in the model. The constant change in the source levels and the spectral characteristics due to interactions between rotating blades, unsteady inflow, and turbine operational conditions can be taken into account. After each time step of the source calculation, each blade is represented with a single point source within the PE domains and independent simulations are carried out for each receiver. This approach ensures that the directivity, source strength, and realistic flow field between the source and receiver are taken into account. Using the time-dependent flow fields and source locations and strengths, successive PE simulations are conducted. Subsequently, the near- and far-field noise levels of a 5 MW wind turbine for different incoming shear values and wind speeds are investigated.

The article is organized as follows. Section II describes the numerical methods and gives details about their implementation. Section III provides the modular methodology. Results are presented in Sec. IV, which is followed by the conclusions in Sec. V.

II. NUMERICAL METHODS

In this study, the National Renewable Energy Laboratory (NREL) 5 MW reference wind turbine is used. The wind turbine has a rotor diameter of 126 m and a hub-height of 90 m. The structural and aerodynamic characteristics of the wind turbine are detailed in Ref. [23] and the necessary inputs are released with FAST v8 simulation tool [24]. The controller is not used because the rotational speed of the wind turbine is kept constant at 7.8 rpm and 10.17 rpm for a 6 m/s and 9 m/s hub-height wind speed, respectively. The next three subsections detail the flow, source, and propagation models.

A. Flow model

The Technical University of Denmark's (DTU) pseudo-spectral incompressible Navier-Stokes solver is used to model the flow around the wind turbine [25]. The code solves the filtered continuity and momentum conservation equations in three-dimensional (3D) form with the Smagorinsky subgrid scale model [26]. The flow is driven by a pressure gradient wherein the turbulence is maintained solely because of shear stresses rather than buoyancy forces. This will also impact the sound propagation model as the temperature distribution, and thus the speed of sound is assumed to be constant. To capture the desired boundary layer characteristics, a wall model is applied at the bottom boundary. With this setup, the simulations are run until the boundary layer is established for a given hub-height wind speed (U_h) and a surface roughness value (z_0). After this and with the same initial conditions, two simulations are conducted with and without the turbine for each case listed in Table I.

The wind turbine rotor is modelled via the AL technique [27], in which a body force distributed along the blade 'lines' are used to represent the rotor blades. The AL technique is an efficient method to mimic the effect of wind turbines on the flow. It utilizes the tabulated airfoil lift and drag coefficients and the instantaneous velocity fields to determine the blade forces. Comparisons with field and wind tunnel experiments showed that the AL simulations can capture the wind turbine blade loading as well as the flow around it within an acceptable accuracy [28, 29].

To avoid the downwind flow affecting the flow upwind of the wind turbine due to periodic boundary conditions in the horizontal direction, a buffer zone is applied to smoothly adjust the flow from the very-far-wake downwind to that of the precursor simulation. Figure 1 shows a snapshot of the streamwise velocity in Case 1 interpolated onto slices at five azimuthal angles between the turbine and the selected receiver locations.

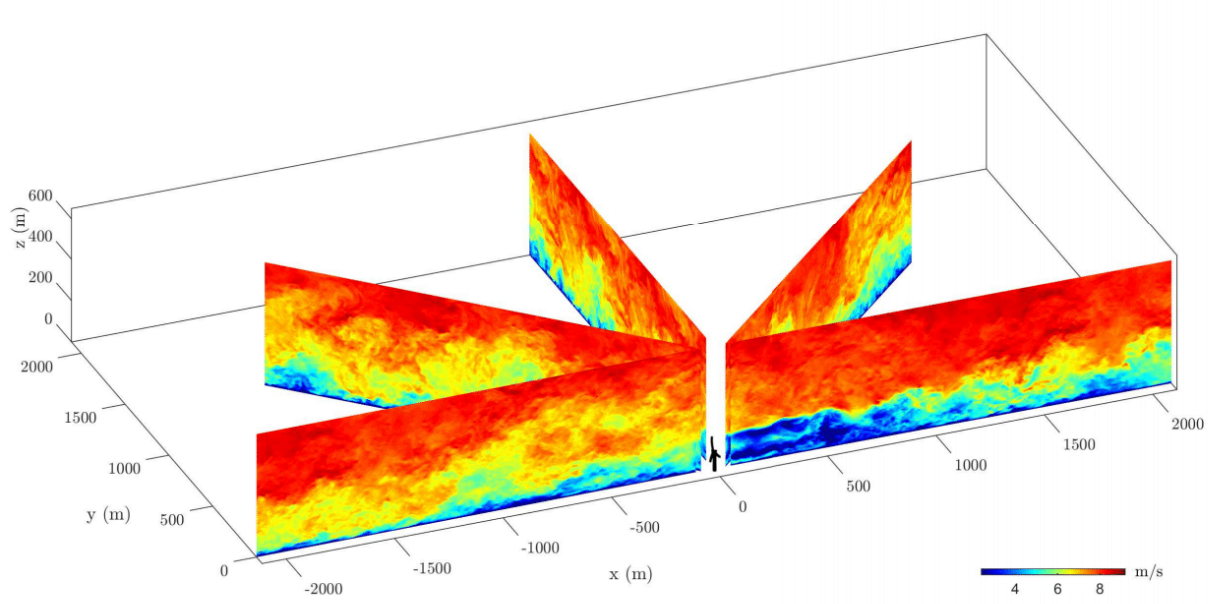

FIG. 1. (Color online) Snapshot of the streamwise velocity in Case 1 for five azimuthal angles used for propagation calculations.

TABLE I. Numerical setup for the flow simulations. Grid points and spacing are tabulated in the streamwise, lateral, and vertical directions, respectively.

	$N_x \cdot N_y \cdot N_z$	$\Delta_x \cdot \Delta_y \cdot \Delta_z$ (m)	z_0(m)	U_h(m/s)
Case 1	800×200×300	4 × 4 × 2	0.5	6
Case 2	800×200×300	4 × 4 × 2	0.005	6
Case 3	800×200×300	4 × 4 × 2	0.5	9
Case 4	800×200×300	4 × 4 × 2	0.005	9

B. Aerodynamic noise source model

For the wind turbine noise source model, we use an aeroacoustics module based on NREL AirFoil Noise (NAFNoise) code [30] within the FAST v8 modular framework. In this article, we call this integrated code FAST v8+AA (aeroacoustics), which allows the modelling of aerodynamic noise generated by the blades in consideration of wind turbine structural dynamics and its interaction with the incoming turbulent flow. Using the blade element theory, each blade is divided into a number of two-dimensional (2D) airfoil elements. The total noise level at a given receiver location is predicted as the sum of the contributions from all the blade elements. This prediction method implicitly assumes that the noise generation mechanisms for all blade elements and all models are uncorrelated. Limitations of this assumption were investigated in Ref. [31], in which a correction method for 3D correlation was proposed. Considering that the span-over-chord ratio for each element is around 1.5 in the outer part of the blade, the error caused by this assumption does not exceed 2 dB for 20 Hz and decreases with frequency (negligibly small for frequencies above 100 Hz). Because it is rather complicated to calculate sound pressure levels (SPL) with 3D correlated formulae, we use the uncorrelated version in this study. Furthermore, it is worthwhile to mention that the convective amplification and Doppler effects are not taken into account in the present model.

Figure 2 shows a snapshot of the flow field that the turbine is exposed to, two selected receivers, and the symbolic rays traced from the blade elements. For each element and time step, the local angle of attack and relative velocity are output from the aeroelastic solver. The changing angle of attack and the turbulence intensity are the main contributors of the noise modulation. The time-averaged angle of attack in the rotor area is shown in Fig. 3. The vertical wind shear is the dominant factor causing the angle of attack variation and Case 1 has a more drastic change over one revolution than Case 2. In addition, there is an asymmetry along the y axis because of a relatively small horizontal wind shear and the effect of the tower on the incoming flow.

In the present study, only two types of aerodynamic noise have been included: turbulent boundary layer trailing-edge and turbulent inflow noise. The models and methods used for obtaining the necessary inputs are explained below.

1. *Turbulent boundary layer trailing-edge noise (TBLTE):*

The total SPL of noise generated from the interaction of the turbulent boundary layer with the trailing edge is

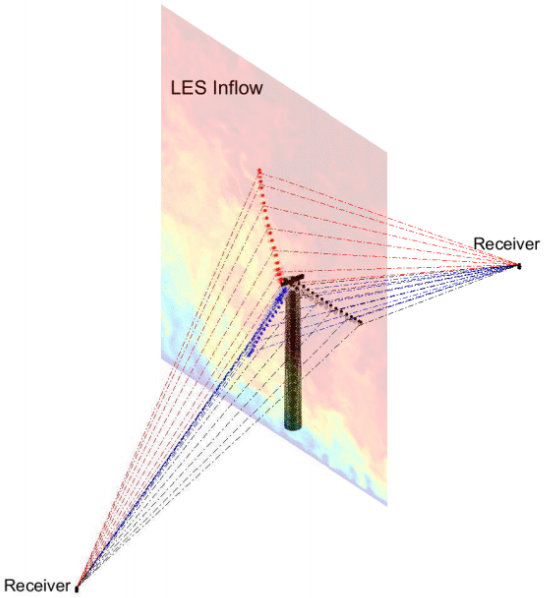

FIG. 2. (Color online) Schematic of the wind turbine noise-generation model and inflow. Each airfoil segments' noise contribution is summed up at each receiver location.

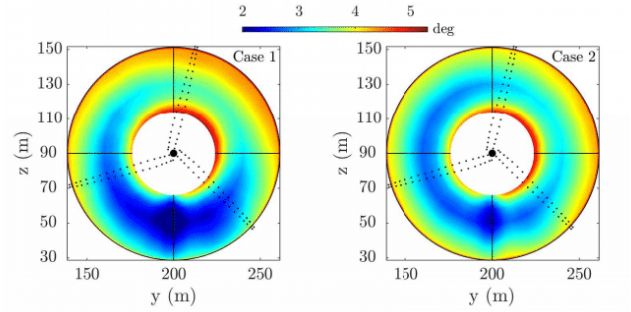

FIG. 3. (Color online) Time-averaged angle of attack at the rotor plane for Case 1 (left) and Case 2 (right).

calculated through the summation of the different contributions of noise on the pressure side, the suction side, and angle-dependent noise. These three noise mechanisms can be modelled semiempirically using scaling laws (see Brooks, Pope, and Marcolini (BPM) [32]). Different from the classical BPM noise generation model, the boundary layer characteristics in this study are obtained from Q^{3}UIC (DTU's viscous-inviscid interactive boundary layer flow solver), which is more accurate than XFOIL (a viscous-inviscid interactive code for subsonic isolated airfoils) [33]. For a range of Reynolds numbers and angles of attack, the boundary layer thickness values are calculated and used as inputs to FAST v8. At each time step, each blade element's boundary layer thickness is interpolated for the corresponding airfoil, local angle of attack, and Reynolds number. Additionally, the angle of attack values used for the separation flag (a conditional switch used in the classical BPM model) is modified according to the lift coefficient curves of the blade airfoils used.

2. *Turbulent Inflow Noise:*

The turbulent inflow noise model developed in Refs. [34, 35] is used for inflow noise estimation, including a correction for airfoil thickness proposed in Ref. [36]. The turbulence intensity (TI) is calculated by taking into account the inflow characteristics obtained from the flow simulations (Sec. II A) and instantaneous airfoil locations. First, TI is calculated in the 2D plane at 1 RD upstream of the turbine for each 10-minute data set and stored. This calculation is used as input to FAST v8 and then at each time instant the TI value at each airfoil location is interpolated and assigned. The integral turbulent length scale (L) is calculated using the relationship in Ref. [37] that can be expressed as a function of a nondimensional roughness parameter, α_r, and height, z: $L = 25z^{0.35}\alpha_r^{-0.063}$. A more up-to-date expression for length-scale distribution with height can be found in Ref. [38]. However, in this study we consider only the given expression with the α_r values 0.01 and 0.2 to represent open sea flat terrain and open country, respectively.

As explained in Sec.II A, the flow solver models only the shear-generated turbulence. This approach results in higher turbulence levels for higher shear cases. Figure 4 shows the averaged streamwise velocity and TI for Cases 1 and 2. The corresponding SPL spectra for a ground-level receiver 2 RD downstream of the turbine are depicted in Fig. 5. It is observed that the low-frequency content (below 130 Hz) is dominated by the turbulent inflow noise. Therefore, Case 1 levels are higher than those in Case 2 within this frequency range. The other dominant noise source is from the TBLTE suction side. It dominates the midrange frequencies (between 200 Hz and 800 Hz). The difference between the two cases in this frequency range is negligibly small. This observation is in line with Ref. [39]. While the incoming shear is not that effective on sound generation, it has a significant effect on sound propagation, thus the far-field levels [40]. This effect will be investigated in detail in Sec. IV.

C. Sound propagation model

For the sound propagation modelling, we use DTU's WindSTAR-Pro (Wind turbine Simulation Tool for AeRodynamic Noise Propagation). The tool implements a variety of 2D PE models in a FORTRAN environment with a message passing interface parallelization strategy

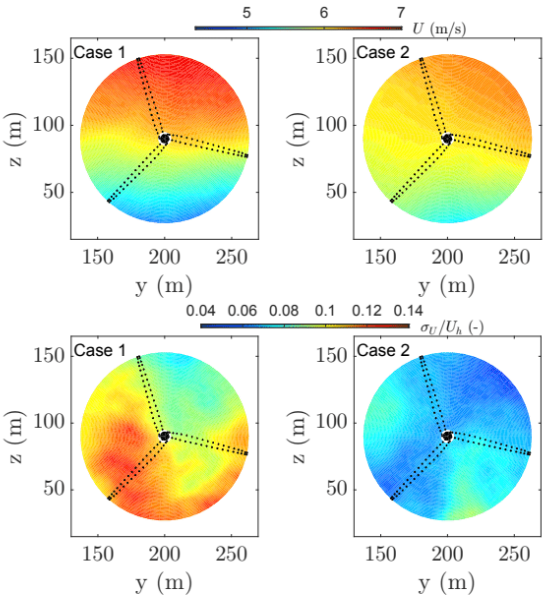

FIG. 4. (Color online) Time-averaged streamwise velocity (top) and turbulence intensity (bottom) at 1 RD upstream of the turbine for Case 1 and Case 2.

in frequency and realization/time step. The code has been validated and used for various propagation calculations in Ref. [9]. In this study, the two-dimensional, wide-angle, Crank-Nicholson, parabolic equation is used with the starter function and the implementation details given in Ref. [41]. The method uses the effective speed of sound approach wherein the moving atmosphere is replaced by a hypothetical motionless medium with an effective sound speed $c_{\text{eff}} = c + v_x$, where v_x is the wind velocity component along the direction of propagation between the source and receiver [42]. In this study, the speed of sound is kept constant ($c(x, z) = 340$ m/s) in the whole domain, and the propagation phenomena (i.e., refraction, diffraction, scattering) is solely due to the wind speed and its fluctuations around the wind turbine. This approach is representative of a neutrally stratified atmosphere on a day with high wind or thick cloud layers [43]. Figure 6 shows the time-averaged effective sound speed profiles at multiple locations in the midvertical plane obtained from the simulations listed in Table I. It is observed that each case has a distinct shear even though the hub-height wind speeds are the same for the first two and last two. Additionally, for the same surface roughness increasing the hub-height wind speed from 6 m/s to 9 m/s results in increasing shear. It is clear that Cases 3 and 4 have higher shear values than Cases 1 and 2, respectively. While the upstream profiles are the main parameters for the upwind propagation characteristics, the wake evolution is the determining factor for the downwind propagation (see Sec. IV).

For the Crank-Nicholson parabolic equation calculations, the spatial resolution in both directions is set to one-eighth of the wavelength ($\Delta x = \Delta z = \lambda/8$, where λ is the wavelength of the considered frequency). Only flat terrain is considered and the ground impedance is characterized using the four-parameter model proposed in Ref. [44] with effective flow resistivity of 200 kPas/m^2 and $200 \cdot 10^4$ kPas/m^2; representative values for grassland and hard ground, respectively. These two ground covers were selected to define land-based and offshore conditions. The latter is important because the noise from offshore wind farms can be audible in long distances, as a result of hard ground and various atmospheric phenomena [45]. The other parameters of the impedance model are kept constant: pore shape factor ($s_p = 0.75$), Prandtl number ($N_{Pr} = 0.72$), grain shape factor ($n' = 0.5$), porosity ($\Omega = 0.3$), ratio of specific heats ($\gamma = 1.4$), and density ($\rho = 1.19$ kg/m^3).

All simulations are carried out for 1/3-octave band centre frequencies from 20 Hz to 800 Hz, because the frequencies above have a negligible contribution (less than 0.1 dB for Case 1 calculations) to the overall SPL due to atmospheric absorption as well as the dominant part of the spectra shown in Fig. 5. The corresponding sound pressure levels in each band are summed logarithmically to obtain the overall SPL:

$$Lp_{sum} = 10\log_{10}\Big(\sum_{i=1}^{N} 10^{Lp(f_i)/10}\Big). \tag{1}$$

Here, N is the number of frequencies used and $L_p(f_i)$ is the sound pressure level defined as:

$$L_p(f_i) = L_W(f_i) - 10\log_{10}(4\pi R^2) - \alpha(f_i)R + \Delta L(f_i), \tag{2}$$

where the first two terms on the right-hand side (source power level and geometrical spreading) are obtained from the source model explained in Sec. II B for each receiver location. The third term represents the atmospheric absorption wherein the absorption coefficient is calculated according to International Standards Organization 9613-1 for air at 20°C with 80% relative humidity. The last term is the relative SPL that represents the deviation of a source from the free field as a result of ground and atmospheric effects. This last term is calculated using the PE method. Figure 7 shows a schematic of nine 2D PE domains from three blades to three receiver locations at one time instant. For each frequency and receiver, each blade is modelled as a monopole source, depicted with the red spheres in the figure.

III. MODULAR METHODOLOGY

This section is devoted to the explanation of the modular methodology that allows for a loose coupling of the

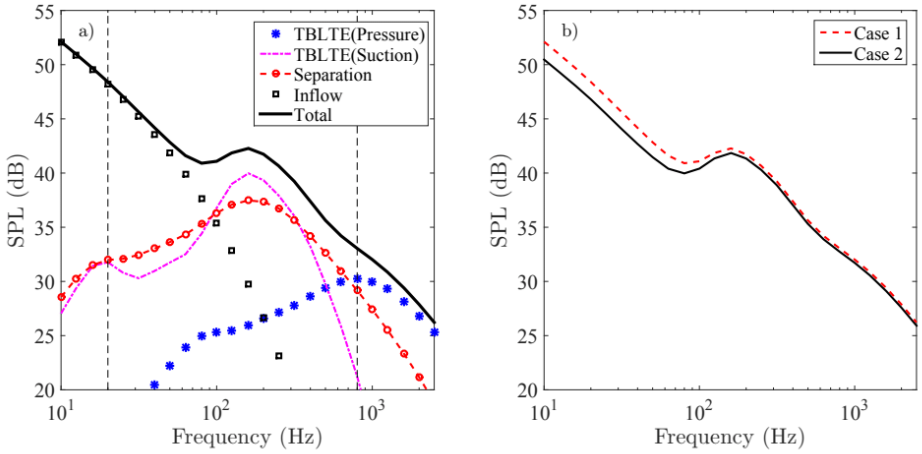

FIG. 5. (Color online) Time-averaged SPL spectra obtained from the FAST v8 calculations 2 RD downwind of the turbine. Left: Various noise source mechanisms for Case 1. Right: Comparison of Case 1 and 2.

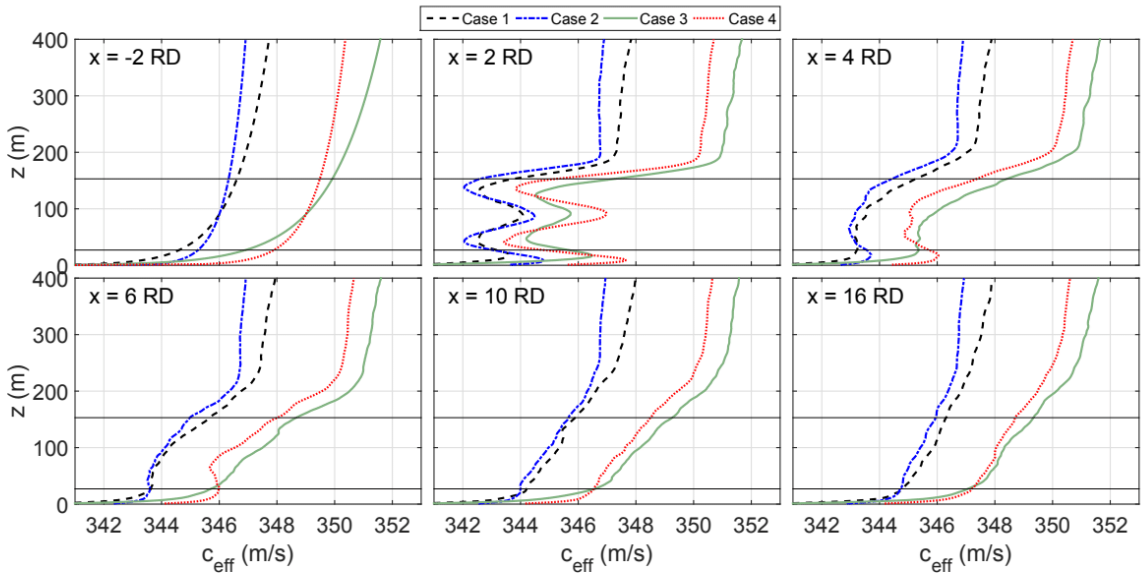

FIG. 6. (Color online) Time-averaged effective sound speed profiles for four cases listed in Table I at multiple locations. Horizontal black lines represent the bottom and top tip height of the wind turbine.

three models explained in Sec. II.

1. First, the flow field is simulated using LES. A 2D slice in spanwise and vertical directions (y-z slice) 1 RD upstream of the wind turbine is stored at each time step (0.02 s) to be used as input for the source simulations. The entire 3D flow field is also stored with a sampling frequency of 10 Hz to be used for propagation simulations.

2. The flow field sampled upstream of the turbine is used as input to FAST v8, forcing a fully aeroelastic turbine to a realistic atmospheric flow. While the time step used in the aeroelastic simulations is 0.02 s, the integrated aeroacoustic module is called every 0.1 s. The smaller time step for the aeroelastic simulations is due to the FAST v8 stability requirements. Additionally, we observe that a 10 Hz resolution for the aeroacoustic source simulations is sufficient because higher frequency content is calculated semiempirically.

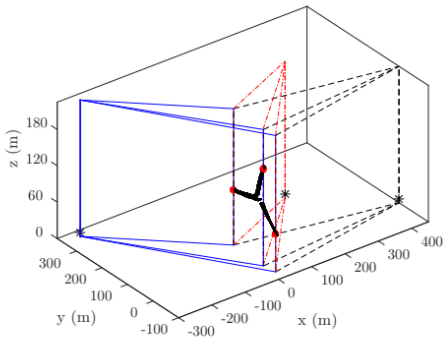

FIG. 7. (Color online) Schematic of nine 2D PE domains from three blades to three receivers at one time instant. Red spheres around the blade tips represent sample source locations for a single frequency. The black stars represent the receiver locations at a 2 m height.

3. Frequency-dependent sound pressure levels at receiver locations are calculated and stored via the integrated aeroacoustics module in FAST v8. In total, 75 receiver locations are distributed over 5 propagation angles from 0° to 180° with 45° increments (see Fig. 8). Along each propagation angle, 15 locations are chosen, from 252 m (2 RD) to 2016 m (16 RD) from the turbine.

4. At these receiver locations, the coordinates of the element with the largest frequency-dependent SPL magnitude along the blade are stored, enabling the frequency and blade-dependent source localization.

5. A 2D PE domain is constructed between each blade and each receiver based on the detected source locations (shown in Fig. 7). While only one element for each blade is represented in the propagation model, the source power levels of the whole blade are used as the L_W term in Eq. 2 for each 2D PE. The reasons for using only one blade element instead of all of them are threefold: a) the dominant noise source of a wind turbine blade lies around the tip region due to its high speed, b) for a far-field receiver it is hard to distinguish blade elements independently, c) using a fewer number of elements decreases the computational time significantly. The effective sound speed is obtained by interpolating the flow field and projecting along the propagation planes.

6. At each time step, 2D PE simulations are carried out for 3 blades, 17 frequencies, and 75 receivers (total of 3825 calculations). This procedure is repeated 6000 times (a 10-minute simulation with 0.1 s time resolution) using the time-dependent flow fields, source locations, and strengths for the four flow cases listed in Table I and for two ground covers (grassland and hard ground).

For each case, approximately 23 million independent propagation simulations are executed. The computational time required for sound propagation is 5000 processor hours. The flow solver requires 6000 processor hours after establishing the desired boundary layer. The stored flow fields are used for propagation simulations with various ground covers.

It is worthwhile noting that the SPL obtained from the successive PE simulations are evaluated at the source time. Even though the receiver time is the most common for noise measurements, it is disregarded in this paper. The term "time-dependent SPL" is used to refer to the PE output. Additionally, the simulations that follow the six-step procedure are referred to as "coupled simulations" from now on.

Figure 8 shows a snapshot of the overall SPL obtained from the coupled simulations for Case 1. The contour plot is obtained via linear interpolation of the results on an equidistant grid with 20 m radial and 2 degree azimuthal spacing. It is observed that the noise directivity of the wind turbine is well captured, considering the crosswind levels are significantly lower than the upwind and downwind levels. This point will be elaborated in the following sections. Additionally, it is also observed that even though the downwind and upwind levels have initially similar values, the atmospheric effects take over after a certain distance at which the upwind levels become much lower than the downwind ones.

IV. RESULTS

Using the methodology explained in Sec. III, three sets of calculations are carried out as described below.

1. Source-only simulations ($\mathrm{SPL_S}$): Output of FAST v8+AA at various receiver locations are stored including the impact of the atmospheric absorption. The last term in Eq. 2 is neglected (i.e., the propagation effects).

2. Source and propagation over a grassland simulation ($\mathrm{SPL_{S+P_G}}$): Coupled source and propagation simulations with a ground impedance value that is representative of a grassland. The 3D flow field is incorporated as explained in Section III.

3. Source and propagation over hard ground simulations ($\mathrm{SPL_{S+P_{HG}}}$): Coupled source and propagation simulations with a ground impedance value that is representative of a fully reflective hard ground. The 3D flow field is incorporated as explained in Section III.

Note that, unless stated otherwise, the results show overall sound pressure levels summed from 20 Hz to 800 Hz.

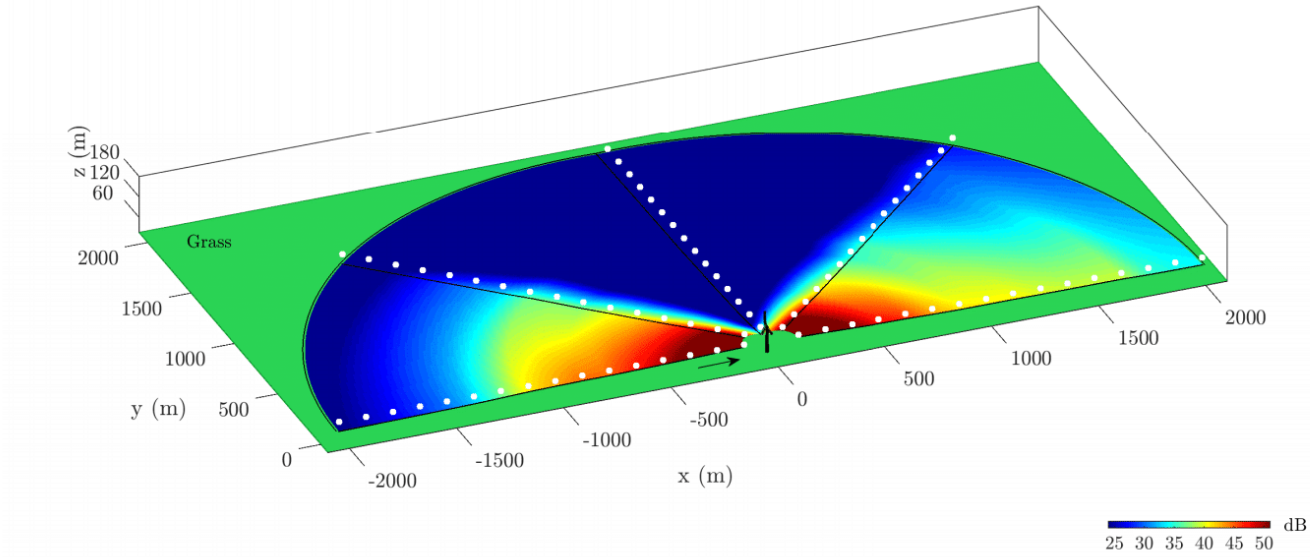

FIG. 8. (Color online) Snapshot of the overall SPL at a 2 m receiver height for flow Case 1 obtained from the coupled simulation. White dots represent the receiver locations. The arrow shows the wind direction.

A. Time-averaged results

First, the output obtained from the source-only simulations (SPL_S) is investigated. Figure 9 shows the time-averaged SPL for Case 1. It is observed that the levels upwind and downwind of the turbine are considerably higher than the crosswind levels (approximately 25 dB). This pattern is caused by the wind turbine noise directivity and is observed for all cases listed in Table I. However, this result differs from field experiments in Refs. [46, 47], which show that the difference between the crosswind and downwind levels do not exceed 7 dB. The mismatch between the model output and the experiments is due to many reasons, such as background noise, binning of the wind direction (i.e., $\pm 10°$) to represent the crosswind results, and inaccuracy of the directivity functions used in calculations. Nevertheless, because the main focus of our work is the propagation effects on wind turbine noise, this large difference due to directivity is not further investigated.

Note that SPL_S includes only the atmospheric absorption and geometrical spreading for the propagation. As a result, the sound pressure levels decrease with distance equally upwind and downwind of the turbine. This pattern changes when the atmospheric propagation effects are considered.

Figure 10 shows the time-averaged output obtained from the coupled simulations (SPL_{S+P_G}). Similar to Fig. 9, the SPL in the crosswind direction is less than

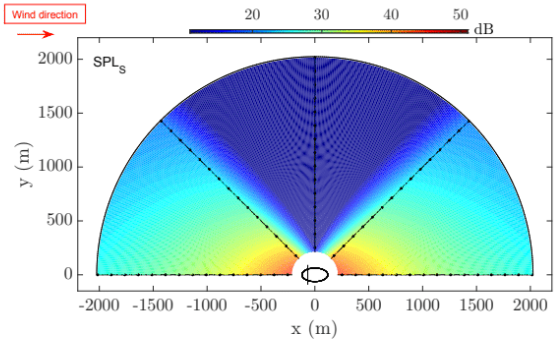

FIG. 9. (Color online) Top view of the time-averaged SPL_S at a 2 m receiver height for Case 1. The black points represent the receiver locations.

that in the downwind or upwind directions. Different than Fig. 9, the upwind levels are lower than the downwind levels after a certain distance.

A more detailed comparison of all cases is depicted in Fig. 11, which shows the average upwind and downwind SPL_{S+P_G} for the grassland. It follows from the figure that the SPL at the first receiver location for Cases 1 and 2 are approximately 9 dB lower than Cases 3 and 4 in either direction. This is an expected result, because the rotational speed of the wind turbine increases with the increasing wind speed within this operation range. Subsequently, the tip speed increases from 51 m/s to

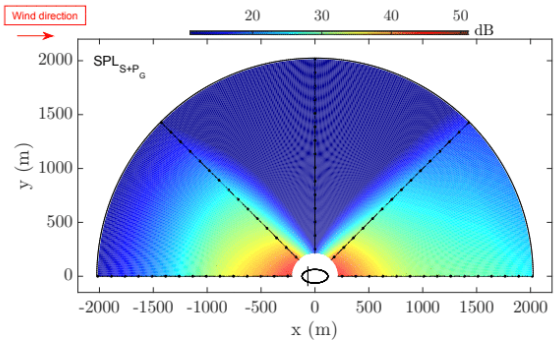

FIG. 10. (Color online) Top view of the time-averaged SPL_{S+P_G} at a 2 m receiver height for Case 1. The black points represent the receiver locations.

66 m/s, which results in increased sound pressure levels. Also note that $SPL_{S+P_{HG}}$ has a similar averaged footprint, though not shown here. Furthermore, for the same hub-height wind speed, it is observed that an increase in shear causes a slight increase (approximately 1 dB) in source levels at the closest receiver location, 2 RD away from the turbine. This result was discussed and attributed to the increased turbulent inflow noise in the low-frequency content in Sec. II B.

Figure 11 shows the A-weighted SPL, which decreases the SPL considerably, because the low-frequency content dominates the overall levels (see Fig. 5). However, the trends of the weighted and unweighted SPL distributions with distance are very similar. Because the focus of the study is on the propagation effects only, the unweighted results are reported further.

The small SPL differences between different shears in the near field vary significantly with distance depending on the atmospheric conditions. To isolate the propagation effects, the differences in SPL values are depicted in Fig. 12. Δ_{SPL_G}=SPL_{S+P_G}-SPL_S for the grassland case and $\Delta_{SPL_{HG}}$=$SPL_{S+P_{HG}}$-SPL_S for the hard ground case are shown. In all the subplots, Δ_{SPL_G} is the top and $\Delta_{SPL_{HG}}$ is the bottom half domain.

We start with the common features of all the flow cases. First, it is observed that $\Delta_{SPL_{HG}}$ values are consistently higher than Δ_{SPL_G}. This is due to the more absorbing character of grassland than the hard ground. The SPL difference between two ground covers for the same flow case increases with distance. The difference values reach approximately 6 dB for the overall SPL at a 2 km distance.

Second, it is observed that the higher the shear, the earlier the shadow zones start upwind of the turbine (see Figs. 12a and 12b). Additionally, for the same shear, the shadow zones are larger for higher frequencies (see Figs. 12e and 12m). These observations are in line with field experiments in Refs. [49, 50] and other numerical simulations in Refs. [42, 51]. These phenomena are captured only with the coupled model, thus negative Δ_{SPL} values are seen in these regions in Fig. 12. Even though these zones are insonified because of diffraction and scattering (depending on the turbulence scales and acoustic wavelength [48]), the time-averaged levels of the coupled simulations are consistently lower than the source-only simulations.

A counterintuitive observation that can be deduced from Figs. 11 and 12 is that the sound pressure levels upwind of the wind turbine are higher than the downwind up to a certain distance. This distance varies with the considered case. For example, the upwind levels are higher than the downwind levels up to 1200 m for Case 1, whereas this value is 950 m for Case 4. This difference is due to the combined effects of refraction and ground reflection/absorption. The spectra at multiple locations are investigated to gain insight for the upwind and downwind SPL difference using one more set of simulations wherein the flow upstream of the turbine is used to simulate the downwind propagation. This means that the effects of the wake are neglected downwind of the turbine, and referred to as "no-wake simulations."

Figure 13 shows the spectra for Case 4. It is observed that for the upwind propagation, the ground caused dips in the near field are much less pronounced than both of the downwind ones. This is the main reason for the high upwind levels. As we get farther away from the turbine, the upwind levels start to decrease and eventually become lower than the downwind ones. Downwind of the turbine the levels obtained from the no-wake simulations are initially higher than the ones including the realistic wake flow. However, after a certain distance the opposite is true. This observation is in agreement with some of the results obtained in Refs. [6, 8, 9]. The main reason for this result is the wake-induced refraction behind a wind turbine, which plays a role similar to a SOFAR channel in underwater acoustics [52], wherein the sound waves are ducted within the minima of the speed of sound. After a certain distance, waves are refracted downwards as the wake recovery takes place. This distance depends mainly on the considered flow case. For example, for Case 1 the wake is not persistent enough because of the high incoming turbulence. Hence, a relatively narrow SPL amplification region (1300 m−1600 m) and low amplification levels are observed (approximately 1 dB). However, for Case 4, in which the turbulence is low, the wake-induced SPL amplification levels reach up to 3 dB and the SPL amplification region is smeared to a larger area (1000 m−2000 m). The wake effects will be investigated with the time-dependent results in the following section.

In Fig. 12a, if we compare the upper and lower half, in the crosswind direction, the increased levels reach up to 8 dB and 4 dB for the hard ground and grassland, respectively. It is also observed that the regions where Δ_{SPL} values are greater than or equal to zero, are longer in the crosswind direction than in the downwind direction for both ground covers (note that this is not valid in the downwind regions with wake-induced SPL

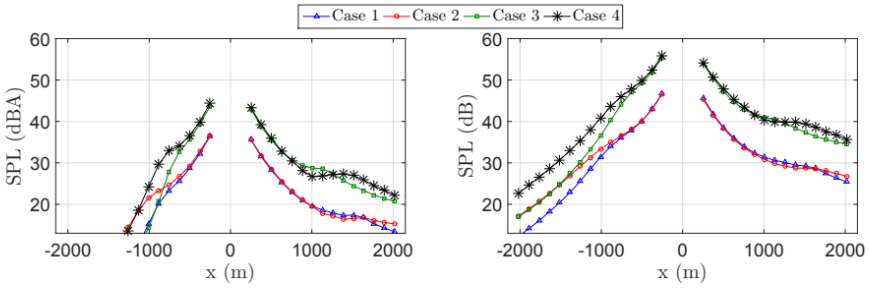

FIG. 11. (Color online) Time-averaged SPL at a 2 m receiver height for the downwind and upwind propagations over the grassland in the cases listed in Table I. Both A-weighted and unweighted results are shown. The turbine is located at x = 0 m.

amplifications explained previously). For the same flow and ground impedance case, the main difference between the Δ_{SPL} values in the crosswind and downwind directions is caused by the flow field. Although sound waves propagate through the wake-induced flow field downwind of the turbine, the crosswind sound waves are affected only by the turbulent perturbations because the mean crosswind velocity is close to zero and we assume a neutral atmosphere in which there is no temperature gradient. This means that the refraction-related propagation effects play a larger role in SPL attenuation in the downwind case than in the crosswind case at certain distances. This outcome does not necessarily mean that the neutral atmosphere causes less attenuation. On the contrary, it highlights the complexity of the propagation phenomena. Nevertheless, because the wind turbine noise is dominated by a dipole emission pattern the overall levels are significantly lower in the crosswind direction than in the downwind direction.

B. Time-dependent results

In this study, the quantification of the wind turbine noise amplitude modulation (AM) is done using the method proposed by the UK Institute of Acoustics Noise Working Group on Wind Turbine Noise Amplitude Modulation. The details of the method can be found in Ref. [53]. Only a brief description of the calculation procedure is given here. The method is based on transforming a SPL time series of 10 s blocks into the frequency domain to detect the blade passage frequency and its next two harmonics. Afterward, some threshold checks are applied (i.e., a harmonic is kept only if its reconstructed time signal has a peak-to-trough ratio bigger than 1.5 dB). The harmonics that pass the threshold checks are used for the conversion from frequency to time domain. Figure 14a shows a sample 10 s block and Fig. 14b shows the power spectrum that is calculated by taking the square of the absolute discrete Fourier transform (DFT), $F(x)$, of the time signal and dividing it by the square of number of points. Figure 14c shows the real part of the DFT for all frequencies (white bars) as well as the ones that are included for reconstructing a new signal after the aforementioned threshold checks (red bars). Figure 14d shows the original and the reconstructed signal. The modulation depth is then determined by subtracting the fifth percentile (L_{95}) of the reconstructed signal from the ninety-fifth percentile (L_5). Dashed lines in Fig. 14d show these percentiles. This method is applied to the three cases described earlier and the AM levels are referred to as $\mathrm{AM_S}$, $\mathrm{AM_{S+P_G}}$, and $\mathrm{AM_{S+P_{HG}}}$. Different from the Institute of Acoustics method, the detected AM levels in each 10 s block are averaged over a 10-minute simulation.

Figure 15 shows the AM levels of the source-only and coupled simulations with grassland for Case 3. The source-only simulation captures the near-field AM in the crosswind direction. This is relatively well understood [54] to be caused by the directivity and the blade rotation. The coupled simulation, on the other hand, shows a different trend. The results indicate a significant increase in AM levels when the propagation effects are taken into account in the far-field downwind or upwind of the turbine.

If we look closely at some of the time series (see Fig. 15) certain observations can be deduced. The time series obtained from receiver number 1 (downwind 1260 m) shows that the relatively small modulations observed from the source-only simulation are enhanced with the propagation effects. This increase in the downwind AM levels can be explained with the random phase and amplitude fluctuations caused by the turbulence that is only considered with the coupled simulation. It is worth noting that the turbulence scales smaller than the LES grid size are not resolved, and thus the full scattering phenomenon might not be captured, especially at the highest frequencies considered. Apart from the atmospheric and wake-induced small-scale turbulence, another reason could be the overall unsteady behaviour of the wind turbine wake (also known as wake meandering [55]). This may cause the sound waves refract through full or partial wake, which results in increased SPL fluctuations at the selected downwind locations. For a better understanding of this phenomenon, the top view of the instantaneous streamwise velocity in Case 3 at two

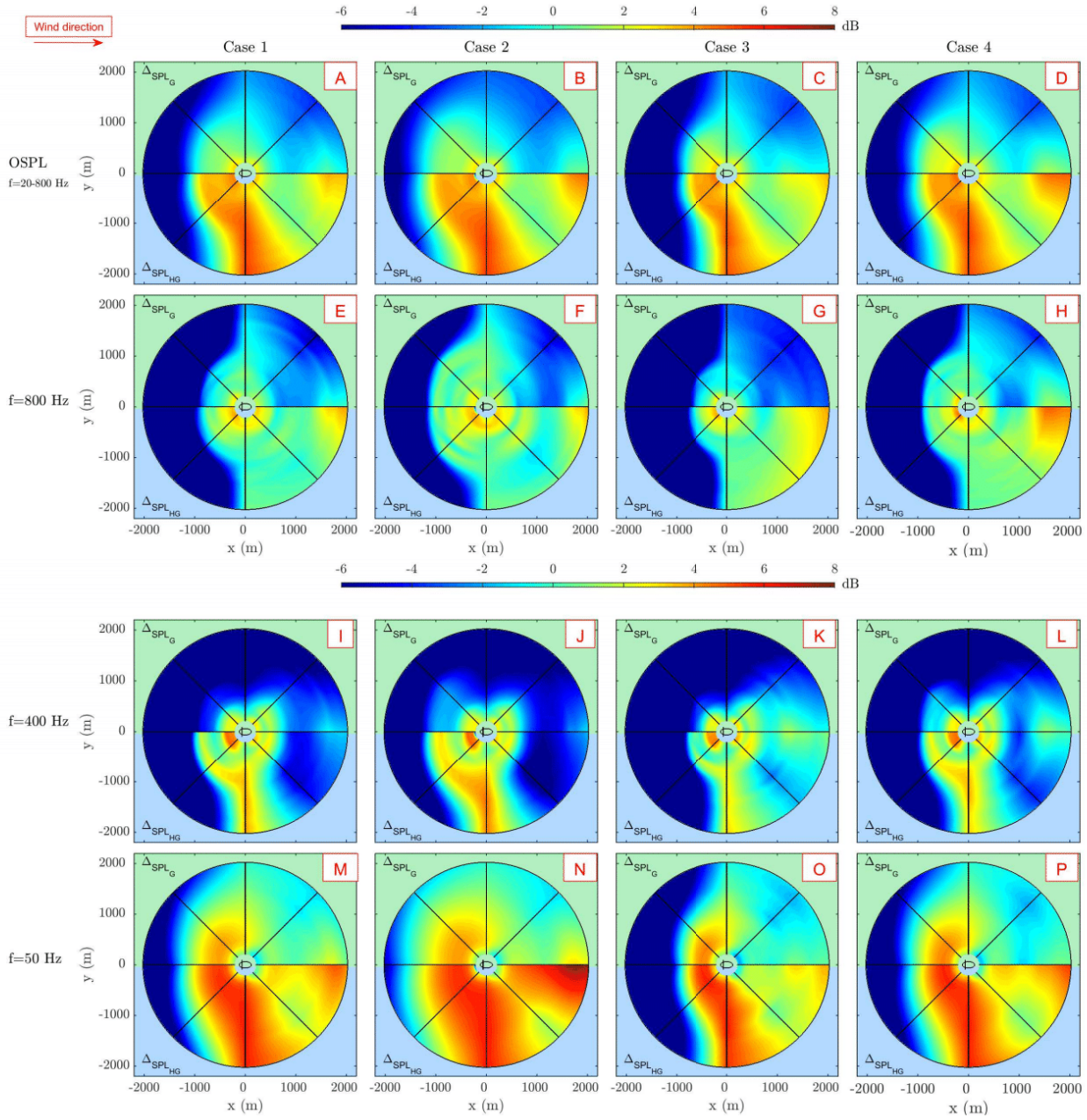

FIG. 12. (Color online) Top view of the time-averaged SPL difference at a 2 m receiver height. From left to right: varying cases listed in Table I. From top to bottom: overall levels and frequency-dependent levels. In each subplot, the upper half domain is with the grass-covered land: $\Delta_{\mathrm{SPL_G}}$=$\mathrm{SPL_{S+P_G}}$-$\mathrm{SPL_S}$. The lower half domain is the hard ground: $\Delta_{\mathrm{SPL_{HG}}}$=$\mathrm{SPL_{S+P_{HG}}}$-$\mathrm{SPL_S}$. Wind direction is from left to right and the turbine is located at the center of the domain.

different time instants are shown in Fig. 16. It is clear that the wake has a dynamic nature. Note that, the time scale of the large-scale wake movement is much longer than the blade rotation time scale. Therefore, at each instant sound waves emitted from each source propagate through different refractive regions. It is hard to distinguish which effect is the main contributor of the enhanced downwind AM. However, a comparison of the AM levels obtained from the simulations with and without the wake (see Fig. 17) emphasizes the importance of the wind turbine wake.

The time series of receiver number 2 (upwind 1260 m) in Fig. 15 shows an overall SPL attenuation for the coupled simulation. However, the modulation depths are considerably higher than in the source-only simulation. One reason for this could be the constant change of the

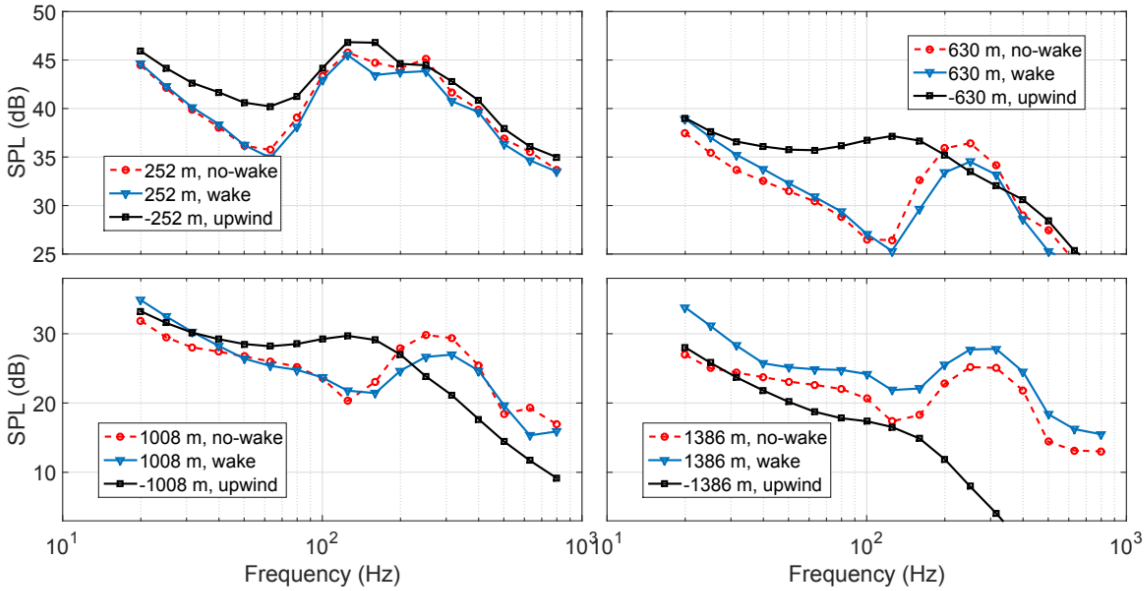

FIG. 13. (Color online) Time-averaged spectra at multiple locations for Case 4.

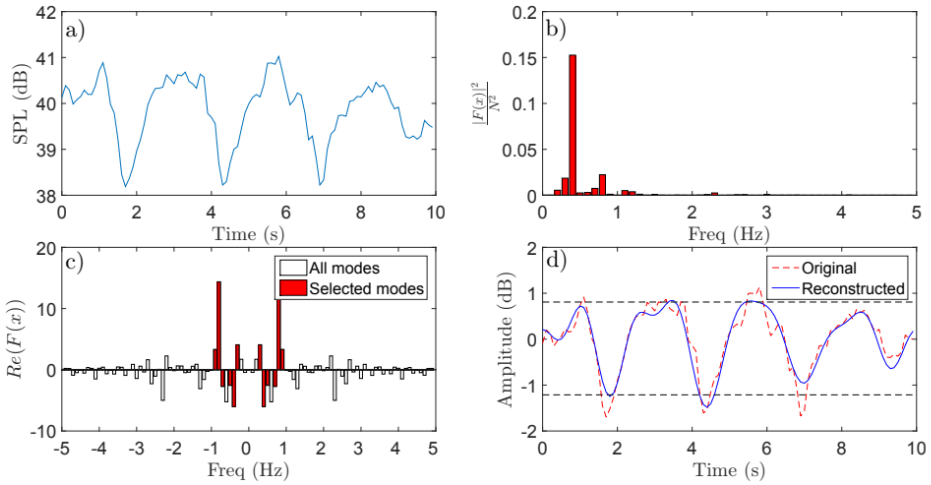

FIG. 14. (Color online) Procedure for AM quantification: a) original signal, b) power spectrum, c) real part of the DFT, d) original and reconstructed signal with percentiles (L_{95} and L_5) used for determining AM levels (horizontal dashed lines).

upwind extent of shadow zones caused by the blade rotation. For the sake of argument, let us consider the idealized upwind propagation without turbulence. It is well known that for a low-elevation source the shadow zones start within a shorter distance than an elevated source [49]. This means that under idealized conditions, the start of the shadow zone is determined only by the highest source. In this study, each blade is represented with one source within the propagation model and the source is often located around the tip of each blade (see Sec. II B). Two time instants are selected during the turbine rotation: A and B. At instant A, one source goes through the top tip height (153 m), whereas the other two sources are at a 58 m height. This means the shadow region start is dominated by the source at 153 m. At instant B, one source goes through the bottom tip height (28 m) and the other two sources are located at a 117 m height. This is the instant when the highest source among the three is at the lowest height. Therefore, the shadow zone will start closer to the turbine than in instant A. Figures 18a and 18b show the contour plots of the logarithmically summed SPL for 800 Hz

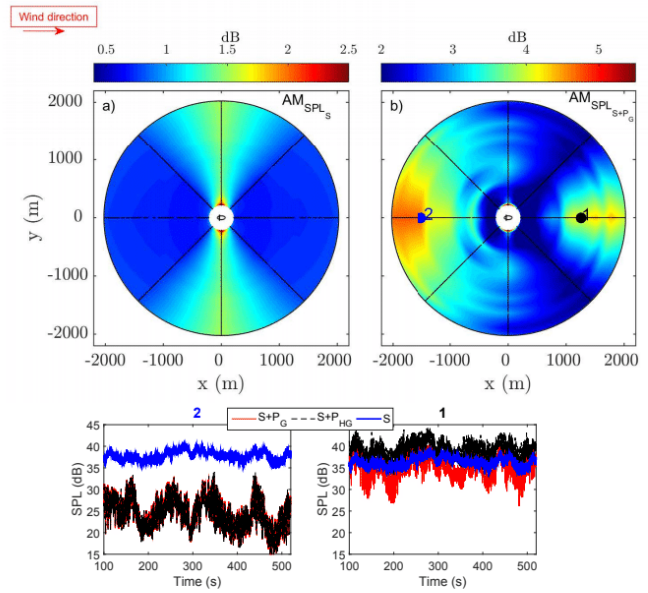

FIG. 15. (Color online) Top: top view of the AM levels at a 2 m receiver height for Case 3: a) source-only simulation and b) the coupled simulation. Wind direction is from left to right and the turbine is located at the centre of the domain. Bottom: SPL time series for two selected receivers enumerated and colour coded in the top plot.

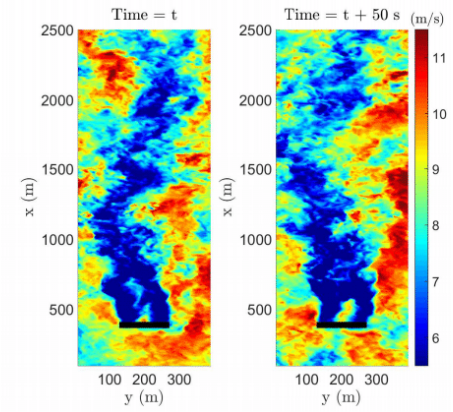

FIG. 16. (Color online) Top view of the instantaneous streamwise velocity at hub height in Case 3 at two different time steps. The black line represents the wind turbine rotor.

obtained from three independent 2D PE simulations for this idealized case. If we measure the noise around the start of a shadow zone, the amplitude fluctuations would be significantly larger (i.e., at instant A we hear something but at instant B we do not hear anything). Figure 19 shows the time signals at multiple locations. The AM levels calculated around the shadow zone boundaries (Figs. 19b and 19c) are much higher than the ones before (Fig. 19a) or after (Fig. 19 d) the shadow zone. The idealized situation changes when the turbulence is

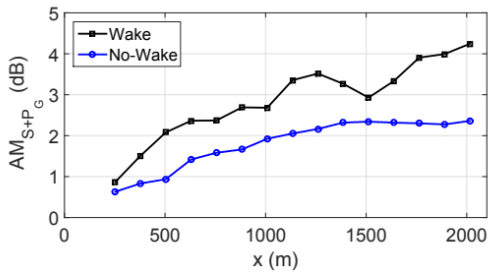

FIG. 17. (Color online) Downwind AM levels obtained from the simulations with and without the wake effect.

accounted for, because it is not possible to determine a distinct boundary of the shadow zone. Nevertheless, with the rotation of the blades and because of the turbulent flow field between the sources and receivers, these regions constantly change shape (see video MM1.avi) resulting in increased upwind AM levels. An important caveat is that these simulations do not model the background noise. It is very likely that the attenuated levels at the upwind would be lower than the background noise in field measurements. Therefore, it may not be always possible to measure these SPL fluctuations.

A more detailed study is shown in Fig. 20. Similar to the previous subsection, to isolate the propagation effects on AM, the difference contour plots are depicted (Δ_{AM_G}=AM_{S+P_G}-AM_S for grassland and $\Delta_{AM_{HG}}$=$AM_{S+P_{HG}}$-AM_S for hard ground). It is observed that in Case 3 the region with high upwind AM is the widest, namely from 500 m to 1900 m. The same thing is valid for the downwind AM. Additionally, the Case 3 levels are higher than those in all other cases. The comparison of Case 1 and 2 shows that Case 1 has narrower AM regions with higher levels than Case 2. Figure 20 shows that the shear, wake flow evolution, and ground characteristics play a role in AM levels both upwind and downwind of the turbine.

V. CONCLUSION

In this article, a consistent and modular modelling technique for wind turbine noise propagation was developed. A flow solver based on LES/AL, a wind turbine noise generation model based on FAST v8/NAFNoise, and a propagation model based on the PE method were loosely coupled. The unsteady flow fields were used for both noise generation and propagation calculations. The focus of the present study was on the propagation effects for varying wind shear, wind speed, and ground covers. Various phenomena, such as shadow zone existence, absorbing character of grass versus hard ground were captured when the propagation effects were included in the noise calculations. A clear increase in the source level was observed with increasing wind speed (9 dB difference at 2 RD away from the turbine, from U_h=6 m/s to

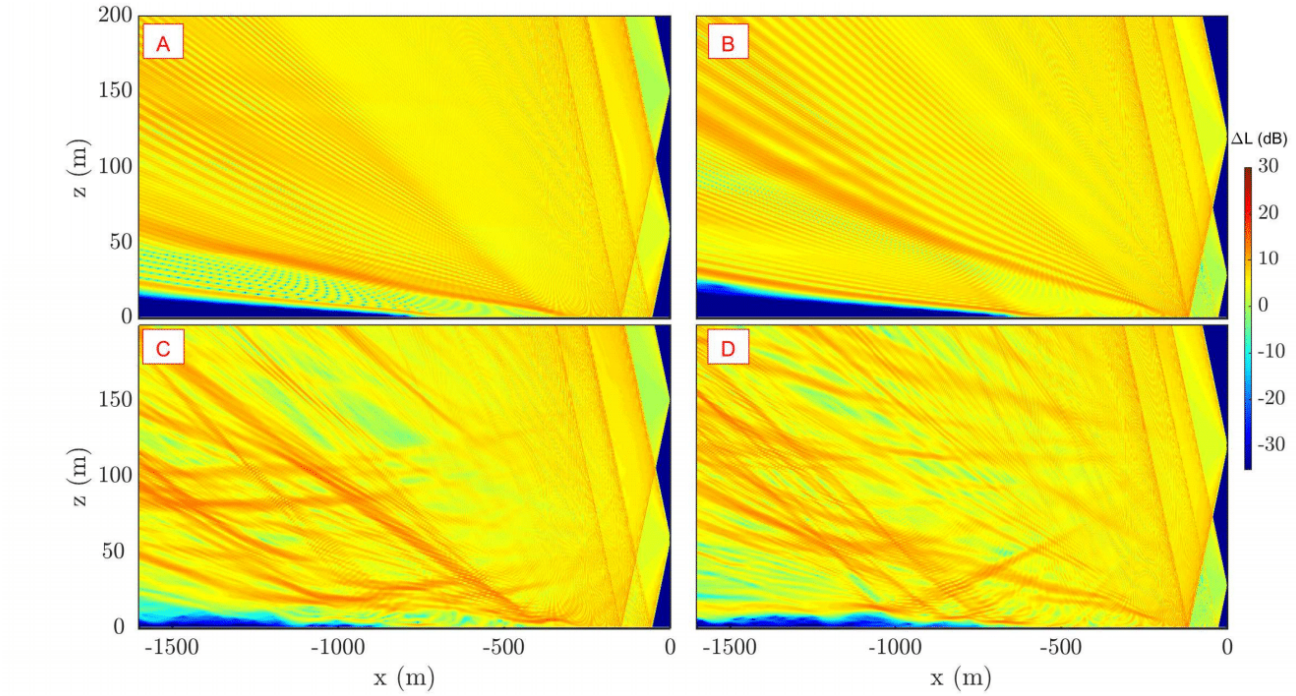

FIG. 18. (Color online) Snapshots of transmission loss (ΔL in Eq. 2) for 800 Hz obtained from three independent logarithmically summed 2D PE simulations using the Case 3 flow fields: a) and b) the simulations with time-averaged LES flow field and c) and d) the simulations with the instantaneous LES flow fields. Left and right columns correspond to time instants A and B, respectively.

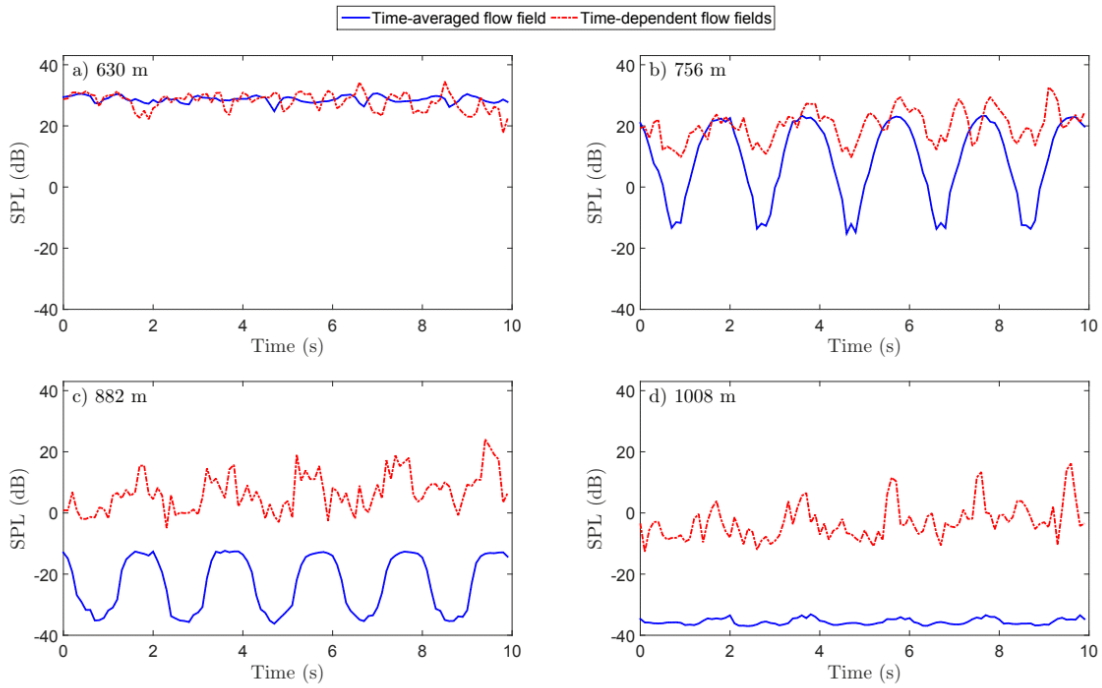

FIG. 19. (Color online) SPL time signal of 800 Hz at multiple downwind locations. The simulations are carried out with the coupled methodology explained in Sec. III and using instantaneous or time-averaged flow fields from Case 3.

U_h=9 m/s). It was shown that for the same hub-height wind speed, increased shear resulted in a small increase

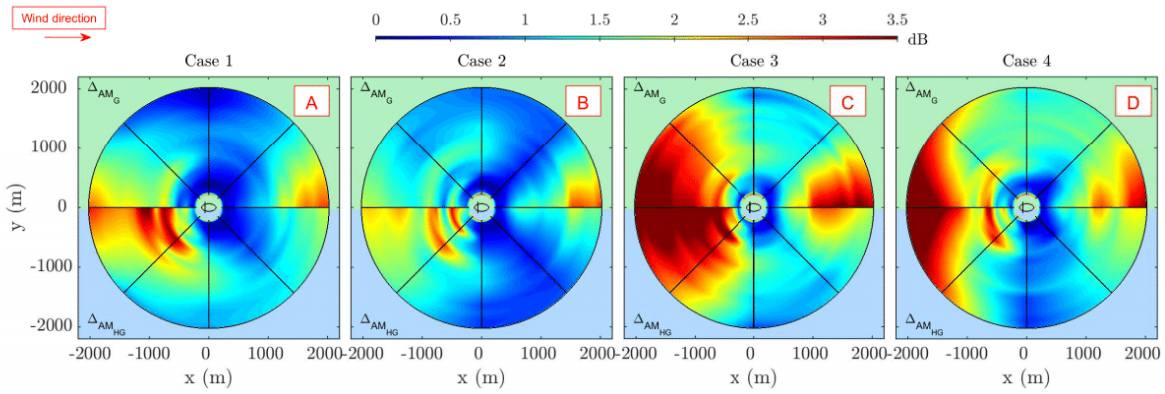

FIG. 20. (Color online) Top view of the amplitude modulation levels difference at a 2 m receiver height. From left to right: varying cases listed in Table I. For each subplot the upper half domain is grass-covered land: $\Delta_{\mathrm{AM_G}}$=$\mathrm{AM_{S+P_G}}$-$\mathrm{AM_S}$. The lower half domain is the hard ground: $\Delta_{\mathrm{AM_{HG}}}$=$\mathrm{AM_{S+P_{HG}}}$-$\mathrm{AM_S}$. Wind direction is from left to right and the turbine is located at the centre of the domain.

(approximately 1 dB) in the source levels. However, small SPL differences between various cases in the near field were enhanced in the far field as a result of the propagation effects. This observation was valid both for the steady and unsteady investigations. The SPL time signals evaluated at the source time showed enhanced far-field AM levels both upwind and downwind of the turbine.

The developed modular technique for the coupled model in this article allows for substitution of each part of the model with an alternative. This approach can be a good way to overcome the limitations, such as inaccurate airfoil noise calculations, simple wind turbine representations within the flow, or propagation models. Although the submodels are easily replaceable with their higher fidelity versions, more accurate modelling of the flow around wind turbines in complex terrain is one of the major challenges that lies ahead for accurate noise prediction.

ACKNOWLEDGMENTS

This work was supported by the National Natural Science Foundation of China Grant No. 11672261 and the Green-Tech Wind project, a collaboration of the EuroTech Universities. This work was also supported by the U.S. Department of Energy under Contract No. DE-AC36-08GO28308 with the National Renewable Energy Laboratory. Funding for the work was provided by the DOE Office of Energy Efficiency and Renewable Energy Wind Energy Technologies Office. The U.S. Government retains and the publisher, by accepting the article for publication, acknowledges that the U.S. Government retains a nonexclusive, paid-up, irrevocable, worldwide license to publish or reproduce the published form of this work, or allow others to do so, for U.S. Government purposes.

[1] ISO 9613-2, "Acoustics attenuation of sound during propagation outdoors, Part 1: General method of calculation," *International Standards Organization, Geneva, Switzerland,* (1996).

[2] B. Plovsing, "Proposal for Nordtest method: Nord2000. Prediction of outdoor sound propagation. Nordtest Proposal AV 1106/07," (2007).

[3] B. Søndergaard and B. Plovsing, "Validation of the Nord2000 propagation model for use on wind turbine noise," Technical Report PSO-07 F&U project no 7389 (2009).

[4] J. M. Prospathopoulos and S. G. Voutsinas, "Noise propagation issues in wind energy applications," J. Solar Energy Eng. **127**, 234–241 (2005).

[5] J. M. Prospathopoulos and S. G. Voutsinas, "Application of a ray theory model to the prediction of noise emissions from isolated wind turbines and wind parks," Wind Energy **10**, 103–119 (2007).

[6] D. Heimann, Y. Kasler and G. Gunter, "The wake of a wind turbine and its influence on sound propagation," Meteorol. Z. **20**(4), 449–460 (2011).

[7] K. Kaliski, E. Duncan, D. K. Wilson and S. Vecherin, "Improving predictions of wind turbine noise using PE modeling," in *NOISE-CON 2011*, Portland, OR (2011), pp. 1–13.

[8] S. Lee, D. Lee and S. Honhoff, "Prediction of far-field wind turbine noise propagation with parabolic equation," J. Acoust. Soc. Am. **140**(2), 767–778 (2016).

[9] E. Barlas, W.J. Zhu, W. Z. Shen, M. Kelly and S. J. Andersen, "Effects of wind turbine wake on atmospheric sound propagation," Appl. Acoust. **122**, 51–61 (2017).

[10] E. Barlas, W. J. Zhu, W. Z. Shen and S. J. Andersen, "Wind turbine noise propagation modelling: An unsteady approach," J. Phys. Conf. Ser. **753**(2) (2016).

[11] W. J. Zhu, N. Heilskov, W. Z. Shen and J. N. Sørensen, "Modeling of aerodynamically generated noise from wind turbines," J. Solar Energy Eng. **127**(4), 517-528 (2015).

[12] P. Fuglsang and H. A. Madsen, "Implementation and verification of an aeroacoustic noise prediction model for wind turbines," Technical Report, Risoe-R-867 (1996).

[13] K. Boorsma and J.G. Schepers, "Enhanced wind turbine noise prediction tool SILANT," in *4th Int. Meeting on Wind Turbine Noise,* Rome, Italy (2011).

[14] S. McBride and R. Burdisso, "An efficient noise modelling tool for wind turbines including sound propagation in arbitrary weather conditions," in *23rd Int Congress on Sound Vib.*, Rome, Italy (2016).

[15] B. Schaffer, S. J. Schlittmeier, K. Heutschi, M. Brink, R. Graf, R. Pieren and J Hellbruck, "Annoyance potential of wind turbine noise compared to road traffic," in *EuroNoise 2015*, Maastricht, Netherlands (2015).

[16] S. Yokoyama, S. Sakamoto and H. Tachibana, "Study on the amplitude modulation of wind turbine noise: part 2 − Auditory experiments," in *Internoise 2013*, Innsbruck, Austria (2013).

[17] S. V. Legarth, "Auralization and assessments of annoyance from wind turbines," in *2nd Int. Meet. Wind Turbine Noise*, Lyon, France (2007).

[18] E. Pedersen, F. van den Berg, R. Bakker and J. Bouma, "Response to noise from modern wind farms in The Netherlands," J. Acoust. Soc. Am. **126**, 634−643 (2009).

[19] E. Pedersen and K. Persson Waye, "Perception and annoyance due to wind turbine noise a dose response relationship," J. Acoust. Soc. Am. **116**(6), 3460−3470 (2004).

[20] G. P. Van Den Berg, "Effects of the wind profile at night on wind turbine sound," J Sound Vib. **277**(4), 995−970 (2004).

[21] C. Larsson and O. Öhlund, "Amplitude modulation of sound from wind turbines under various meteorological conditions," J. Acoust. Soc. Am. **135**(1), 67−73 (2014).

[22] N. Sedaghatizadeh, M. Arjomandi, B. Cazzolato and R. Kelso, "Wind farm noises: Mechanisms and evidence for their dependency on wind direction," Ren. En. **109**, 311−322 (2017).

[23] J. Jonkman, S. Butterfield, W. Musial and G. Scott "Definition of a 5-MW Reference Wind Turbine for Offshore System Development," Technical Report NREL/TP-500-38060 (2009).

[24] M. A. Sprague, J. M. Jonkman and B. J. Jonkman, "FAST Modular Framework for Wind Turbine Simulation: New Algorithms and Numerical Examples," in *AIAA SciTech 2015: 33rd Wind Energy Symposium,* Kissimmee, Florida (2015).

[25] K. O. Dag, "Development of Large Eddy Simulation Tools for Simulation of Atmospheric Boundary Layers in Wind Farms," Ph.D. dissertation, Technical University of Denmark, 2016.

[26] J. Smagorinsky, "General circulation experiments with the primitive equations," Mont. Weath. Rev., **91**, 99−164 (1963).

[27] J. N. Sørensen and W. Z. Shen, "Numerical modelling of wind turbine wakes," J. Fluids Eng., **124**, 393−399 (2002).

[28] W. Z. Shen, W. J. Zhu and J. N. Sørensen, "Actuator line/Navier−Stokes computations for the MEXICO rotor: comparison with detailed measurements," Wind Energy, **15**(5), 811−825 (2012).

[29] J. N. Sørensen, R. F. Mikkelsen, D. S. Henningson, S. Ivanell, S. Sarmast and S. J. Andersen, "Simulation of wind turbine wakes using the actuator line technique," Phil. Trans. R. Soc. A **373**(2035) (2015).

[30] P. Moriarty, "NAFNoise Users Guide," National Wind Technology Center, National Renewable Energy Laboratory, Golden, Colorado (2005).

[31] M. Roger and S. Moreau, "Back-scattering correction and further extensions of Amiet's trailing-edge noise model. Part 1: theory," J Sound Vib. **286**(3) 477−506 (2005)

[32] T. F. Brooks, D.S. Pope and M.A. Marcolini, "Airfoil self-noise and prediction," NASA reference publication 1218 (1989).

[33] N. Ramos-Garcìa, J. N. Sørensen and W. Z. Shen, "A strong viscous-inviscid interaction model for rotating airfoils," Wind Energy **17**(12), 1957−1984 (2014).

[34] R. K. Amiet, "Acoustic radiation from an airfoil in a turbulent stream," J Sound Vib. **41** 407−420 (1975).

[35] M. V. Lowson, "Assessment and prediction of wind turbine noise," Department of Trade and Industry W/13/00284/REP (1993).

[36] P. Moriarty, G. Guidati and P. Migliore, "Prediction of turbulent inflow and trailing-edge noise for wind turbines," in *11th AIAA/CEAS Aeroacous. Conf.*, Monterey, California (2005).

[37] ESDU-Report, Characteristics of atmospheric turbulence near the ground, Part II: single point data for strong winds (neutral atmosphere), No. 85020, April 1993.

[38] V. E. Ostashev and D. K. Wilson, "Relative contributions from temperature and wind velocity fluctuations to the statistical moments of a sound field in a turbulent atmosphere," Acta Acusti. Acustic. **86**(2), 260−268 (2000).

[39] S. Oerlemans, "Effect of wind shear on amplitude modulation of wind turbine noise," Int. J. Aeroacou. **14**(5−6), 715−728 (2015).

[40] O. Öhlund and C. Larsson, "Meteorological effects on wind turbine sound propagation," Appl. Acoust. **89**, 34−41 (2015).

[41] M. West, K. Gilbert and R. A. Sack, "A tutorial on the parabolic equation (PE) model used for long range sound propagation in the atmosphere," Appl. Acoust. **37**, 31−49 (1992).

[42] V. Ostashev and D. K. Wilson, *Acoustics in Moving Inhomogeneous Media, 2nd ed.* (CRC Press, 2015).

[43] D. K. Wilson, C. L. Petit and V. E. Ostashev, "Sound propagation in the atmospheric boundary layer," Acoust. Soc. Am., Acoustics Today, **11**(2) (2015).

[44] K. Attenborough, "Acoustical impedance models for outdoor ground surfaces," J. Sound Vib. **99**, 521−544 (1985).

[45] K. Bolin, M. Boué and I. Karasalo, "Long range sound propagation over a sea surface," J. Acoust. Soc. Am. **126**, 2191−2197 (2009).

[46] Y. Okada, K. Yoshihisa, K. Higashi and N. Nishimura, "Radiation characteristics of noise generated from a wind turbine," Acoust. Sci. Tech. **36**(5), 419−427 (2015).

[47] M. Friman, "Directivity of sound from wind turbines: A study on the horizontal sound radiation pattern from a wind turbine," M.Sc. Thesis, KTH, Department of Aeronautical and Vehicle Engineering (2011).

[48] B. Cotté and P. Blanc-Benon, "Estimates of the relevant turbulent scales for acoustic propagation in an upward refracting atmosphere," Acta Acusti. Acustic. **93**(6), 944−958 (2007).

[49] C. Larsson and S. Israelsson, "Effects of meteorological conditions and source height on sound propagation near the ground," Appl. Acoust. **33**(2), 109121 (1991).

[50] K. E. Gilbert and M. J. White, "Application of the parabolic equation to sound propagation in a refracting atmosphere," J. Acoust. Soc. Am. **85**(2), 630−637 (1989).

[51] S. Cheinet, "A numerical approach to sound levels in near-surface refractive shadows," J. Acoust. Soc. Am. **131**(3), 1946−1958 (2012).

[52] M. Ewing and J. L. Worzel "Long-Range Sound Transmission," Geolog. Soc. Am., Memoir 27 (1948).

[53] Institute of Acoustics IOA Noise Working Group (Wind Turbine Noise) "Amplitude Modulation Working Group Final Report, A Method for Rating Amplitude Modulation in Wind Turbine Noise," (2016).

[54] A. Fischer, H. A. Aagaard , K. A. Kragh and F. Bertagnolio, "Analyses of the mechanisms of amplitude modulation of aero-acoustic wind turbine sound," in *Proceedings of EWEA* (2014).

[55] G. C. Larsen, H. A. Madsen, K. Thomsen and T. J. Larsen, "Wake meandering: a pragmatic approach," Wind Energy, **11**(4), 377−395 (2008).

Chapter 6

Diurnal Variability of Wind Turbine Noise

6.1 Chapter Overview

This chapter is devoted to the investigation of wind turbine noise variations over a diurnal cycle. The change in noise levels over a day is an important topic as many country regulations dictate different limits for day and night time. Quantifications of these variations can pave the way towards better estimations of noise levels before or after the wind farm installation.

The corresponding publication in this chapter (Sec. 6.2) addresses this issue with the combined model that is previously introduced. Large eddy simulation with a rotational actuator disk wind turbine model is used to model the wind and temperature around a mega-watt scale wind turbine over a diurnal cycle. The time dependent output is used as input to the wind turbine noise generation-propagation model introduced in the previous chapter. The results highlight the significant variation of the wind turbine far field noise depending on the atmospheric conditions. For example, the SPL difference between night time and afternoon is 2.5 dBA at 650 m and reaches 6.5 dBA at 3600 m downwind of the wind turbine. Furthermore, peak AM levels are observed at distances of 1200 m during evening and night time, while in the afternoon no specific peaks are detected.

6.2 Publication

Variability of Wind Turbine Noise over a Diurnal Cycle

Emre Barlas[a], Ka Ling Wu[b], Wei Jun Zhu[c,a], Fernando Porté-Agel[b], Wen Zhong Shen[a]

[a] *Department of Wind Energy, Technical University of Denmark, Kgs. Lyngby, 2800 Denmark*
[b] *Wind Engineering and Renewable Energy Laboratory (WiRE), École Polytechnique Fédérale de Lausanne (EPFL), Lausanne, Switzerland*
[c] *School of Hydraulic, Energy and Power Engineering, Yangzhou University, CN*

Abstract

The diurnal variation of atmospheric conditions over land has a significant effect on the wind and temperature distributions which greatly influence the generation and propagation of wind turbine aerodynamic sound. In this paper, a new fully consistent unsteady approach is developed to study wind turbine noise such that large eddy simulation with a rotational actuator disk wind turbine model is used to model the wind and temperature around a mega-watt scale wind turbine over a diurnal cycle, and time dependent flow and temperature fields are used as input to the coupled wind turbine noise generation-propagation model. Computations are carried out for four different 10 minutes datasets selected at certain periods of a day for a same hub height wind speed. The results show the variations of the time dependent as well as the time averaged sound pressure levels in near and far fields. It is observed that the source levels are affected mostly by the incoming turbulence more than by the wind shear. Hence the time-averaged near field (2 diameters away from the turbine) A-weighted overall sound pressure levels in the afternoon are slightly higher than those in the night ($\approx$ 0.5 dBA). This value is similar in all directions. However, as we move away from the turbine, the propagation effects take over and downwind of the turbine the night time levels exceed the day time levels. At 650 m the difference is 2.5 dBA and at 3600 m the difference reaches 6.5 dBA. Furthermore, the regions with enhanced far field amplitude modulation (AM) levels also vary with time in the day. Peak AM levels are observed at distances of 1200 m during evening and night time, while in the afternoon no specific peaks are detected.

Keywords: `wind turbine noise`, diurnal cycle, variability, large eddy simulation, parabolic wave equation
2010 MSC: 00-01, 99-00

1. Introduction

Emerging interest in clean energy has resulted in large deployment of wind power within short periods of time. While many people have interest in contributing to green energy transition, not all of them are satisfied with the wind turbines being erected nearby their houses. Two major reasons for opposing onshore wind turbines are visual impact [1, 2, 3] and noise annoyance [4]. In this paper we will limit our study with the latter. The character of noise emitted from wind turbines has been the main factor for increased annoyance. The variability and the unsteadiness are some of the characteristics of wind turbine noise different from other noise sources [5].

Today the wind turbines are placed within clusters rather than stand alone, and thus the interest in flow interaction between them has grown significantly. The wake flow behind a wind turbine has an important effect on both loads and energy production of the downstream turbines. This issue was addressed extensively via numerical models [6, 7], field experiments [8] as well as wind tunnel studies [9, 10]. Numerical techniques range from simple analytical wake models [11, 12, 13, 14] to linearized flow solvers [15] and more sophisticated tools [16, 17, 18]. Various representation methods of wind turbine within flow solvers were used to develop efficient but accurate methods for wind turbine and wind farm flow computations [19, 20, 21]. With increasing computational capabilities more comprehensive studies were carried out for understanding the detailed flow behaviors around the wind turbines [22, 23, 24, 25, 26]. Nevertheless most of the published papers were limited to the flow itself however, the wake has also an effect on the wind turbine sound generation and propagation. Particularly, the diurnal variation of atmospheric conditions over land which has a significant effect on the wind and temperature distributions, and thus wakes and wind turbine sound. Based on thermal stratification and the turbulence generation mechanisms, the atmospheric boundary layer (ABL) can be classified into neutral, convective and stable [27]. Stable boundary layer (SBL) is observed when the ground surface is colder than the air, such as during a clear night over land. SBL is associated with high wind and temperature shear, and low turbulence intensity (TI). This is caused by the negative buoyancy fluxes that reduce the shear generated turbulence. While a decreased TI may reduce the wind turbine noise emission levels, an increased wind shear and temperature inversion may cause a more severe downward refraction (sound waves bend towards the ground). Therefore, an increase in the immission levels (high noise levels at far field receivers) may be observed. Furthermore, a low TI results in longer wake deficit behind the turbines. This causes

*Wen Zhong Shen
Email address: `wzsh@dtu.dk` (Wen Zhong Shen)

a ducting effect of the sound waves and refraction patterns are significantly modified. This effect was observed with various propagation and source models in [28] [29] [30] [31]. Additionally, as it was pointed out in [32] stable conditions have other effects on wind turbine noise. For example, large wind speed and direction changes along the rotor cause a large variation of the angle of attack on the blades over one revolution. High angles of attack in the top tip region may trigger the flow separation and cause a transient stall, thus changing the frequency content and the strength of aerodynamic noise. Moreover, since SBL flow is associated with high wind shear and low near-ground wind velocity, it is likely that the background noise levels at the ground level are lower in SBLs, compared with their convective counterparts, at the same hub height wind speed.

Contrary to SBL, convective boundary layer (CBL) is observed whenever the surface is warmer than the air, such as during a sunny day with slow winds over land. CBL is associated with enhanced mixing and increased turbulence levels. This, in turn, decreases the wind and temperature shear. As aforementioned, the wind turbine aerodynamic noise generation is known to be increased, with increasing the incoming turbulence [33]. Thus it can be expected that under convective conditions far field noise levels are higher. However, low wind shear and faster wake recovery may prevent the ducting of the sound waves hence the propagation effects may play a role in favour of sound pressure levels (SPL) attenuation.

The dynamic interaction of atmosphere, wind turbine noise generation and propagation is a complex phenomenon. So far the issue is addressed mostly with field experiments. While the findings in [34] show relatively small effects of atmospheric conditions on far field SPL variation, the conclusions of long term measurements carried out in [35] show the opposite. The findings in [35] demonstrate variations of 6 - 14 dBA at propagation distances of 1 - 2 km from 12 wind turbines, depending on the refraction and ground properties. Same authors also investigated the possible relationship between the far field amplitude modulation and meteorological conditions [36]. They observed enhanced AM levels under high wind shear and low turbulence, namely at night time.

While experiments capture the far field SPL variation, the issue has not been addressed numerically in an unsteady manner. In this paper a fully consistent unsteady approach is developed where wind and temperature fields obtained from a diurnal cycle simulation with Large Eddy Simulation (LES) and a rotational actuator disk wind turbine model (AD-R), and for sound propagation, a physics-based model, namely a wide-angle Crank-Nicholson parabolic wave equation model (CNPE) is used. The wind turbine as a sound source is represented in a quasi-three-dimensional and unsteady manner. The source levels on each blade is obtained from aero-elastically coupled semi-empirical wind turbine noise generation models.

2. Computational Models

2.1. Flow Modelling

For the flow modelling, the WiRE LES code [37] is used. The wind turbine is modelled with a rotational actuator disk model. The model relies on the tabulated airfoil data and the blade geometry to calculate the aerodynamic forces on the blades. WiRE LES and AD-R has been validated and extensively used for various wind energy studies (e.g. [38][39][40][41][42]). In this study a single turbine is simulated. The turbine simulated is a Vestas V80-2MW turbine, which has a diameter of D = 80 m and a hub height of 70 m [43]. The computational domain is broken into 192 × 320 × 160 grid points with a spatial resolution of 25 m × 15 m × 10 m in the streamwise, spanwise and vertical directions, respectively. With these setup the simulations are carried out for two full diurnal cycles. Four different 10 minutes datasets are selected on the second diurnal cycle and the three dimensional flow and potential temperature fields are stored at each 0.1 s. The selected periods are early morning (from 05:00 to 05:10), afternoon (from 13:00 to 13:10), evening (from 19:00 to 19:10) and night (from 23:00 to 23:10).

Figure 1 shows the contours of instantaneous effective speed of sound in the middle vertical plane for different time instants in the day. The effective speed of sound is calculated as C_{eff} (x,z)=c(x,z)+V_x (x,z) where V_x is the wind velocity component projected along the direction of propagation between source and receiver and c is the speed of sound and calculated as c= $\sqrt{\gamma RT}$ where γ is the specific heat ratio, R is the gas constant and T is the temperature. Since the temperature is not an output of the code the relation between the potential temperature and the absolute temperature (T) is assumed to be the lapse rate for dry adiabatic atmosphere. Thus $\theta \approx T - 0.01$ Km^{-1}·z.

The effective speed of sound is a parameter of interest because it is the main input for the propagation calculations (see next section). In addition, Fig. 2 shows the time-averaged vertical profiles of streamwise velocity (U [m/s]), potential temperature (θ [K]) and streamwise turbulence intensity (σ_u/U_{hub}) at 3D upstream of the turbine. The averaging time span is 10 minutes for each case.

From Figs. 1 and 2 various observations can be deduced regarding the atmospheric conditions relevant for sound propagation. In the morning we observe a very clear low level jet where the highest wind speed is reached at around 150 m height. As aforementioned the negative buoyancy flux damps the turbulence, which leads to lower turbulence intensity levels (maximum 5 %). This suppressed mixing results in a longer wake deficit region. Furthermore, the temperature decrease with altitude is another factor that directly influences the sound propagation. Overall, the conditions in the morning have considerable effects on propagation via trapping the sound waves and causing a severe downward refraction. This phenomenon will be detailed in Sec 3.

Contrary to the morning, in the afternoon the turbulent mixing is enhanced due to the positive buoyancy flux. This results in a faster wake recovery. A very low temperature and wind shear is observed. These conditions result in a situation similar to the homogeneous atmosphere (constant speed of sound with height) where the refraction effects are not dominating the propagation.

The selected evening period is the start of the transition from low wind shear, high turbulent, convective conditions to high shear, low turbulent, stable conditions. Turbulence levels are

maximum 8 % and the wind shear power law exponent derived by fitting the wind profile is 0.33.

The night time and morning conditions are very similar to each other in terms of wind turbine noise generation. The turbine is exposed to an almost identical flow field with regard to turbulence levels and wind shear (see Fig. 2). However, while the source levels may be similar, the propagation effects play different roles for the two different time instants of the day. This is also investigated in detail in Sec 3.

2.2. Noise Modelling

A new technique which couples wind turbine noise generation and propagation models was presented in [44]. For sound propagation the model uses DTU's Parabolic wave Equation (PE) based tool WindSTAR-Pro (Wind turbine Simulation Tool for AeRodynamic Noise Propagation) [45]. The sound source modelling is carried out with the aeroacoustics module based on NRELs NAFNoise [46] integrated in the FAST8 modular framework [47]. This subsection briefly explains the technique and gives details about the used parameters in this study.

It is a common approach to model the wind turbine aerodynamic noise generation via dividing the blades into a number of two dimensional airfoil elements and predicting the total noise level at a given receiver location as the sum of the contributions from all the elements. At each element, the local relative velocity and angle of attack are the main parameters for the prediction of airfoil self noise based on semi empirical relationships obtained in [48] with scaling laws. Using the time and location dependent angle of attack, the boundary layer displacement thickness values at trailing-edge are interpolated using the pre-tabulated data obtained from XFOIL [49].

In addition to the trailing-edge noise, the turbulent inflow noise is calculated using the model that is originally proposed by Amiet [50] and further developed by Lowson [51]. A correction about airfoil thickness is also used [52]. It is worthwhile noting that the SPL is calculated from all the elements in an uncorrelated way. The spanwise correlation appears to have a small effect for low frequencies (<100Hz).

To obtain the necessary inputs (i.e. turbulence intensity, turbulent length scale, angles of attack and relative velocity) the LES flow field sampled at 2 diameters upstream of the turbine is fed into FAST8 as inflow. The turbulence intensity distribution is calculated at the sampled two-dimensional plane for each 10 minutes dataset. This is used as input for FAST8 and then at each time-instant the TI value at airfoil location is interpolated and assigned. The integral turbulent length scale (L) is calculated using the relationship in Ref. [53] that can be expressed as a function of a non-dimensional roughness parameter α_r and height z: $L = 25 \cdot z^{0.35} \cdot \alpha_r^{-0.063}$. In this study we consider the α_r values 0.08, 0.03, 0.05, 0.08 to represent the time instants of the day from morning to night, respectively. Since the detailed design of the turbine used in the flow simulations is confidential, a generic 2 MW turbine with the same diameter and hub height is used in FAST8. The 40 m blades were divided into 24 elements and the rotational speed of the turbine is kept constant at 15 rpm which matches the power output of the turbine used in the flow simulations at 8 m/s (average wind speed for all selected periods during the day). Frequency dependent sound pressure levels at the selected receiver locations are calculated and stored for all the periods of the day. In total 99 receiver locations are distributed around the turbine shown in Fig. 4. The closest receiver is 160 m (2D) away from the turbine and the furthest one is 3600 m (45D) away. The distances between source and receiver vary depending on the propagation angle. This receiver distribution pattern is purposefully selected from the experience gained in previous studies. In addition to the frequency dependent SPL, the coordinates of the blade element with the highest SPL contribution along each blade are stored. Thereby the frequency and blade dependent source localization is carried out to be used for the sound propagation model at each time-step.

Figure 3 shows the angle of attack time signal at 85 % radius of a single blade for two periods of the day. The high wind shear at night time causes the large peak-to-trough variation ($\approx 6\,^\circ$) over one revolution. However, the fluctuations are very regular due to the low turbulence. On the contrary, the low wind shear and high turbulence associated with the day time results in lower peak-to-trough ratios ($\approx 2\,^\circ$) over one revolution but more random fluctuations with time. Note that while the peak-to-trough ratios vary with the time of the day, the averaged angle of attack values are almost identical. It is also worthwhile to mention that this is the situation only for one blade. Considering that the other two blades go through similar changes over one revolution with phase shifts in time, the sum of all three blades' angles of attack can be very similar. This observation will be relevant for noise simulation results later on.

Although FAST8's aero-acoustics module can predict the noise levels at various receiver locations, it does not take into account the propagation effects, such as atmospheric absorption, refraction, ground absorption and reflection. This part is modelled using the PE method. A two-dimensional, wide-angle, Crank-Nicholson parabolic wave equation (CNPE) method [54] is used. With this method the moving atmosphere is replaced by a hypothetical motionless medium with an effective speed of sound. These values are calculated using the fields obtained from the flow solver described in Sec 2.1. A semi-implicit marching scheme is used, with central differences in the vertical direction (z) and the Crank-Nicholson scheme in the horizontal direction (x). The spatial resolution for both directions is set to $\Delta x = \Delta z = \lambda/8$, where λ is the wavelength of the frequency solved. To avoid unwanted reflection from the top boundary a 50 λ thick absorption layer is used on top of the 700 m domain height. Only flat terrain is considered and the ground impedance is characterized using the 4 parameter model proposed in [55]. An effective flow resistivity value of 200 kPa s/m^2 is chosen, as this is a typical value for grassland where onshore turbines are commonly located. The other parameters of the impedance model are the pore shape factor ($s_p = 0.75$), grain shape factor ($n' = 0.5$), porosity ($\Omega = 0.3$). All simulations are carried out for 1/3-octave band centre frequencies from 20 Hz to 800 Hz. At each time-step for each receiver, each frequency and each blade a two-dimensional PE domain is constructed. The source locations and the source levels obtained from the noise generation model are used.

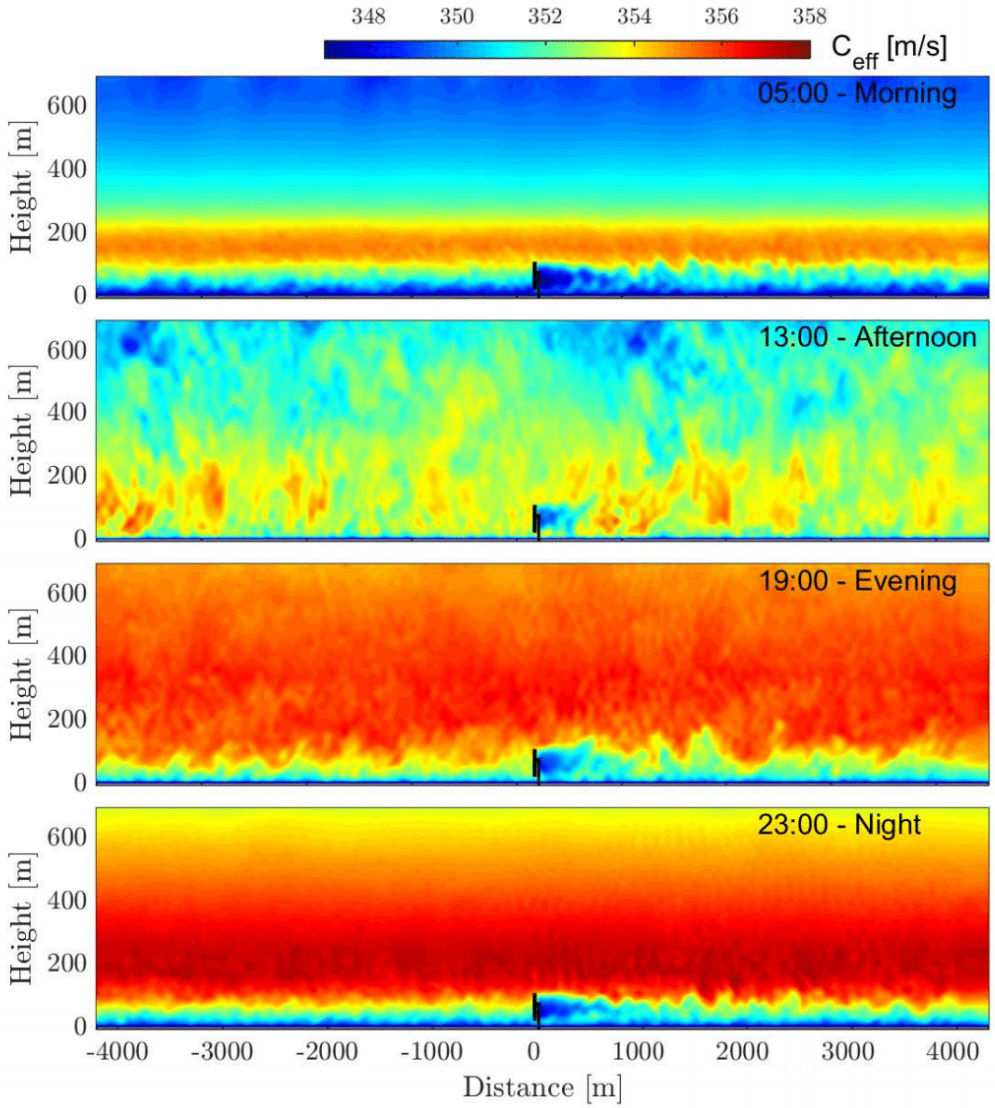

Figure 1: Instantaneous effective speed of sound fields in the middle vertical plane for different time instants in the day. **From top to bottom:** Morning (05:00), afternoon (13:00), evening (19:00), night (23:00).

For 99 receivers, 3 blades, 17 frequencies, 6000 time-steps and 4 cases, a total of 121 million independent simulations are carried out for the propagation calculations.

3. Results

In this section we first investigate the SPL averaged over 10 minutes for various time instants in the day. The focus is on both overall as well as frequency dependent results. Subsequently, the time dependent SPL is investigated and amplitude modulation depths are quantified.

3.1. Time Averaged Results

Figure 5 shows the contours of time-averaged A-weighted overall sound pressure levels (OASPL) at the receivers of 2 m height seen from top. It is observed that close to the turbine, crosswind levels are considerably lower than the upwind and downwind levels. This is an expected outcome due to the wind turbine noise directivity and it is valid for all periods of the day. On the other hand, the OASPL distribution downwind and upwind of the turbine varies with the time of the day. For a clearer comparison, line plots are shown in Figs. 6 and 7. Initially all lines collapse (up to 350 m) and the maximum OASPL difference at 2D is 0.5 dBA. This difference is due to the change

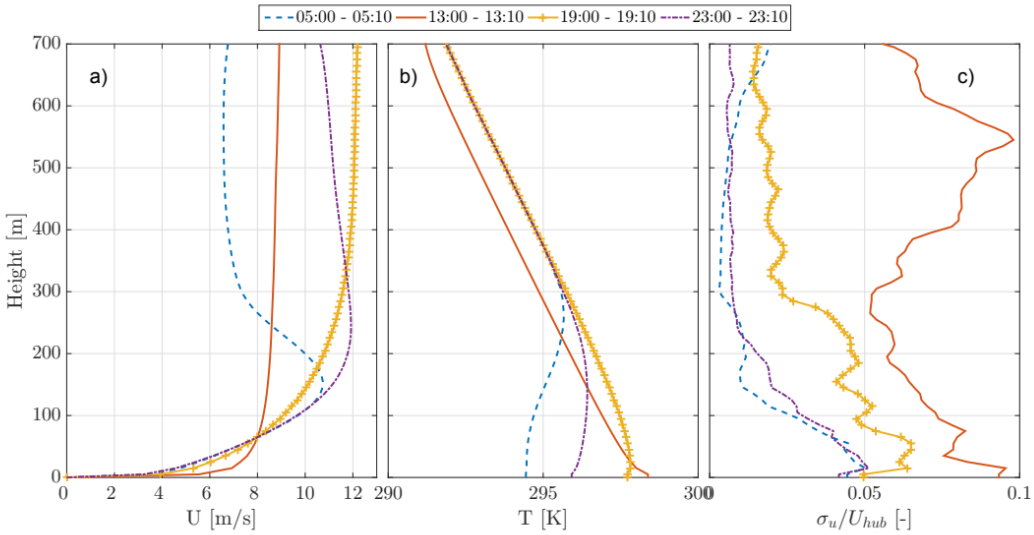

Figure 2: Time-averaged streamwise velocity, temperature and streamwise turbulence intensity at 3 diameter upstream of the turbine for different times of the day.

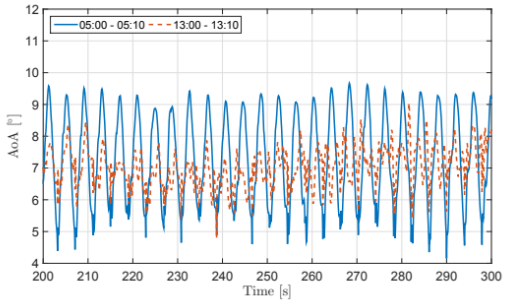

Figure 3: Time signal of angle of attack at 85 % radius of blade number 1.

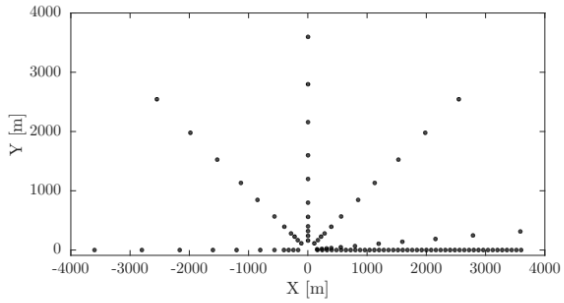

Figure 4: Top view of the receiver locations selected around the turbine. Turbine is at the center of the domain.

in source levels and it will be elaborated using spectra plots later on. As the distance from the source increases (i.e. as the propagation becomes effective) OASPL distributions show larger variations. Already at 650 m downwind of the turbine, the OASPL difference between night time (23:00-23:10) and afternoon (13:00-13:10) is 2.5 dBA and it reaches 6.5 dBA at 3500 m. This increased variation is caused by the atmospheric conditions explained in Sec 2.1. Due to severe downwards refraction as well as persistent wake induced ducting effects, far field noise levels in the night time are higher than in the afternoon. Night time levels are important because of two reasons. First, in most countries the night time noise limits are more restrictive than the day time ones. Second, due to the high wind shear in night time the wind speed at the receiver height in night time is lower than that in the day at the same hub height wind speed. This results in lower background noise. Therefore, the wind turbine noise becomes more noticeable for a receiver on the ground in the night time. In this study the wind speed at 5 m height (the first grid point of the flow solver) is 3.5 m/s and 5.5 m/s in the night time and in the afternoon, respectively.

Since the atmospheric conditions are similar during the night and in the morning, the OASPL distributions with distance are similar. At both times of the day, a long wake deficit and low level jets are observed from the effective speed of sound plots. In the morning the shear of the low level jet is higher. Nevertheless, the OASPL difference between the two periods of the day does not exceed 1 dBA. To investigate deeper and for a better visual understanding, instantaneous OASPL contours in the mid-vertical plane are shown in Fig. 8. In the morning, downwind of the turbine the low level jet traps the reflected waves and refracts them downwards. This causes a SPL enhancement in the far field $\approx$ 2500 m. It is not very clear why downwind SPL at certain distances (e.g. 1800 - 2600) during the evening is higher than in the morning and at night. One explanation can be the evening effective speed of sound profile. This has a more continuously downwards refraction effect, than the other two cases (evening and night) where the profiles change slope towards upward refraction after a certain height.

Upwind of the turbine, contrary to the downwind case, the lines collapse at slightly longer distance (up to 320 m). The main reason for this is the wake deficit which is not present upwind. Thus the sound waves for all cases can initially refract downwards without the wake deficit trapping them. Again different from the downwind propagation after certain distances shadow zones (regions with very low SPL) are observed. This is due to the upward refraction of sound waves and the extent of these regions which varies with the time of the day. The effective speed of sound profiles are similar upwind of the turbine in the morning, evening and night time. Thus the OASPL evolution with distance is also similar. One major difference is the very strong low level jet observed in the morning. This manifests itself after 2500 m as an increase in OASPL. We can again refer to Fig. 8 for explanation. It is observed that in the morning, initially upward refracted waves are trapped by the low level jet and they start bending downwards, causing enhanced SPL regions in the very far field. Nevertheless, the levels upwind of the turbine are still very low to be of interest since the enhanced SPL region is far away and the source levels are not high enough.

OASPL upwind of the turbine in the afternoon starts deviating from the other times of the day after a 700 m distance propagation. Due to the low shear, the upward refraction in the afternoon is relatively weak. Therefore, the day time levels are higher than the levels in other times of the day upwind of the turbine once the propagation effects become important.

Since the propagation effects are frequency dependent, the time averaged spectra contours in the night time and in the afternoon are shown in Fig. 9. The aforementioned observation on the weaker upward refraction in the afternoon than in the night is clearly visible. One additional output of the figure is the frequency dependency of the shadow zones. The high frequencies are influenced by the atmospheric refraction faster than the low frequencies. Additionally, atmospheric absorption is more effective on high frequencies. This results in a later start of the low frequency shadow zones. Therefore, we can state that accurate modelling of the low frequency bands is more important for correct far field noise predictions.

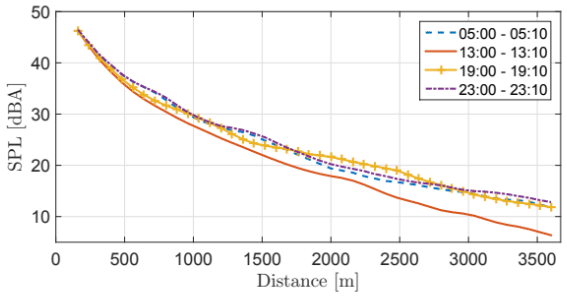

Figure 6: Time averaged OASPL for the receivers at 2 m height downwind of the turbine in four periods of the day.

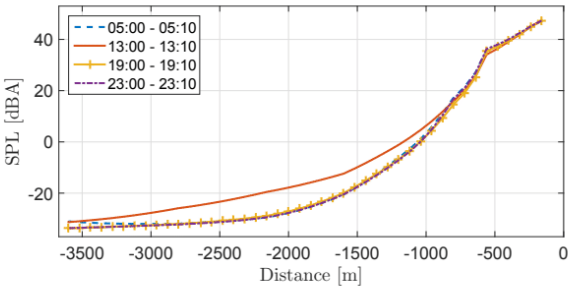

Figure 7: Time averaged OASPL for the receivers at 2 m height upwind of the turbine in four periods of the day.

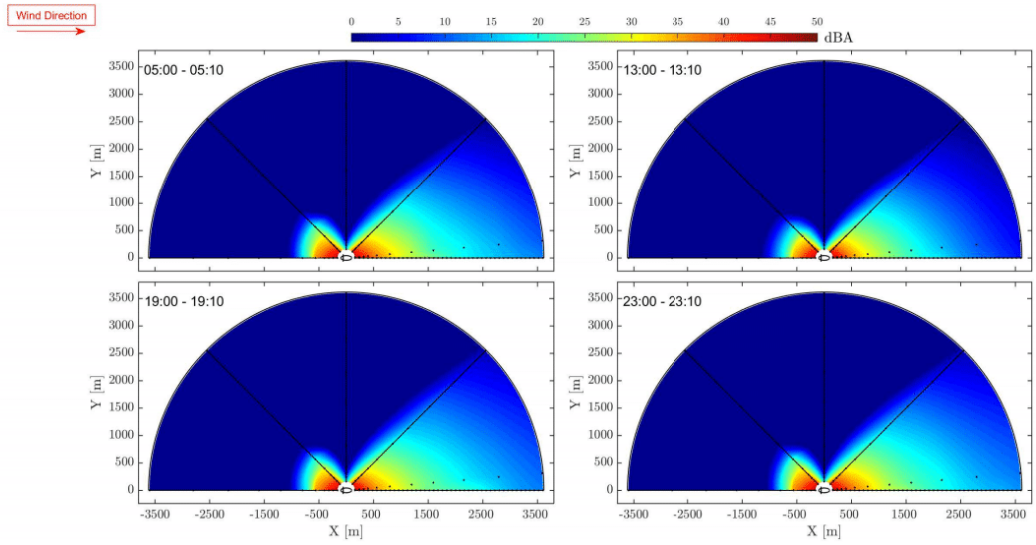

Figure 5: Top view of the time averaged OASPL at 2 m receiver height in four different periods of the day. Black points represent the receiver locations.

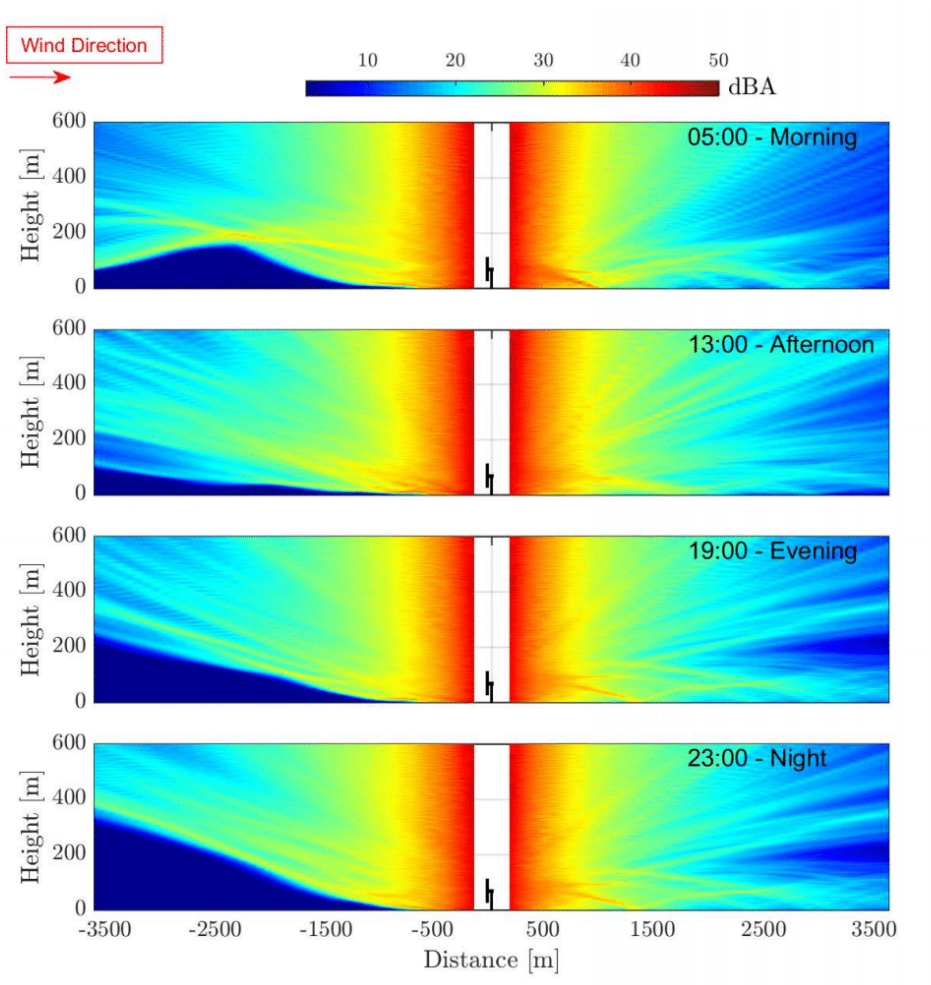

Figure 8: Instantaneous SPL fields in the middle vertical plane at different times of the day. **From top to bottom:** Morning (05:00), afternoon (13:00), evening (19:00), night (23:00).

For a clearer comparison of the downwind levels, line plots of the spectra at the selected distances are shown in Fig. 10. One of the major atmospheric differences between night time and afternoon is the turbulence level. The enhanced turbulence levels in the afternoon result in an increase of SPL at the low frequency range (e.g. below 100 Hz) where the turbulent inflow noise dominates the spectrum. The SPL difference in the near field (2D away from the turbine) varies from 1 dB to 4 dB depending on the frequency band below 100 Hz. In the mid frequency range, where the trailing-edge noise is the main contributor, the sound pressure levels at 2D are very similar in both periods. The effect of wind shear on angle of attack and trailing-edge noise was briefly discussed in Sec 2.2. Even though the wind shear values are significantly different, the sound pressure levels in the mid frequency range are almost identical. However, these are only the time averaged spectra, the time dependent signals show small variations and the results are detailed in Sec 3.2. More importantly, as the distance increases, the trend changes and the night time noise levels start to exceed the levels in the afternoon. This is a clear indication of the propagation effects. During the night time, there is a strong downward refraction as opposed to the almost homogeneous atmospheric conditions in the afternoon. Subsequently, the SPL attenuation is weak in the night. From the spectra it is observed that at 30 D downwind, SPLs of all frequency bands in the night are either equal to or more than the afternoon levels, even though at 2D the opposite is true.

3.2. Time Dependent Results

The time dependent results focus on the downwind of the turbine since previous studies showed that the unsteady nature of the wake and the aerodynamic noise emitted from rotating blades result in far field modulations [56]. A quantification of the unsteadiness is carried out by investigating the amplitude modulation (AM) levels and then time signals at the selected receiver locations are shown. AM levels are quantified using

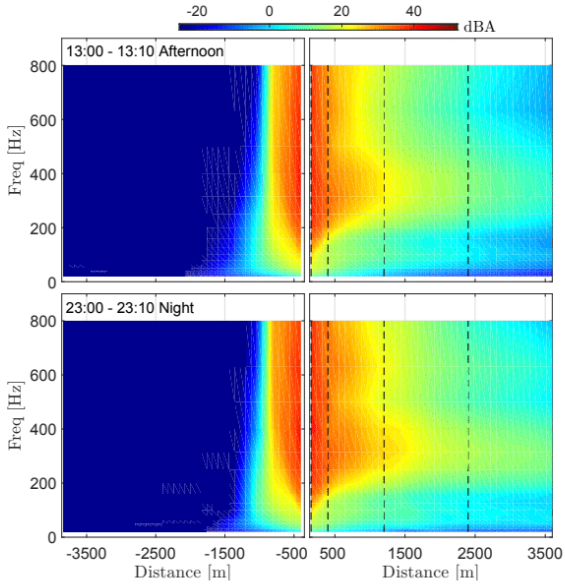

Figure 9: Contours of the time averaged spectra at receivers of 2 m height both upwind and downwind of the turbine. **From top to bottom** Afternoon and night time.

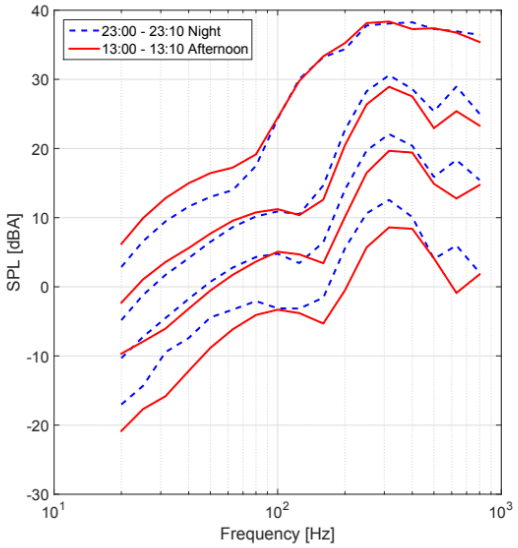

Figure 10: Time averaged spectra at the receivers of 2 m height and various downwind locations in two periods of the day. **From top to bottom:** 2D, 5D, 15D, 30D distance downwind of the turbine.

the method proposed by the UK Institute of Acoustics (IoA) Noise Working Group on Wind Turbine Noise Amplitude Modulation. The method is based on transforming a SPL time series of 10 second blocks into frequency domain in order to detect the blade passage frequency and its next two harmonics. After certain checks and filtering, an inverse Fourier transform is applied and the modulation depth is determined from the reconstructed signal. This procedure is repeated 60 times for each 10 minute dataset and the detected AM values are averaged. Thus, at each receiver one value is obtained as representative for each period of the day. Figure 11 shows the AM levels downwind of the turbine for receivers at 2 m height at various time instants in the day. In near field the AM levels are around 1 dBA in the night time and in the morning while in the afternoon the levels are the lowest, 0.6 dBA. The small difference between the night time and afternoon SPLs (≈ 0.4 dbA) is associated with the incoming wind shear and it is detailed via SPL time signals later on. Starting from the near field up to a distance of 1200 m the AM levels increase with distance. This is valid for all times of the day; however the peak values show a variation. In the night time and in the morning there are two distinct peaks, one at ≈ 1200 m and another one at ≈ 2700 m. The first peak is due to the sound waves that are refracted downwards after being trapped within the long wake deficit. The second peak is due to the secondary downward refraction. This can be seen from the side view contours in Fig. 8. As the blades rotate, the emitted waves go through the wake deficit region and refract differently. Thus, the location of the enhanced SPL regions changes. This results in high SPL modulations. It is also observed that at both distances (1200 m and 2700 m) the AM levels in the night time are slightly higher than in the morning. The reason behind this is not very clear to the authors.

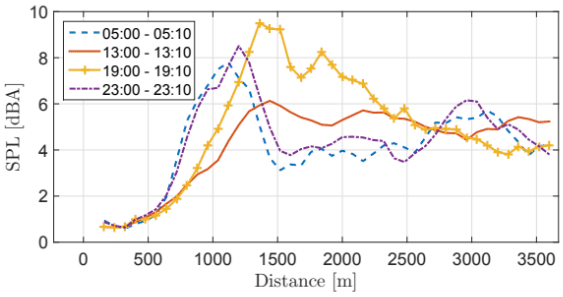

Figure 11: Amplitude modulation levels downwind of the turbine for receivers at 2 m height at various times of the day.

Figure 12 shows SPL time signals for two periods of the day (night time and afternoon) and at two receiver locations downwind of the turbine (near field (2D) and far field (15D)). At 2D the average overall sound pressure levels are similar (within 0.5 dBA) but the SPL time signal in the afternoon shows more fluctuations than that in the night. This can be attributed to the high incoming turbulence levels associated with the convective conditions in the afternoon. There is no clear trend of increased peak-to-trough ratios of OASPL for different times of the day in the near field downwind of the turbine. In addition to the overall SPL, two frequency bands are also shown: 50 Hz band where the turbulence inflow noise dominates the spectrum and 315 Hz band where the trailing-edge noise is dominant. The 50 Hz time signal at 2D distance shows clearly that the levels in the afternoon are higher than in the night. This is again due

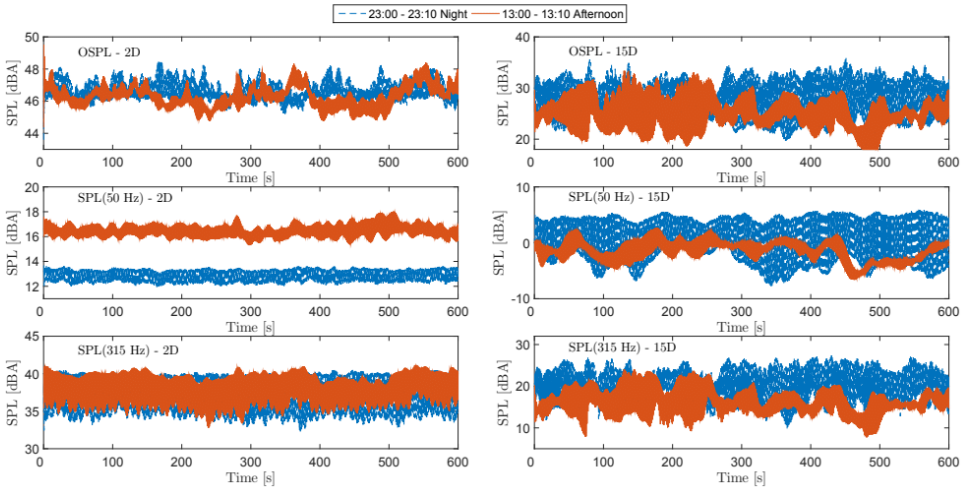

Figure 12: Time signals of overall and frequency dependent sound pressure levels at receivers of 2 m height in the near field (2D downwind) and far field (15D downwind).

to the high turbulence. The 315 Hz band, on the other hand, shows very similar mean levels in the near field. However, the peak-to-trough ratios are slightly higher in the night. This can be explained by the high wind shear associated with stable conditions in the night time.

Far field levels have a different trend. The variation of source levels combined with propagation caused fluctuations result in higher peak-to-trough ratios than in the near field. The selected receiver location in the far field is at 15 D (1200 m) where the AM levels in the night time are considerably higher than in the afternoon (see Fig. 11). This is also observed in Fig. 12. While a larger SPL variation is observed in the afternoon (levels vary more during 10 minutes), SPL in the night time has more regular fluctuations with higher peak-to-trough ratios. This can again be explained with the damped turbulence and the persistent wake deficit associated with the night time.

4. Conclusion

In this study a fully consistent unsteady approach has been developed for modelling wind turbine noise and both time averaged and time dependent variability of wind turbine noise over a diurnal cycle have been studied with a propagation model based on Parabolic Equation method. The flow and temperature input is obtained from Large Eddy Simulation with a rotating actuator disk model, while the source levels are predicted using aero-elastically coupled semi empirical noise models. It was observed that for a wind turbine with a hub height of 70 m and a diameter of 80 m, the near field levels are similar (within 0.5 dBA) for the same hub height wind speed. The small difference is mostly caused by the varying turbulence levels during the diurnal cycle and manifests itself at the low frequency range of the spectrum (below 150 Hz). However, far field levels showed a larger variation depending on the atmospheric conditions. The largest difference in A-weighted overall sound pressure level was observed between night time and afternoon, in other words between convective and stable conditions. The difference in SPL is 2.5 dBA at 650 m and reaches 6.5 dBA at 3600 m downwind of the turbine. The quantification of unsteadiness was carried out with an amplitude modulation detection procedure. It was observed that enhanced far field amplitude modulation (AM) levels also vary with the time of the day. Peak AM levels were observed at distances of 1200 m during evening and night time, while in the afternoon no specific peaks were detected.

In conclusion, this paper has presented the importance of the atmospheric conditions for far field receivers and how SPL varies with distance even with similar source levels. Future work will focus on a statistical approach to study the far field noise levels combined with the prevalence of various atmospheric conditions. Furthermore, unsteady simulations for wind turbines operating under wake conditions and yaw error will be carried out.

Acknowledgements

The work has been funded by the GreenTech Wind project, a collaboration of the EuroTech Universities. In addition, Chinese National Nature Science Foundation under grant number 11672261 is acknowledged.

References

[1] V. Betakova, J. Vojar, P. Sklenicka, Wind turbines location: How many and how far?, Applied Energy 151 (2015) 23–31.

[2] K. Molnarova, P. Sklenicka, J. Stiborek, K. Svobodova, M. Salek, E. Brabec, Visual preferences for wind turbines: Location, numbers and respondent characteristics, Applied Energy 92 (2012) 269–278.

[3] T. Tsoutsos, A. Tsouchlaraki, M. Tsiropoulos, M. Serpetsidakis, Visual impact evaluation of a wind park in a greek island, Applied Energy 86 (4) (2009) 546–553.

[4] E. Pedersen, H. I. Halmstad, Noise annoyance from wind turbines: a review, Naturvårdsverket, 2003.

[5] E. Pedersen, F. van den Berg, R. Bakker, J. Bouma, Response to noise from modern wind farms in the netherlands, The Journal of the Acoustical Society of America 126 (2) (2009) 634–643.

[6] A. Crespo, J. Hernandez, S. Frandsen, Survey of modelling methods for wind turbine wakes and wind farms, Wind energy 2 (1) (1999) 1–24.

[7] W. Z. Shen, J. Srensen, Numerical modeling of wind turbine wakes, J. Fluids Eng 124 (2) (2002) 393–399.

[8] R. J. Barthelmie, S. C. Pryor, An overview of data for wake model evaluation in the virtual wakes laboratory, Applied energy 104 (2013) 834–844.

[9] E. Barlas, S. Buckingham, J. van Beeck, Roughness effects on wind-turbine wake dynamics in a boundary-layer wind tunnel, Boundary-Layer Meteorology 158 (1) (2016) 27–42.
URL http://dx.doi.org/10.1007/s10546-015-0083-z

[10] L. P. Chamorro, F. Port-Agel, A wind-tunnel investigation of wind-turbine wakes: boundary-layer turbulence effects, Boundary-layer meteorology 132 (1) (2009) 129–149.

[11] N. O. Jensen, A note on wind generator interaction, 1983.

[12] G. C. Larsen, A simple wake calculation procedure, 1988.

[13] M. Bastankhah, F. Port-Agel, A new analytical model for wind-turbine wakes, Renewable Energy 70 (2014) 116–123.

[14] L. Tian, W. Zhu, W. Shen, Y. Song, N. Zhao, Prediction of multi-wake problems using an improved jensen wake model, Renewable Energy 102 (2017) 457–469.

[15] S. Ott, Linearised cfd models for wakes, Tech. rep. (2011).

[16] M. Churchfield, S. Lee, P. Moriarty, Overview of the simulator for wind farm application (sowfa) (2012).

[17] W. Z. Shen, J. N. Srensen, H. Yang, Actuator line/navier-stokes computations for flows past the yawed mexico rotor, 2011.

[18] N. N. Srensen, A. Bechmann, J. Johansen, Cfd for wind farm siting analysis.

[19] F. Castellani, A. Vignaroli, An application of the actuator disc model for wind turbine wakes calculations, Applied Energy 101 (2013) 432–440.

[20] L. A. Martnez Tossas, M. J. Churchfield, S. Leonardi, Large eddy simulations of the flow past wind turbines: actuator line and disk modeling, Wind Energy 18 (6) (2015) 1047–1060.

[21] W. Z. Shen, J. H. Zhang, J. N. Srensen, The actuator surface model: a new navier-stokes based model for rotor computations, Journal of Solar Energy Engineering 131 (1) (2009) 011002.

[22] H. Zhong, P. Du, F. Tang, L. Wang, Lagrangian dynamic large-eddy simulation of wind turbine near wakes combined with an actuator line method, Applied Energy 144 (2015) 224–233.

[23] E. S. Politis, J. Prospathopoulos, D. Cabezon, K. S. Hansen, P. K. Chaviaropoulos, R. J. Barthelmie, Modeling wake effects in large wind farms in complex terrain: the problem, the methods and the issues, Wind Energy 15 (1) (2012) 161–182.

[24] A. A. Veisi, M. H. S. Mayam, Effects of blade rotation direction in the wake region of two in-line turbines using large eddy simulation, Applied Energy 197 (2017) 375–392.

[25] C. Schulz, L. Klein, P. Weihing, T. Lutz, Investigations into the interaction of a wind turbine with atmospheric turbulence in complex terrain, Vol. 753, IOP Publishing, 2016, p. 032016.

[26] K. Nilsson, S. Ivanell, K. S. Hansen, R. Mikkelsen, J. N. Srensen, S. P. Breton, D. Henningson, Large eddy simulations of the lillgrund wind farm, Wind Energy 18 (3) (2015) 449–467.

[27] R. B. Stull, An introduction to boundary layer meteorology, Vol. 13, Springer Science & Business Media, 2012.

[28] D. Heimann, Y. Ksler, G. Gross, The wake of a wind turbine and its influence on sound propagation, Meteorologische Zeitschrift 20 (4) (2011) 449–460.

[29] E. Barlas, W. J. Zhu, W. Z. Shen, S. J. Andersen, Wind turbine noise propagation modelling: An unsteady approach, in: Journal of Physics: Conference Series, Vol. 753, IOP Publishing, 2016, pp. 022003–.

[30] S. Lee, D. Lee, S. Honhoff, Prediction of far-field wind turbine noise propagation with parabolic equation, The Journal of the Acoustical Society of America 140 (2) (2016) 767–778.

[31] E. Barlas, W. J. Zhu, W. Z. Shen, M. Kelly, S. J. Andersen, Effects of wind turbine wake on atmospheric sound propagation, Applied Acoustics 122 (2017) 51–61.

[32] G. Van den Berg, Wind turbine power and sound in relation to atmospheric stability, Wind Energy 11 (2) (2008) 151–169.

[33] S. Buck, S. Oerlemans, S. Palo, Experimental characterization of turbulent inflow noise on a full-scale wind turbine, Journal of Sound and Vibration 385 (2016) 219–238.

[34] T. Evans, J. Cooper, Effects of different meteorological conditions on wind turbine noise, in: Proceedings of Acoustics 2013 Victor Harbor, 2013.

[35] O. Ohlund, C. Larsson, Meteorological effects on wind turbine sound propagation, Applied Acoustics 89 (2015) 34–41.

[36] C. Larsson, O. hlund, Amplitude modulation of sound from wind turbines under various meteorological conditions, The Journal of the Acoustical Society of America 135 (1) (2014) 67–73.

[37] F. Porte-Agel, Y.-T. Wu, H. Lu, R. J. Conzemius, Large-eddy simulation of atmospheric boundary layer flow through wind turbines and wind farms, Journal of Wind Engineering and Industrial Aerodynamics 99 (4) (2011) 154–168.

[38] M. Abkar, F. Porte-Agel, The effect of free-atmosphere stratification on boundary-layer flow and power output from very large wind farms, Energies 6 (5) (2013) 2338–2361.

[39] H. Lu, F. Porte-Agel, Large-eddy simulation of a very large wind farm in a stable atmospheric boundary layer, Physics of Fluids 23 (6) (2011) 065101–.

[40] F. Porte-Agel, Y.-T. Wu, C.-H. Chen, A numerical study of the effects of wind direction on turbine wakes and power losses in a large wind farm, Energies 6 (10) (2013) 5297–5313.

[41] Y.-T. Wu, F. Porte-Agel, Large-eddy simulation of wind-turbine wakes: evaluation of turbine parametrisations, Boundary-layer meteorology 138 (3) (2011) 345–366.

[42] Y.-T. Wu, F. Porte-Agel, Simulation of turbulent flow inside and above wind farms: model validation and layout effects, Boundary-Layer Meteorology (2013) 1–25.

[43] Y.-T. Wu, F. Porte-Agel, Modeling turbine wakes and power losses within a wind farm using les: An application to the horns rev offshore wind farm, Renewable Energy 75 (2015) 945–955.

[44] E. Barlas, W. J. Zhu, W. Z. Shen, K. O. Dag, P. Moriarty, Coupled modelling of wind turbine noise from source to receiver, The Journal of the Acoustical Society of America.

[45] W. J. Zhu, W. Z. Shen, E. Barlas, F. Bertagnolio, J. Nrkr Srensen, Wind turbine noise generation and propagation modeling at dtu wind energy: A review, Renewable and Sustainable Energy Reviews.

[46] P. Moriarty, NAFNoise Users Guide,National Wind Technology Center, National Renewable Energy Laboratory, USA,Golden, Colorado, 2005. (2005).

[47] J. M. J. Sprague M. A., B. J. Jonkman, Fast modular framework for wind turbine simulation: New algorithms and numerical, in: AIAA SciTech 2015 33rd Wind Energy Symposium Kissimmee, Florida., 2015.

[48] P. D. S. Brooks, T. F., M. M. A., Airfoil self-noise and prediction, Tech. rep., NASA-RP-1218, L-16528, NAS 1.61:1218 (1989).

[49] M. Drela, Xfoil: An analysis and design system for low reynolds number airfoils, in: Low Reynolds number aerodynamics, Springer, 1989, pp. 1–12.

[50] R. Amiet, Acoustic radiation from an airfoil in a turbulent stream, Journal of Sound and vibration 41 (4) (1975) 407–420.

[51] M. V. Lowson, Assessment and prediction of wind turbine noise, Tech. rep. (1993).

[52] P. Moriarty, G. Guidati, P. Migliore, Prediction of turbulent inflow and trailing-edge noise for wind turbines, in: 11th AIAA/CEAS Aeroacoustics Conference, 2005, pp. 2881–.

[53] E. S. D. U. D. Sheets, Characteristics of atmospheric turbulence near the ground, Part II, Single point data for strong winds (neutral atmosphere), Engineering Sciences Data Item (85020).

[54] M. West, K. Gilbert, R. Sack, A tutorial on the parabolic equation (pe) model used for long range sound propagation in the atmosphere, Applied Acoustics 37 (1) (1992) 31–49.

[55] K. Attenborough, Acoustical impedance models for outdoor ground surfaces, Journal of Sound and Vibration 99 (4) (1985) 521–544.

[56] E. Barlas, W. J. Zhu, W. Z. Shen, K. O. Dag, P. Moriarty, Investigation of amplitude modulation noise with a fully coupled noise source and propa-

gation model, in: International Conference on Wind Turbine Noise, 2017.

Chapter 7

Preliminary Wind Farm Study

This chapter addresses the last objective of the thesis, namely the code preparation for wind farm noise mapping. The intricacy of the wind farm flow in complex terrain, sound propagation through multiple wakes and many other issues restrict the present chapter to be only as a preliminary study for the future work.

7.1 Flow Around a Wind Farm

For this study a wind farm in Shanxi region of China is selected. In total 25 turbines with hub heights of 70 m and rotor diameters of 93 m are located over a hilly terrain. For the flow modelling Reynolds-Averaged Navier-Stokes (RANS) option of DTU flow solver EllipSys3D was used [70, 71]. The wind turbines were modelled with actuator disk technique and the Menter's k-ω turbulence model was adapted accordingly [72, 73]. This turbulence model combines the k-ω model by Wilcox in the inner region of the boundary layer with the standard k-ϵ model in the outer region and the free steam outside the boundary layer. The details of the wind farm flow field study and comparison with measurements can be found in [74]. Figure 7.1 shows the streamwise velocity around the farm for one wind direction. The effects of the undulating terrain and the merging wakes are visible in the figure. These flow fields are later on used as input to the sound propagation calculations.

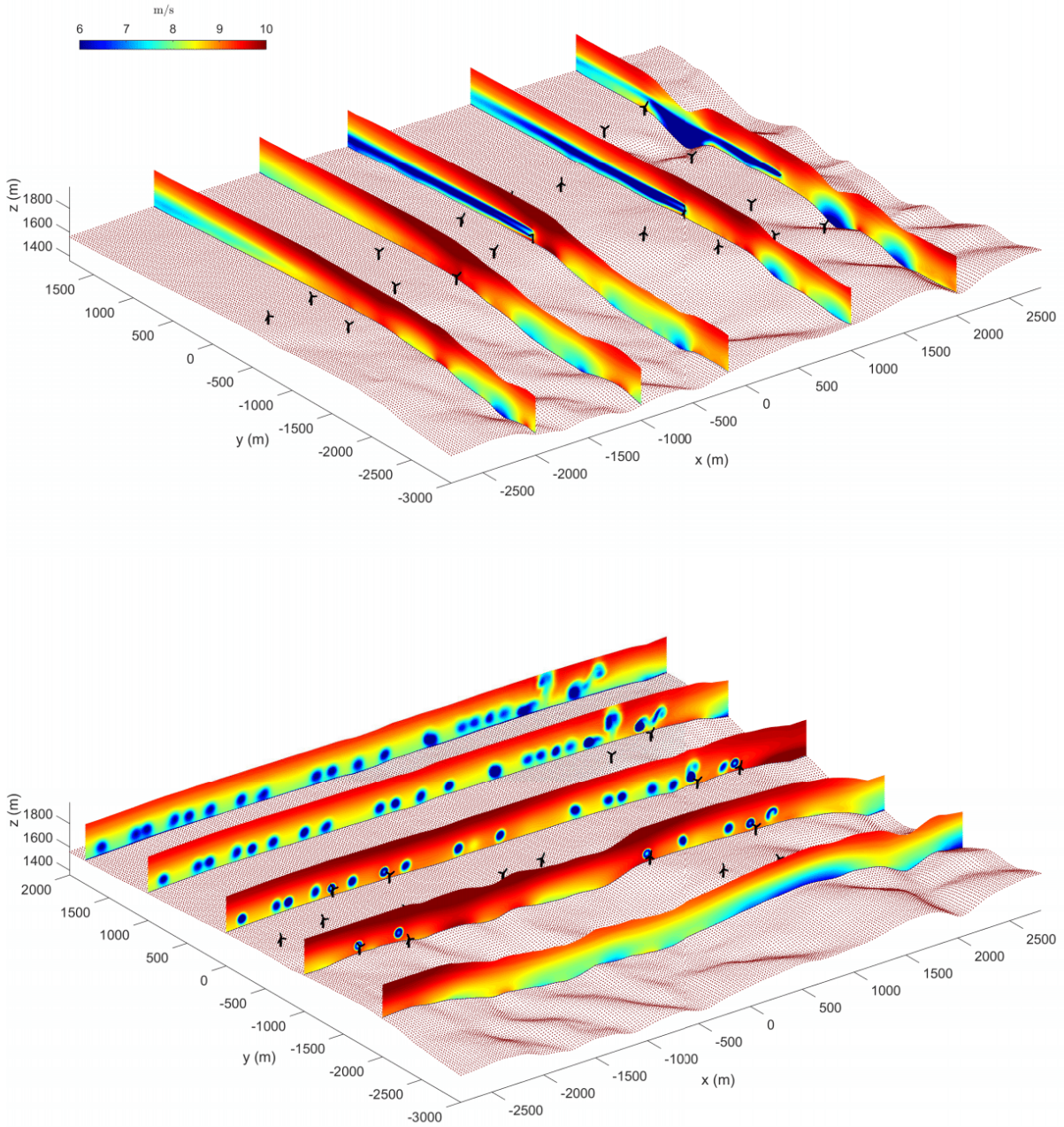

Figure 7.1: Streamwise velocity at various 2D slices around wind farm. Wind direction is along y axis.

7.2 Noise Around a Wind Farm

Source Representation

Similar to the previous two chapters the wind turbine noise source was represented via a point source for each blade at 85 % radius in a quasi three dimensional form. To capture the overall wind turbine noise directivity pattern, the airfoil turbulent inflow and trailing-edge noise directivity functions given in [75] were used. The former is associated with the low frequencies (i.e. the range of wavelength that is larger than the blade chord) and has a dipole directivity pattern. The latter is associated with relatively higher frequencies and has a cardioid directivity pattern. These functions, referred to as D_l and D_h respectively, including the convective amplification factors in the denominator are given:

$$D_l(\theta,\phi) = \frac{sin^2(\theta)sin^2(\phi)}{\Big(1 - Mcos(\theta)\Big)^4} \tag{7.1}$$

$$D_h(\theta,\phi) = \frac{2sin^2(\theta/2)sin^2(\phi)}{\Big(1 - Mcos(\theta)\Big)^4} \tag{7.2}$$

where θ and ϕ are the directivity angles that vary with respect to the source and observer locations (see Fig. B3 in [75]). Using the proportionality of directivity functions with the square of pressure [76] the additional term was added to the equation:

$$L_p(f_i) = L_W(f_i) - 10\log_{10}(4\pi R^2) - \alpha(f_i)R + \Delta L(f_i) + 10\log_{10}(D_x), \tag{7.3}$$

where the terms on the right hand side represent source power level, geometrical spreading, atmospheric absorption, transmission loss obtained from the propagation calculations and the directivity function, respectively. The directivity function was normalized via dividing the values by its maximum. The term D_x, was substituted with D_l for the frequencies lower than 200 Hz, and with D_h for the frequencies higher than 200 Hz.

The simulations were carried out for one full rotation. The sources were rotated with 30° blade azimuth angle increments for all turbines. At each blade azimuth angle 30 independent turbulence realizations were carried out. The von Karman spectral density function was used with the parameters: $C_T^2/T_0^2 = 6 \times 10^{-7} m^{-2/3}$,

$C_v^2/c_0^2 = 1 \times 10^{-6} m^{-2/3}$, $K_0 = 0.12$, number of modes $N = 2000$. The same source power level was used for all sources and all realizations (see Fig. 7.5 for the spectrum). 1/3-octave band centre frequencies from 50 Hz to 800 Hz were used for single wind turbine simulations. The frequency range for the wind farm simulations are explained later on. The ground impedance value was selected to represent grassland.

To gain insight of this setup, first the single turbine simulations were carried out over flat terrain. Figure 7.2 shows the time averaged noise maps at 2 m height around a wind turbine for four cases. Figure 7.2)a shows the SPL distribution for a non moving atmosphere without the directivity term in eq. 7.3. As expected the SPL attenuation in all directions are identical.

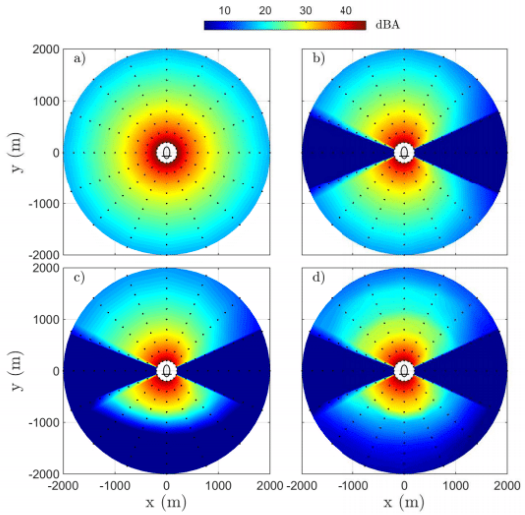

Figure 7.2: Time averaged noise map at 2 m height around a wind turbine over flat terrain: a) non moving atmosphere without source directivity, b) non moving atmosphere with source directivity c) moving atmosphere without turbulence and with source directivity, c) moving atmosphere with turbulence and with source directivity.

In Fig. 7.2)b the directivity is the only factor that causes SPL azimuthal variation. The upwind and downwind levels are similar while the crosswind levels are significantly smaller. This observation is in line with the numerical study in [77]. It is clear that the crosswind levels reach unrealistically low levels as a result of the directivity functions' behaviour. An advantage of this study is that the directivity term is simply a post processing issue, and thus it is easy to modify if experimental

input is provided. Nevertheless, the expected dipole-like pattern is captured with this approach. Figure 7.2)c shows a clear indication of increased SPL attenuation upwind of the turbine (note that the wind direction is from south to north). The effective speed of sound for the moving atmosphere is parametrized using a logarithmic wind speed profile with a surface roughness value of 0.1 m and constant speed of sound. The simulations including turbulence (Fig. 7.2)d) show similar SPL distribution downwind of the wind turbine, however the extent of the shadow zone upwind of the wind turbine is decreased due to turbulent scattering. The number of realizations can be increased for a more statistically correct approach, however here, the idea is to gain insight of the directivity pattern that will be implemented for the wind turbines located in the farm (see Sec. 7.2).

Wind Farm Noise

The wind farm noise simulations were carried out using the aforementioned setup. First, the streamwise and the lateral velocity fields were interpolated from RANS results for the corresponding 2D PE slice from each source to each receiver. The receiver points were distributed around the wind farm in a gridded manner. Even though the wide angle PE option was selected, to ensure the validity of the results the receivers within 200 m distance to any turbine were eliminated. Figure 7.3 shows the turbine layout and the receivers in which the remaining receivers after elimination were circled. Figure 7.4 shows the sketch of the 2D PE domains constructed from all sources to one receiver for single time step. Similar to the single turbine simulations, at each blade azimuthal location 30 independent turbulent realizations were carried out.

Different to the single wind turbine simulations the frequency range was dynamically adjusted. This means that if the distance between the source and receiver was longer than a given threshold, certain frequencies were not simulated. This helps to decrease the computational time. To justify these distances and frequencies only the atmospheric absorption was subtracted from the source power level at different distances (see Fig. 7.5). It is clear that the high frequencies are attenuated much more than low ones. The simulations were carried out such that if the distance is longer than 1000 m, 2000 m, 3000 m and 4000 m, the frequencies larger than 900 Hz, 800 Hz, 600 Hz and 500 Hz were not simulated, respectively. This setup can be easily changed in the code.

Before the whole wind farm results were discussed a PE contour plot for one point source is shown in Fig. 7.6. The same figure also shows the streamwise velocity that has been used as an input to the sound propagation calculations. Two receiver

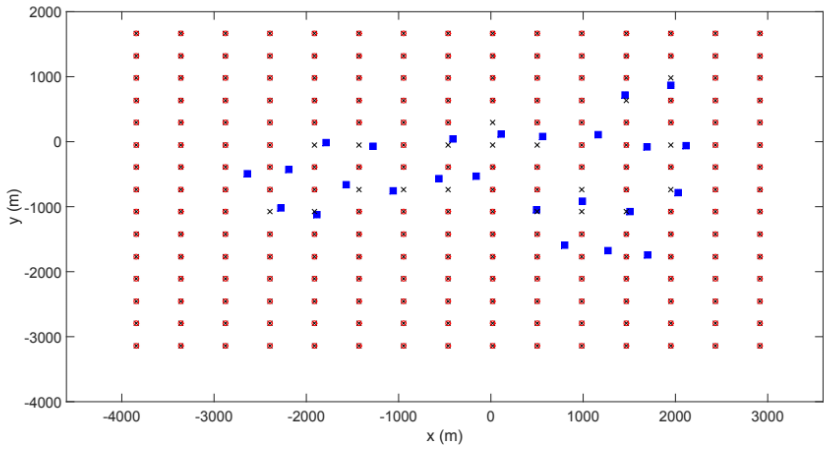

Figure 7.3: The top view of the receiver locations and farm layout. Crosses with circles are the receiver locations that are not within 200 m to any turbine, squares are the turbines.

locations, upwind and downwind of the turbine, were selected and the simulations were carried out for 500 Hz. Downwind of the turbine the wake effect on propagation is seen and the waves are guided downwards at a certain location. This effect was discussed extensively throughout the thesis. Upwind of the turbine the terrain effect on sound propagation results in a shadow zone in the trough of the valley and causes the transmission loss values to be higher further away from the source. Note that this figure shows a single blade simulation that is represented as a point source without the directivity function, atmospheric absorption, geometrical spreading or turbulence. Therefore, it should only be used to qualitatively inspect the sound propagation over complex terrain including the realistic time averaged flow field.

The wind farm simulation outputs were saved only at a single receiver height (2 m) for the locations shown in Fig. 7.3. Figure 7.7 shows the interpolated noise map for the wind direction corresponding to the flow field shown in Fig. 7.1. It is observed that the directivity does not play a role as effective as the single turbine case since the crosswind levels are usually insonified by other turbines. Similar to Fig. 7.6 the terrain undulation sometimes causes *unexpectedly* high levels further away from the turbines. To investigate the effects of terrain, realistic flow and turbulence on noise separately other sets of simulations were carried out.

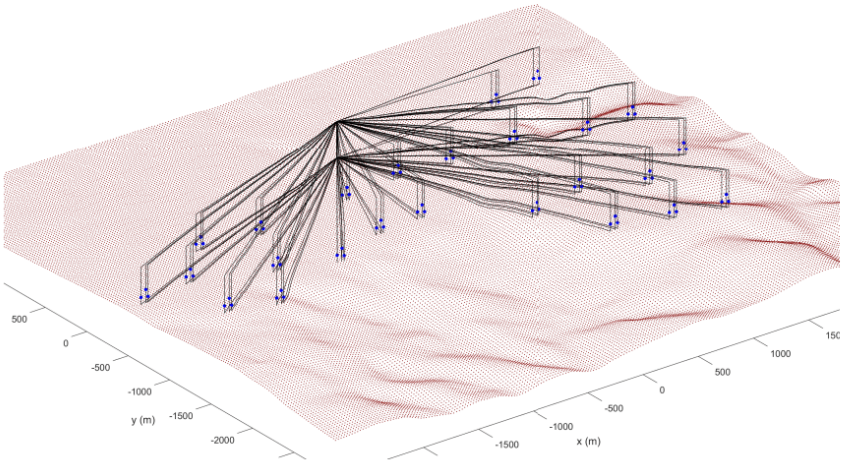

Figure 7.4: Sketch of the 2D PE domains from all sources to one receiver location for single time step

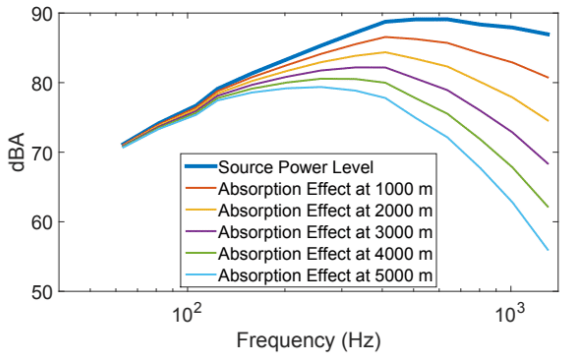

Figure 7.5: Source power level subtracted the atmospheric absorption at various distances

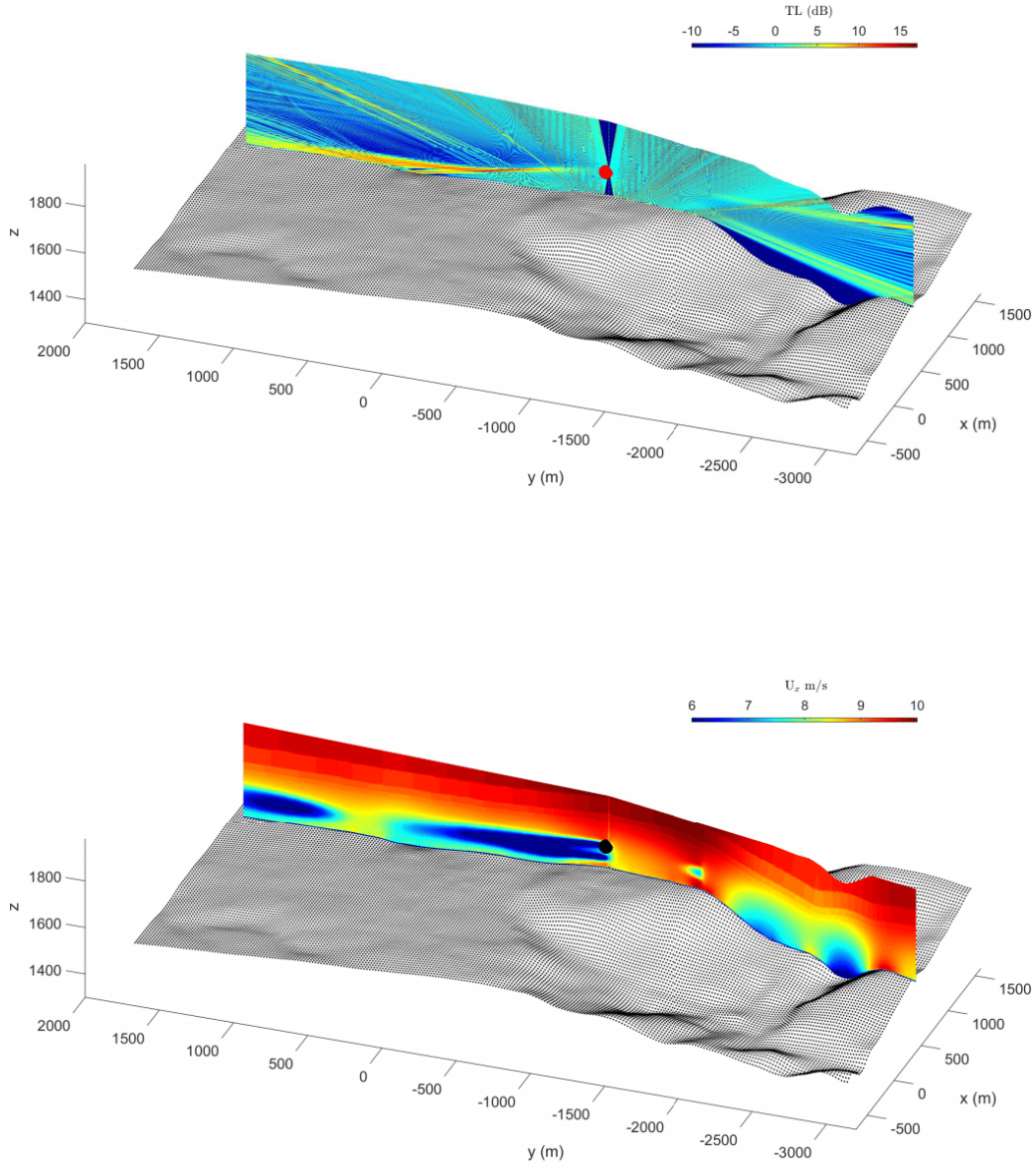

Figure 7.6: Top: The transmission loss for 500 Hz. The red sphere shows the source location. Bottom: The corresponding streamwise velocity in which the sound propagation takes place. The black sphere shows the source location.

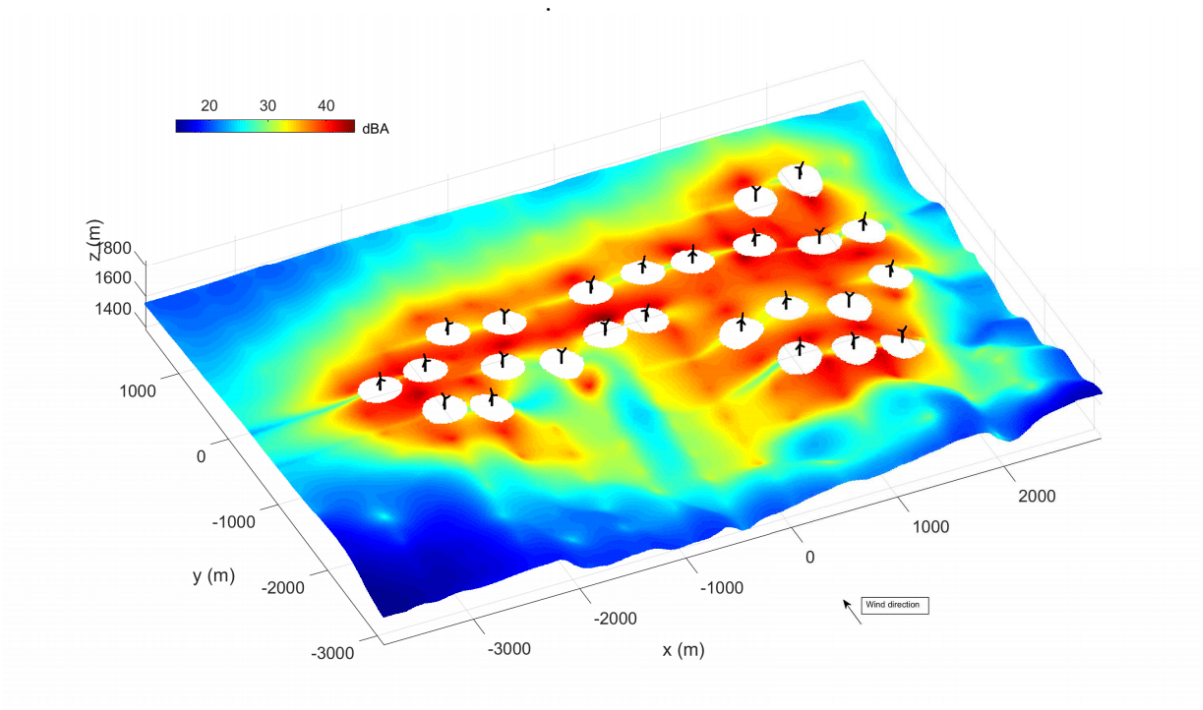

Figure 7.7: OASPL at 2 m receiver height around the wind farm. The wind direction is along the y axis.

- **Case 1**: Flat terrain simulations with the homogeneous atmosphere (no wind - flat terrain - SPL_1).
- **Case 2**: Flat terrain simulations with the logarithmic effective sound speed profile (logarithmic wind - flat terrain - SPL_2).
- **Case 3**: Complex terrain simulations with the logarithmic effective sound speed profile (logarithmic wind - complex terrain - SPL_3).
- **Case 4**: Complex terrain simulations with the flow field obtained from RANS (RANS wind - complex terrain - SPL_4).

Figure 7.8 shows each of the case that are itemized above. The distribution of Case 1 shows a regular SPL attenuation in all directions and the directivity is the main cause of azimuthal deviation. In Case 2 it is clear that the upwind noise levels are much lower than the downwind ones and the upwind SPL attenuation is very regular as the complex terrain is not considered. Similarly, Case 3 shows higher levels in the downwind than the upwind. However, the upwind SPL attenuation distributed in a more complex manner than Case 2. There are regions with amplified as well as attenuated SPL in comparison to Case 2. To visualise the effect better a differential SPL plot is depicted in Fig. 7.9. Downwind of the turbines the terrain is very smooth, and thus the differential levels are close to 0 dBA. However, at the upwind of the turbines the differential SPL changes depending on the receiver location. The variation reaches approximately $\pm$ 11 dBA, which shows a significant error if the terrain was not taken into account. Lastly, the Case 4 is compared with Case 3. This comparison shows the effect of realistic flow field and turbulent realizations. The SPL difference is not as high as the previous comparison. Nevertheless, the differential values reach -4 and +8 dBA. It is observed that the upwind levels are amplified in Case 4 due to the turbulence scattering, which is an expected outcome. The downwind levels are mostly attenuated when the realistic flow field and turbulence is taken into account. There can be multiple reasons for this. For example, it is possible that the logarithmic wind profile used in Case 3 causes a stronger downwind refraction than the RANS flow. It is also possible that the wake effects are causing local SPL amplification or attenuation regions that we can not asses with the few amount of receiver locations. It is difficult to derive conclusions from this preliminary study. Nevertheless, it is clear that the realistic flow field is an important parameter to take into account for accurate noise prediction. Note that this interpretation is only valid for the given wind direction and the turbulence realizations, hence it should not be generalized for all wind farm noise simulations.

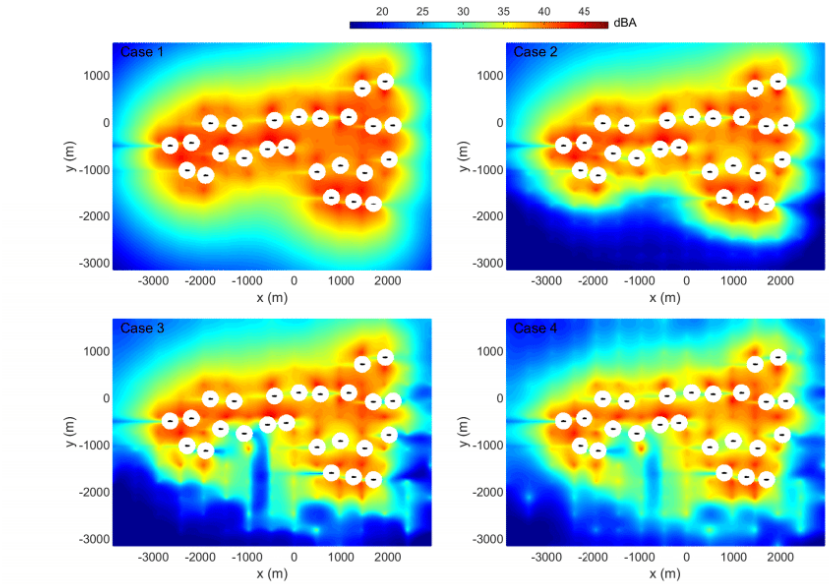

Figure 7.8: Top view of OASPL distribution at 2 m receiver height around the wind farm. Four cases are itemized in the text. The black points represent the wind turbines.

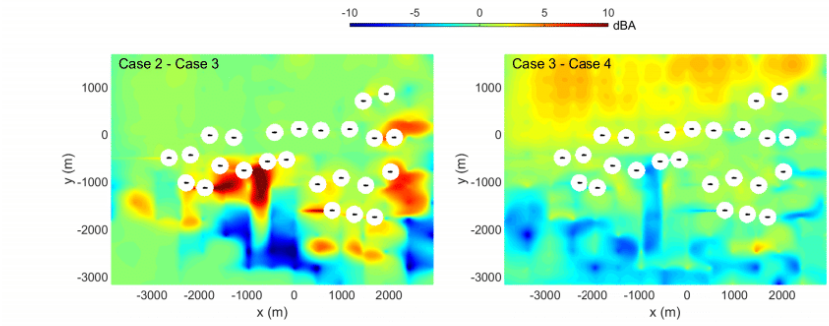

Figure 7.9: Top view of differential OASPL distribution at 2 m receiver height around the wind farm. **Left:** SPL_3 is subtracted from the SPL_2 to investigate the effect of terrain. **Right:** SPL_3 is subtracted from the SPL_4 to investigate the effects of RANS flow and turbulence realizations. The black points represent the wind turbines.

Chapter 8

Conclusions and future work

In this thesis the wind turbine aerodynamic far field noise was investigated with a wave-based propagation model with various source and flow input methods. The developed propagation tool was based on the parabolic equation (PE) method. The PE method is a numerical technique that solves the wave equation with various approximations (i.e. frequency domain, far field, one way propagation). A two-dimensional implementation was carried out. The main inputs for the PE method are the wind speed and speed of sound distribution, ground impedance and terrain along the propagation path. Throughout the thesis various cases with different atmospheric conditions, ground types were studied. The wind turbine as a sound source was represented either as a single point source at hub height or moving sources around the tips. Steady as well as unsteady flow input including the temperature effects were incorporated to the simulations. The relevant observations regarding the wind turbine noise generation and propagation phenomena are listed below;

- The source simplification studies showed that the time averaged SPL can be captured within reasonable accuracy via 2D moving source approach as long as the source levels are correctly weighted.
- The comparison of various fidelity flow models showed that the time averaged SPL can be obtained within reasonable accuracy using the steady flow output.
- The two items above can pave the way for more accurate but computationally less demanding noise mapping tools for wind farms. However as the items below will also point out the quantification of the unsteady effects such as amplitude modulation should be carried out with the combined model in which the source level fluctuations and propagation effects are taken into account consistently.

- It was observed that the wind turbine rotational speed is one of the major parameters that determines the source power levels. This is an expected outcome due to the increased tip speed with the increasing rotational speed.
- Comparison of the simulated wind turbine noise source power levels throughout the day showed lower levels at night than daytime which was associated with the enhanced turbulence intensity under convective atmospheric conditions.
- Throughout the thesis the wake effects on sound propagation has been an underlining factor in regards to far field SPL amplification or attenuation. As the variation in the atmospheric conditions cause a variation in the wake evolution, it can concluded that the atmospheric conditions affect wind turbine noise propagation not only directly (due to varying wind shear, ABL height and turbulence levels etc.) but also indirectly (due to wake evolution).
- Unsteady combined simulations showed that the enhanced far field amplitude modulation can be associated with the unsteady wake dynamics and rotating blades. In other words moving noise sources with constant variation of source power levels (blades) combined with wake deficit and its unsteady dynamics (e.g. meandering) cause increased far field AM levels. Particularly, the increased AM levels were observed at night time with the simulations including wake.
- From the preliminary wind farm study it was concluded that the realistic flow field as well as the terrain undulation are important parameters for an accurate noise prediction around a wind farm.

Future Work

Future work and further applications of the developed tool may address:

- Wind farm noise mapping and further experimental validation of the code.
- Wind turbine and farm control based on instantaneous far field SPL predictions at the specific receiver locations to confine with the regulations.
- A more systematic uncertainty quantification and sensitivity analysis study of various inputs such as flow, terrain and ground impedance.

References

[1] Martin V. Lowson. A new prediction model for wind turbine noise. pages 177–182. IET, 1993.

[2] Wei Jun Zhu, Wen Zhong Shen, Jens Nørkær Sørensen, and Giorgos Leloudas. Improvement of airfoil trailing edge bluntness noise model. *Advances in Mechanical Engineering*, 8(2):1687814016629343, 2016.

[3] C. Doolan. A review of airfoil trailing edge noise and its prediction. 2008.

[4] Thomas F. Brooks, D. Stuart Pope, and Michael A. Marcolini. Airfoil self-noise and prediction. 1989.

[5] Valerian Ilich Tatarskii. Wave propagation in turbulent medium. *Wave Propagation in Turbulent Medium, by Valerian Ilich Tatarskii. Translated by RA Silverman. 285pp. Published by McGraw-Hill, 1961.*, 1961.

[6] Vladimir E Ostashev and D Keith Wilson. *Acoustics in moving inhomogeneous media*. CRC Press, 2015.

[7] Eja Pedersen and Kerstin Persson Waye. Perception and annoyance due to wind turbine noise–a dose-response relationship. *The Journal of the Acoustical Society of America*, 116(6):3460–3470, 2004.

[8] K Persson Waye and E Öhrström. Psycho-acoustic characters of relevance for annoyance of wind turbine noise. *Journal of sound and vibration*, 250(1):65–73, 2002.

[9] Maarten Wolsink, Maarten Sprengers, Armin Keuper, Torben Holm Pedersen, and Chris A. Westra. Annoyance from wind turbine noise on sixteen sites in three countries. pages 273–276, 1993.

[10] Siegfried Wagner, Rainer Bareiss, and Gianfranco Guidati. *Wind turbine noise*. Springer Science & Business Media, 2012.

[11] Renzo Tonin. Sources of wind turbine noise and sound propagation. *Acoustics Australia*, 40(1), 2012.

[12] Gwang-Se Lee, Cheolung Cheong, Su-Hyun Shin, and Sung-Soo Jung. A case study of localization and identification of noise sources from a pitch and a stall regulated wind turbine. *Applied Acoustics*, 73(8):817–827, 2012.

[13] Stefan Oerlemans, Peter Sijtsma, and B Méndez López. Location and quantification of noise sources on a wind turbine. *Journal of sound and vibration*, 299(4):869–883, 2007.

[14] Matthew Cand, Andrew Bullmore, Malcom Smith, Sabine Von-Hunerbein, and Robert Davis. Wind turbine amplitude modulation: research to improve understanding as to its cause & effect. 2012.

[15] Iec 61400-11:2002 edition 2.1 wind turbine generator systems - part 11: Acoustic noise measurement techniques.

[16] Birger Plovsing. Proposal for nordtest method: Nord2000prediction of outdoor sound propagation. *DELTA Acoustics, Report AV*, 1106(07):–, 2007.

[17] B Søndergaard and B Plovsing. Validation of the nord2000 propagation model for use on wind turbine noise. *PSO-07 F&U project*, (7389):1–53, 2009.

[18] Wei Jun Zhu, Nicolai Heilskov, Wen Zhong Shen, and Jens Nørkær Sørensen. Modeling of aerodynamically generated noise from wind turbines. *Journal of Solar Energy Engineering*, 127(4):517–528, 2005.

[19] Peter Fuglsang and Helge Aagaard Madsen. *Implementation and verification of an aeroacoustic noise prediction model for wind turbines*. 1996.

[20] K Boorsma and JG Schepers. Enhanced wind turbine noise prediction tool silant. In *Forth International Meeting on Wind Turbine Noise, Rome*, pages –, 2011.

[21] S. McBride and R. Burdisso. An efficient noise modelling tool for wind turbines including sound propagation in arbitrary weather conditions. In *23rd Int Congress on sound and Vibration*, 2016.

[22] Joseph E Piercy, Tony FW Embleton, and Louis C Sutherland. Review of noise propagation in the atmosphere. *The Journal of the Acoustical Society of America*, 61(6):1403–1418, 1977.

[23] Tony FW Embleton. Tutorial on sound propagation outdoors. *The Journal of the Acoustical Society of America*, 100(1):31–48, 1996.

[24] Richard K Cook and Jessie M Young. Strange sounds in the atmosphere. part i. *Sound: Its Uses and Control*, 1(3):25–33, 1962.

[25] Michael V. Namorato. A concise history of acoustics in warfare. *Applied Acoustics*, 59(2):101–135, 2000.

[26] Charles D Ross. Outdoor sound propagation in the us civil war. *Applied Acoustics*, 59(2):137–147, 2000.

[27] F. Dunn, W. M. Hartmann, D. M. Campbell, and N. H. Fletcher. *Springer handbook of acoustics*. Springer, 2015.

[28] Richard K Cook and Jessie M Young. Strange sounds in the atmosphere. part ii. *Sound: Its Uses and Control*, 1(3):25–33, 1962.

[29] Edmund H. Brown and Freeman F. Hall. Advances in atmospheric acoustics. *Reviews of Geophysics*, 16(1):47–110, 1978.

[30] D Keith Wilson, Chris L Pettit, and Vldimir E Ostashev. Sound propagation in the atmospheric boundary layer. *Acoustics Today, volume11, issue2*, pages 44–52, 2015.

[31] John M. Noble and Harry J. Auvermann. The effects of large and small scale turbulence on sound propagation in the atmosphere. Technical report, 1995.

[32] Loic Ehrhardt, Sylvain Cheinet, Daniel Juve, and Philippe Blanc-Benon. Evaluating a linearized euler equations model for strong turbulence effects on sound propagation. *The Journal of the Acoustical Society of America*, 133(4):1922–1933, 2013.

[33] Sylvain Cheinet, Loic Ehrhardt, Daniel Juve, and Philippe Blanc-Benon. Unified modeling of turbulence effects on sound propagation. *The Journal of the Acoustical Society of America*, 132(4):2198–2209, 2012.

[34] D. Keith Wilson, Edgar L. Andreas, John W. Weatherly, Chris L. Pettit, Edward G. Patton, and Peter P. Sullivan. Characterization of uncertainty in outdoor sound propagation predictions a. *The Journal of the Acoustical Society of America*, 121(5):EL177–EL183, 2007.

[35] Benjamin Cotté and Philippe Blanc-Benon. Estimates of the relevant turbulent scales for acoustic propagation in an upward refracting atmosphere. *Acta Acustica united with Acustica*, 93(6):944–958, 2007.

[36] D. Keith Wilson, James G. Brasseur, and Kenneth E. Gilbert. Acoustic scattering and the spectrum of atmospheric turbulence. *The Journal of the Acoustical Society of America*, 105(1):30–34, 1999.

[37] Richard Michael Jones, Jack Parker Riley, and Thomas Martin Georges. Harpo: A versatile three-dimensional hamiltonian ray-tracing program for acoustic waves in an ocean with irregular bottom. *Unknown*, 1:–, 1986.

[38] Andre L'Espérance, JR Nicolas, P Herzog, and GA Daigle. Heuristic model for outdoor sound propagation based on an extension of the geometrical ray theory in the case of a linear sound speed profile. *Applied Acoustics*, 37(2):111–139, 1992.

[39] Erik M Salomons. Caustic diffraction fields in a downward refracting atmosphere. *The Journal of the Acoustical Society of America*, 104(6):3259–3272, 1998.

[40] Michael B Porter Finn B Jensen, William A Kuperman and Henrik Schmidt. *Computational Ocean Acoustics*. Springer, 2011.

[41] Vladimir E Ostashev, D Keith Wilson, Lanbo Liu, David F Aldridge, Neill P Symons, and David Marlin. Equations for finite-difference, time-domain simulation of sound propagation in moving inhomogeneous media and numerical implementation. *The Journal of the Acoustical Society of America*, 117(2):503–517, 2005.

[42] DK Wilson, David H Marlin, Sandra L Collier, Neill P Symons, David F Aldrige, and Vladimir E Ostashev. Incorporation of atmospheric flow fields and ground interactions into acoustic finite-difference, time-domain simulations. Technical report, 2004.

[43] D Keith Wilson, Neill P Symons, Edward G Patton, Peter P Sullivan, David H Marlin, David F Aldridge, Vladimir E Ostashev, Stephen A Ketcham, Edgar L Andreas, and Sandra L Collier&. Simulation of sound propagation through high-resolution atmospheric boundary layer turbulence fields. pages –, 2004.

[44] Astrid Ziemann, Arthur Schady, and Dietrich Heimann. Meteorological effects on the 3d sound propagation inside an inhomogeneous forest area. *Meteorologische Zeitschrift*, 25(3):327–339, 2016.

[45] Timothy Van Renterghem and Dick Botteldooren. Numerical simulation of the effect of trees on downwind noise barrier performance. *Acta Acustica united with Acustica*, 89(5):764–778, 2003.

[46] D Keith Wilson, Mark L Moran, Lanbo Liu, Vladimir E Ostashev, David F Aldridge, Neill P Symons, and David H Marlin. Development of a high-fidelity simulation capability for battlefield acoustics. In *AeroSense 2003*, pages 51–60. International Society for Optics and Photonics, 2003.

[47] Arthur Schady, Dietrich Heimann, and Joseph Feng. Acoustic effects of trees simulated by a finite-difference time-domain model. *Acta Acustica united with Acustica*, 100(6):1112–1119, 2014.

[48] Didier Dragna, Benjamin Cotté, Philippe Blanc-Benon, and Franck Poisson. Time-domain simulations of outdoor sound propagation with suitable impedance boundary conditions. *AIAA journal*, 49(7):1420–1428, 2011.

[49] Benjamin Cotté and Philippe Blanc-Benon. Time-domain simulations of sound propagation in a stratified atmosphere over an impedance ground. *The Journal of the Acoustical Society of America*, 125(5):EL202–EL207, 2009.

[50] Timothy Van Renterghem. Efficient outdoor sound propagation modeling with the finite-difference time-domain (fdtd) method: A review. *International Journal of Aeroacoustics*, 13(5-6):385–404, 2014.

[51] Maarten Hornikx, Roger Waxler, and Jens Forssén. The extended fourier pseudospectral time-domain method for atmospheric sound propagation. *The Journal of the Acoustical Society of America*, 128(4):1632–1646, 2010.

[52] Didier Dragna, Maarten Hornikx, Philippe Blanc-Benon, Franck Poisson, and Roger Waxler. Chebyshev pseudospectral time-domain method for simulations of outdoor sound propagation. pages –.

[53] Erik M Salomons. *Computational atmospheric acoustics*. Springer Science & Business Media, 2012.

[54] Keith Attenborough, Kai Ming Li, and Kirill Horoshenkov. *Predicting outdoor sound*. CRC Press, 2006.

[55] P Blanc-Benon, L Dallois, and D Juve. Long range sound propagation in a turbulent atmosphere within the parabolic approximation. *Acta Acustica united with Acustica*, 87(6):659–669, 2001.

[56] VE Ostashev, D Juve, and Ph Blanc-Benon. Derivation of a wide-angle parabolic equation for sound waves in inhomogeneous moving media. *Acta Acustica united with Acustica*, 83(3):455–460, 1997.

[57] L. Dallois, Ph Blanc-Benon, D. Juve, and V. Ostashev. A wide angle parabolic equation for sound waves in moving media. pages 195–208, 1998.

[58] P. M. Morse and H. Feshbach. *Methods of theoretical physics*. McGraw-Hill Book Company, 1953.

[59] Kenneth E Gilbert. A numerically stable formulation of the green's function parabolic equation: Subtracting the surface-wave pole. *The Journal of the Acoustical Society of America*, 137(1):EL8–EL14, 2015.

[60] RA Sack and M West. A parabolic equation for sound propagation in two dimensions over any smooth terrain profile: the generalised terrain parabolic equation (gt-pe). *Applied acoustics*, 45(2):113–129, 1995.

[61] Bertrand Lihoreau, Benoit Gauvreau, Michel Brengier, Philippe Blanc-Benon, and Isabelle Calmet. Outdoor sound propagation modeling in realistic environments: Application of coupled parabolic and atmospheric models. *The Journal of the Acoustical Society of America*, 120(1):110–119, 2006.

[62] T. Van Renterghem, Dick Botteldooren, and P. Lercher. Comparison of measurements and predictions of sound propagation in a valley-slope configuration in an inhomogeneous atmosphere. *The Journal of the Acoustical Society of America*, 121(5):2522–2533, 2007.

[63] Santosh Parakkal, Kenneth E. Gilbert, and Xiao Di. Application of the beilis-tappert parabolic equation method to sound propagation over irregular terrain. *The Journal of the Acoustical Society of America*, 131(2):1039–1046, 2012.

[64] Jennifer L. Cooper. *Parameter selection in the Green's function parabolic equation for outdoor sound propagation over varied terrain.* 2003.

[65] Allan P. Rosenberg. A new rough surface parabolic equation program for computing low-frequency acoustic forward scattering from the ocean surface. *The Journal of the Acoustical Society of America*, 105(1):144–153, 1999.

[66] Keith Attenborough, Shahram Taherzadeh, Henry E. Bass, Xiao Di, Richard Raspet, G. R. Becker, A. Gdesen, A. Chrestman, Gilles A. Daigle, and A. LEsprance. Benchmark cases for outdoor sound propagation models. *The Journal of the Acoustical Society of America*, 97(1):173–191, 1995.

[67] Francis M. Wiener and David N. Keast. Experimental study of the propagation of sound over ground. *The Journal of the Acoustical Society of America*, 31(6):724–733, 1959.

[68] Martin Almquist, Ilkka Karasalo, and Ken Mattsson. Atmospheric sound propagation over large-scale irregular terrain. *Journal of Scientific Computing*, 61(2):369–397, 2014.

[69] Wavetools. www.it.uu.se/research/scicomp/software/wavetools/acoustics/.

[70] Jess A. Michelsen. Basis3d-a platform for development of multiblock pde solvers. *Report AFM*, 92:5, 1992.

[71] Niels N. Sørensen. General purpose flow solver applied to flow over hills, 1995.

[72] Robert Mikkelsen. Actuator disc methods applied to wind turbines. *Technical University of Denmark*, 2003.

[73] David C. Wilcox. *Turbulence modeling for CFD*, volume 2. DCW industries La Canada, CA, 1998.

[74] Farmopt project final report. Technical report, Technical University of Denmark, 2017.

[75] Pope D. S. Brooks, T. F. and Marcolini M. A. Airfoil self-noise and prediction. Technical report, NASA-RP-1218, L-16528, NAS 1.61:1218, 1989.

[76] Martin V. Lowson. Assessment and prediction of wind turbine noise. Technical report, 1993.

[77] Steven Buck, Stefan Oerlemans, and Scott Palo. Experimental characterization of turbulent inflow noise on a full-scale wind turbine. *Journal of Sound and Vibration*, 385:219–238, 2016.

Appendix A

Poster Presentations

Development of Wind Turbine Noise Propagation Models

Emre Barlas (ebarlas@dtu.dk), Wei Jun Zhu, Wen Zhong Shen
Dept. of Wind Energy, Fluid Mechanics Section, Technical University of Denmark

Introduction

Problem Statement :

Noise is one of the main obstacles to achieve a broader public acceptance of wind energy. Fewer economic sites are available in EU which implies that the turbines will be placed even closer to the populated areas. There are various studies which show that wind farms do not trigger specific illnesses however annoyance and acceptance is not a negligible issue,

so:
understanding the
• noise generation & propagation mechanisms and the effects of these on people.
and,
• developing wind farms accordingly via involving and informing the public during the planning phases would help to broaden the usage of wind energy

Objective:

This project aims for developing advanced methods which will serve for designing ***low noise*** wind farms with ***high annual energy production***.

Propagation & Modeling

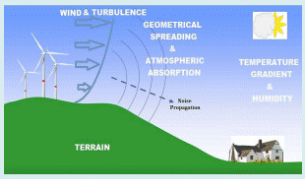

Figure 1 : Sketch of atmospheric noise propagation mechanisms

– Pop Quiz –

Q: Have you ever noticed that sometimes, you don't hear the trains passing by at certain times of the day even though the distance between the station and your house remains unchanged ? Why?

A: One of the most plausible explanations, is that the weather conditions at that moment were causing the sound waves to propagate in a way that you, as a receiver, were not hearing as much as you would at another time of the day.

Propagation of acoustic waves in the atmosphere is affected by numerous (often combined) effects e.g. ground, topography, mean temperature gradients, wind-speed, and their random fluctuations. There are different modeling techniques and each of them comes along with its benefits and drawbacks. An overview is given in the section – Methods & Implementation. (to your right)

Methods & Implementation

Overview of Noise Propagation Models

- **Engineering approach**
  - Ray model (very fast, accurate for high frequencies)
- **Time Domain Numerical Approaches:** (expensive, propagation in all directions, more than one frequency is resolved)
  - DNS, LES/CAA: compute source + propagation, based on solving Navier-Stokes equations.
  - FDTD: given source + propagation, based on solving Euler equations
- **Frequency Domain Numerical Approaches:** (less expensive, mostly one way propagation, one frequency at a time)
  - Parabolic equation (PE)
  - Fast Field Program (FFP) (layered atmosphere and homogeneous ground)

This project employs Parabolic Equation (PE) method which computes the sound field by solving a PDE which is derived from wave equation with the assumptions of harmonic wave, far field and eventually one way propagation. This, in 2D, yields ;

$$\frac{\partial \Omega}{\partial r} = i\sqrt{Q}\,\Omega \quad \text{where} \quad \Omega = \sqrt{r}P,\ Q = \frac{\partial^2}{\partial z^2} + k_{eff}^2 \quad \text{where} \quad k_{eff} = 2\pi f / c_{eff}(r,z)$$

In this set of equations we solve for P (pressure). The effective wave number (k_{eff}) is the main input which contains effective speed of sound (c_{eff}) and the frequency of interest (f). There are various numerical methods to solve the system above. So far the methods implemented within this project are using either Finite Difference Schemes (GTPE) or FFTs (rGFPE). Both methods yield an initial value problem where the simulation is started with the source term which is afterwards solved via space marching. Both models can handle:

- Varying wind (in the propagation direction) and sound speed profile along the propagation path
  (via effective sound speed approach)
- Varying ground properties
  (via bottom B.C., ground impedance derived from various models is an input)
- Atmospheric Turbulence
  (via refractive index fluctuations w.r.t. von Karman Spectrum, various methods exist)
- Complex Terrain
  (via terrain following coordinates, conformal mapping, domain decomposition etc.)
- Different starting fields
  (via modified initial value various starting fields can be an input for directionality etc.)

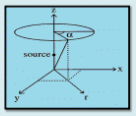

Figure 2 : 2D axisymmetric domain

Results

Effect of Impedance

For an elevated source and a receiver: ground causes interference between direct and the reflected wave. This can result in enhancement or attenuation of the sound pressure level at the receiver height. (due to constructive or destructive interference). In order to investigate this, the effective resistivity parameter was varied using Delany-Bazley model in a non-refracting atmosphere on a homogenous ground. The surfaces from snow to sealed asphalt was represented.

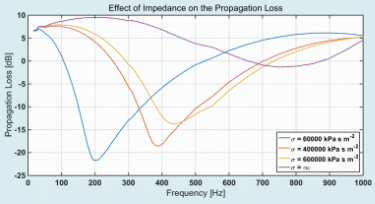

The results show large attenuation values for soft grounds, and then this gradually decreases with increasing resistivity. Another observation is that the lower peak values are shifted towards the higher frequencies with an increasing resistivity.

Effect of Atmospheric Turbulence

For the sound propagation models the turbulent atmosphere is usually described as a medium with a randomly fluctuating effective speed of sound which comes in as a phase multiplier into the equations, $e^{(ik_0\mu\Delta r)}$. Here the refractive index factor (μ) is generated such that the correlation function of it will be representative for turbulence. (in this case von Karman Spectrum fit, shown to the right)

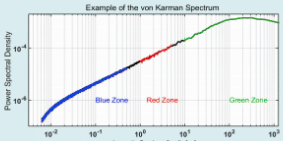

The whole spectrum (**Black Zone**) was divided into three parts; **Green Zone** ($l_0 > 10\,m$), **Red zone** ($1\,m < l_0 < 5\,m$), **Blue zone** ($l_0 < 0.5\,m$) representing those scales. The simulations were run both with the full spectrum content as well as the band pass filtered versions. The reason for this was to investigate the theoretical input which postulates that the turbulence scattering is expected to be dominated by the eddy sizes that are of the order of the wavelength. The investigation is carried out for one frequency, 100 Hz ~ 3.4 m. The results clearly show that the scattering effect that is caused by the whole spectrum (to the left) can also be captured with the band pass filtered version (the middle) - **Red zone**. On the other hand the very large scales (to the right) has almost no effect to the scattering at the receiver. (the very small scales are not shown since it has a very similar behavior with the very large scales, so **Green Zone** and **Blue zone** scales have similar effect for this configuration)

- 100 Hz, Grass Ground
- Source @ (0,2)
- Propagation Direction
- No Turbulence
- Large shadow zone

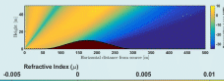

Note: This color map is also valid for the lower three propagation plots

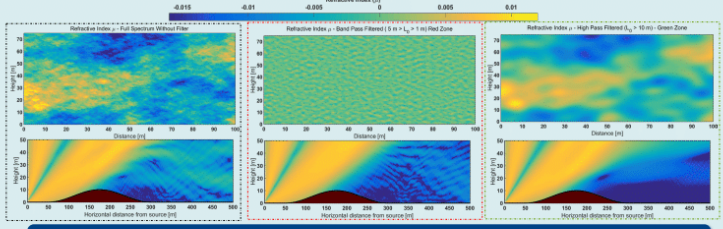

Effect of Terrain

The terrain on which the sound travels also affects the propagation. Below; various simulation outputs are depicted. It is seen that under the same atmospheric conditions the receiver would be exposed to varying noise level dependent on the terrain.

- Source @ (0,15)
- Propagation Direction
- No Turbulence
- Downward Refraction - Log. Wind

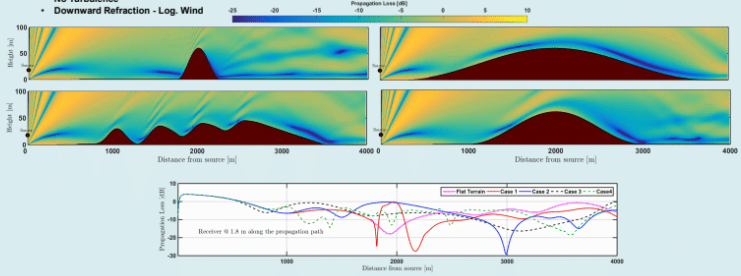

Effect of Sound Speed Distribution

The variation of the atmospheric conditions can be investigated via changing the vertical effective speed of sound distribution. A well representative profile is the logarithmic profile;

$$c_{eff}(z) = c_0 + b * ln\left(\frac{z}{z_0} + 1\right)$$

where $c_0 = 340\frac{m}{s}, z_0 = 0.1$ and b are reference sound speed, aerodynamic roughness and refraction set-up parameter, respectively.

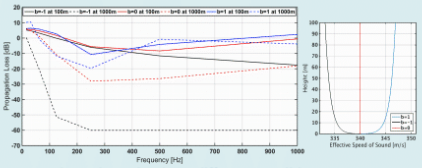

The investigations were carried out for flat grass covered terrain under three different conditions. ($b = 1 \rightarrow$ downward, $b = -1 \rightarrow$ upward and $b = 0 \rightarrow$ non − refractive) . The results show that up to 100 m the atmospheric conditions are not very effective. However, for longer propagation distances the effective sound speed distribution can result in large shadow zones, particularly for high frequency content.

- Source @ (0,2)
- Propagation Direction
- No Turbulence

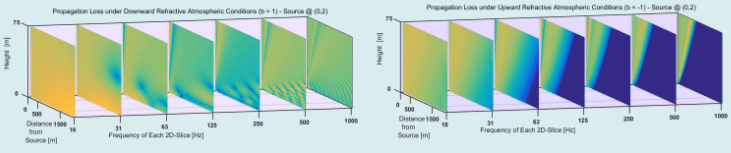

Conclusions & Future Work

Various parametric studies conclude that the noise prediction tools may fail if the realistic atmospheric conditions, terrain and ground characteristics are not correctly taken into account. To this extent Parabolic Equation (PE) method is a promising tool in terms of compromise between accuracy and computational time. It is the aim of this project to further improve wind farm noise propagation tools by taking advantage of the developing computational power and accuracy of the methods.

Acknowledgement

This project is funded by the EuroTech Wind project, in collaboration with Technical University of Denmark, Technische Universität München, Eindhoven University of Technology, École Polytechnique Fédérale de Lausanne.

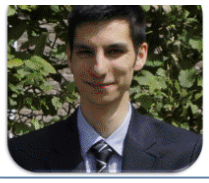

Sensitivities of Wind Farm Noise Propagation

Emre Barlas (ebarlas@dtu.dk), Wei Jun Zhu, Wen Zhong Shen
Dept. of Wind Energy, Fluid Mechanics Section, Technical University of Denmark

Introduction

Wind farm developers rely on noise mapping tools for environmental assessment studies. Inaccurate noise mapping during wind farm development phase may result in two scenarios;

- **Underprediction of the sound levels**
  This causes downregulation of wind turbines under certain atmospheric conditions (wind direction, atmospheric stability etc.).
- **Overprediction of the sound levels**
  This causes turbines to be located at less resourceful sites.

Both of these scenarios increase the cost of energy. With this study it is aimed to investigate the variability of noise levels dependent on the input parameters using a physics based propagation model.

Propagation Phenomenon

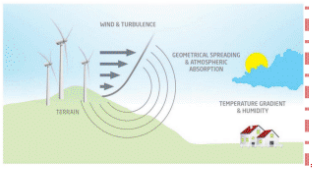

Figure 1 : Sketch of atmospheric noise propagation mechanisms

– Pop Quiz 1 –

Q: Have you ever noticed that sometimes, you don't hear the trains passing by at certain times of the day even though the distance between the station and your house remains unchanged ? Why?

A: One of the most plausible explanations, is that the weather conditions at that moment were causing the sound waves to propagate in a way that you, as a receiver, were not hearing as much as you would at another time of the day.

Propagation of acoustic waves in the atmosphere is affected by numerous (often combined) effects e.g. ground, topography, mean temperature gradients, wind-speed, and their random fluctuations. This study is limited with the effect of steady flow field, wind turbine noise source levels and terrain.

– Pop Quiz 2 –

Q: Why do stars twinkle? (why do we see the stars as if they change their brightness)

A: The movement of air in the atmosphere of Earth causes the starlight to get slightly bent as it travels to the observer. So some of the light reaches us directly and some gets bent slightly away. This is a good analogy to the sound waves propagating in turbulent atmosphere.

Models

Propagation

This work employs Generalized Terrain Parabolic Equation (GTPE) [1] method which computes the sound field by solving a PDE that is derived from the wave equation with the assumptions of harmonic wave, far field and eventually one way propagation. This, in 2D (after mapping for terrain following coordinates), yields ;

$$\frac{\partial^2\varphi}{\partial r^2} + 2ik_0\frac{\partial\varphi}{\partial r} - k_0^2\varphi - 2H'\left(\frac{\partial^2\varphi}{\partial r\partial z} + ik_0\frac{\partial\varphi}{\partial z}\right) - H''\frac{\partial\varphi}{\partial z} + (1+H'^2)\frac{\partial^2\varphi}{\partial z^2} + k^2\varphi = S$$

$$\text{where } \varphi = \exp(ik_0 r)\sqrt{r}P \quad \text{and } k = 2\pi f/c_{eff}(r,z)$$

In this set of equations we solve for P (pressure). The effective wave number (k_{eff}) is the main input which contains effective speed of sound ($c_{eff} = c(T) + v_x$) and the frequency of interest (f). Two of the inputs that this method needs are; background flow and source power levels. The methods used for obtaining inputs are explained below.

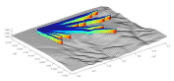

Each 2D PE slice represents the propagation from a turbine to one single receiver. Figures on the left and right shows two samples of this. Subsequently, distributing receiver locations in a circular manner yields a 'noise rose'. (see results)

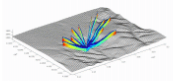

Flow Field

Flow field was obtained from Reynolds Averaged Navier-Stokes solution with Actuator Disk representation of the wind turbines [2]. Effects of wind turbine wake flow field on propagation is extensively studied by the authors in [3][4]

Source Levels

Source power levels are obtained from semi empirical noise model that is developed in [5]. For each turbine location the wind speed and turbulence levels are obtained from flow solver and then the source power levels are calculated.

Results

KEY NUMBERS : 19 Number of wind turbines in the wind farm. **36** Number of receiver locations around the wind farm **15** Number of acoustic frequency simulated. **800** Value of the highest acoustic frequency simulated [Hz]

Wind Farm Noise Map 1

Wind Farm Noise Map 1 (WFNR1) simulates;
Flat Terrain.
Same source strength for all turbines and all directions.
Same logarithmic wind profile for all directions and whole domain.

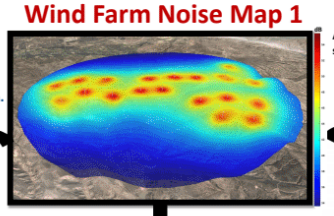

A Wind Farm Noise Map shows the sound pressure levels at ground level.

Terrain

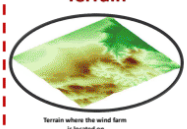

Terrain where the wind farm is located on

If the terrain was taken into account the SPL difference between WFNR1 and this case would be this plot on the right.

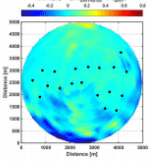

Flow Field

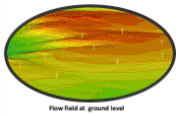

Flow field at ground level

If a realistic flow field was taken into account the SPL difference between WFNR1 and this case would be this plot on the right.

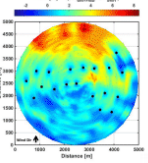

Source

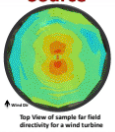

Top View of sample far field directivity for a wind turbine

If realistic source characteristics (changes due to turbulence, local flow and far field directivity) was taken into account the SPL difference between WFNR1 and this case would be this plot on your right

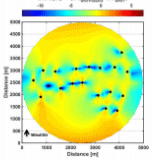

Difference with all parameters

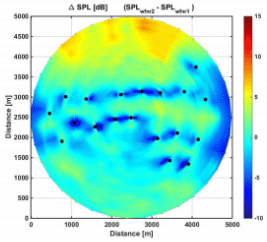

Wind Farm Noise Map 2 (WFNR2) simulates;
Complex Terrain.
Source strength variation w.r.t. local flow, turbulence levels and directivity.
Flow Field that is obtained from RANS.

Conclusions

The effects of three parameters are investigated on wind farm noise, namely terrain, source characteristics and flow field. When all three effects are correctly taken into account the difference in SPL between the simplest case (WFNR1) and the case with all three parameters can reach up to 15 dB. Separate parametric studies show that (for this specific wind farm)

Flow field, that take into account the wind turbine wake and the terrain effects, change the SPL significantly. Certain locations the differences can reach up to 8 dB if a realistic flow field was not taken into account. It is observed that **Terrain** did not play that much of a role on overall far field sound pressure levels in this case. **Source levels,** that take into account wind turbine noise directivity and local flow conditions, generally decrease the overall SPL. There are two reasons for this: 1) due to the dipole pattern directivity of wind turbine noise emission, sound pressure levels perpendicular to the incoming wind direction decrease dramatically. Note that the simplest approach (WFNR1) assumes monopole pattern directivity (which radiates sound equally well in all directions). Therefore the SPL is over estimated for the WFNR1 case. 2) The local flow conditions (local wind speed and turbulence levels) may have different effects. For example, due to wake and terrain turbulence levels are mostly increased (this results in increased source power levels), however due to same reasons (mostly wake) the wind speed is decreased (this results in decreased source power levels).

References

1. A Parabolic Equation for Sound Propagation in Two Dimensions over Any Smooth Terrain Profile, 1994, Applied AcousticsR.A. Sack and M. West.
2. Development of an AD/RANS model for accurately predicting wind turbine wakes, EWEA Offshore 2013 L Tian et al
3. Effects of wind turbine wake on atmospheric sound propagation, submitted to Applied Acoustics journal, E. Barlas et al.
4. Wind Turbine Noise Propagation Modelling : An Unsteady Approach, Torque Conference 2016, E Barlas et al.
5. Modeling of aerodynamically generated noise from wind turbines. Journal of Solar Energy Engineering 127.4 (2005): 517-528, Zhu, Wei Jun et al.

DTU Wind Energy is a department of the Technical University of Denmark with a unique integration of research, education, innovation and public/private sector consulting in the field of wind energy. Our activities develop new opportunities and technology for the global and Danish exploitation of wind energy. Research focuses on key technical-scientific fields, which are central for the development, innovation and use of wind energy and provides the basis for advanced education at the education.

We have more than 240 staff members of which approximately 60 are PhD students. Research is conducted within nine research programmes organized into three main topics: Wind energy systems, Wind turbine technology and Basics for wind energy.

Technical University of Denmark
Department of Wind Energy
Nils Koppels Allé
Building 403
2800 Kgs. Lyngby
Denmark
Telephone 46 77 50 85

info@vindenergi.dtu.dk
www.vindenergi.dtu.dk